REPUBLIQUE DU CAMEROUN

****

Paix-Travail-Patrie

****

REPUBLIC OF CAMEROON

****

Peace-Work-Fatherland

****

UNIVERSITÀ DEGLI STUDI DI PADOVA

DEPARTEMENT DE GENIE CIVIL

DEPARTEMENT OF CIVIL ENGINEERING

****

DEPARTMENT OF CIVIL, ARCHITECTURAL

AND ENVIRONMENTAL ENGINEERING

****

COMPARATIVE DESIGN BETWEEN EUROCODE AND BAEL BY ANALYTICAL AND NUMERICAL METHODS: CASE STUDY OF THE PRESTRESSED BRIDGE OVER THE MAHE RIVER.

A thesis submitted in partial fulfilment of the requirements for the degree of Master of Engineering (MEng) in Civil Engineering.

Curriculum: **Structural Engineering**

Presented by:

TCHINDA NAOUSSI Franky Vanèle

Student number: **15TP20949**

Supervised by:

Prof. Carmelo MAJORANA

Co-Supervised by:

Dr. Eng. Emanuele MAJORANA

Dr. Eng. POH'SIE Guillaume Hervé

Academic year: 2019/2020

BLANK PAGE

DEDICATION

I dedicate my work
To
My family in gratitude for all the love with which you cover me and the support that you bring to me for the success of my studies and my accomplishment as a man.

ACKNOWLEDGEMENTS

Special thanks goes to GOD for covering me with his grace, giving me the patience and the necessary energy to accomplish this work. This document is the fruit of the combined efforts of several individuals that I will like to thank here.

- The **President of the jury,** for the honour accepting to preside this jury.
- The **Examiner of this jury**, for accepting to examine this work.
- I particularly thank **Pr. Eng. Carmelo MAJORANA**, **Dr. Eng. Emanuele MAJORANA and Dr. Eng POH'SIE Guillaume** my supervisors, for their advice and recommendations for the outcome of this work.
- **Pr**. **NKENG George Elambo**, Director of the National Advanced School of Public Works Yaoundé, for his implication in the engineering formation at the NASPW.
- **Pr. Michel MBESSA**, the head of department of Civil engineering in the NASPW, for his guidance and work in civil engineering formation and provision of necessary data for this study.
- My appreciation equally goes to **Dr. WOUNBA Jean François and Dr NZENDA Celestin Silantos** for their advice throughout my training.
- **The teaching and administrative staff** of the NASPW, who devoted themselves to inculpate in us quality values and knowledge in the engineering field and their services rendered.
- I will also thank my classmates and academic elders for their advice and support throughout my writing period.
- I will like to express my deepest gratitude to my parents, **Mr. NAOUSSI Jean** and **Mme. NAOUSSI Martine** and the rest of my family members for all their encouragements, devotion and sacrifices. Thanks to you all for supporting me until the end of this work.
- Also, I really thank all those who directly or indirectly contributed or supported me throughout these years.
- Finally, my deep thanks goes to **KENMEUGNE MIGUE Lyne Alexandra**, **MODI Steve Loïc Michel, SONNA Donko Maël and MBOH Herbert Shayeh** for their support and encouragement throughout my training.

GLOSSARY

BAEL	Béton Armé aux Etats Limites
BPEL	Béton Précontraint aux Etats Limites
EN	European standards
LM1	Load Model 1
Q_{lk}	Characteristic value of breaking loads
$F_{w,x}$	Wind force acting in the x direction
v_b	Basic wind velocity
$v_{b,0}$	Fundamental value of the basic wind velocity
C_{dir}	Directional factor
C_{season}	Seasonal factor
C_{prob}	Probability factor
v_m	Mean wind velocity
C_r	Roughness factor
C_0	Orography factor
r	Roughness length
k_r	Terrain factor
k	Shape parameter
k_l	Turbulence factor
I_v	Turbulence intensity
$C_{f,x}$	Force coefficient in the x direction
q_p	Peak velocity pressure
$F_{w,x}$	Wind force per meter in the x direction
M_t	Torsional moment due to wind action
$\varepsilon_{shrinkage}$	Shrinkage strain
ε_{cd}	Drying shrinkage
ε_{ca}	Autogenous shrinkage
θ	Torsion parameter
α	Stiffening parameter
K_α	Load amplification coefficient
f_{ctm}	Characteristic tensile strength of concrete

fck	Characteristic compressive strength of concrete
fcd	Design concrete strength in compression
fyd	Design tensile strength of steel
f_{pk}	Characteristic breaking strength of prestressing steel
$f_{p0.1k}$	Yield stress of prestressing steel
ULS	Ultimate Limit State
SLS	Serviceability limit state
P_s	Prestressing force at service
FEM	Finite Element Method
CSI	Computers and Software Inc
EN	European Standard

ABSTRACT

The main objective of this work is to differentiate the design approaches of Eurocode and BAEL by assessing their performance in terms of number of parameters, sollicitations and design for the bridge over the Mahe river. In order to achieve this, documentary research was carried out for general site recognition, furthermore data relevant to the design was collected, the actions on the prestressed bridge were evaluated according to the prescriptions in EN 1991-2 and "fascicule 61 titre 2" for the actions on bridges. A numerical model of the bridge was made on which was performed static analysis for load repartition using finite element method and dynamic analysis done to control vibration of the structure. The load was then repartitioned using the Guyon Massonet method on the analytical model. There after the Magnel diagrams were drawn to make a suitable choice of prestress and eccentricity and finally, based on the results obtained, a comparative study was then carried out to differentiate the norms on the basis of the criteria already mentioned. The results obtained after application of this methodology are the general presentation of site, presentation of project, numerical model of the bridge with its vibration modes, frequencies, periods and the bridge response in terms of sollicitations. From the results obtained, the maximum moment in the edge beam due to the traffic loads according to Eurocode is greater than that due to the traffic loads according to BAEL However, a higher effective prestressing force is required to satisfy the stress limitations at service for BAEL This is due to a lower tensile stress limitation in BAEL (3.3 MPa) than Eurocode (3.7 Mpa). The outcome of the comparative study is that fewer parameters are involved to obtain the results in Eurocode compared to BAEL ,the sollicitations are greater in Eurocode than BAEL thus bridges designed according to Eurocode are expected to bear greater sollicitations compared to BAEL and fewer strands were obtained in the beam designed according to Eurocode (54) compared to BAEL(56).

Key words: Comparative study, Prestressed bridge, Eurocode, BAEL.

RESUME

L'objectif principal de ce travail est de différencier les approches de conception de l'Eurocode et du BAEL en évaluant leurs performances en termes de nombre de paramètres, sollicitations et dimensionnement pour le pont sur la rivière Mahe. Pour ce faire, une recherche documentaire a été réalisée pour une reconnaissance générale du site. Ceci est suivi par l'obtention des données pertinentes au dimensionnement. Les actions sur le pont précontraint ont été évaluées selon les prescriptions de l'EN 1991-2 et du « fascicule 61 titre 2 » pour les actions sur les ponts, Un modèle numérique du pont a été conçu sur lequel a été réalisée une analyse statique pour la répartition des charges selon la méthode des éléments finis et une analyse dynamique pour contrôler la vibration de la structure. Puis la charge a été repartitionnée selon la méthode de Guyon Massonet sur le modèle analytique. Ensuite, les diagrammes de Magnel ont été tracés pour faire un choix approprié de précontrainte et d'excentricité et enfin, sur la base des résultats obtenus, une étude comparative a ensuite été réalisée pour différencier les normes sur la base des critères déjà mentionnés. Les résultats obtenus après application de cette méthodologie sont la présentation générale du site, la présentation du projet, le modèle numérique du pont avec ses modes de vibration, fréquences, périodes et la réponse du pont en termes de sollicitations. D'après les résultats obtenus, le moment maximal dans la poutre de rive dû aux charges de trafic selon l'Eurocode est supérieur à celui dû aux charges de trafic selon BAEL Cependant, une force de précontrainte effective plus élevée est nécessaire pour satisfaire les limitations de contraintes en service pour BAEL Cela est dû à une limitation de contrainte de traction plus faible dans BAEL (3,3 MPa) que dans l'Eurocode (3,7 MPa). Le résultat de l'étude comparative est que moins de paramètres sont impliqués pour obtenir les résultats avec l'Eurocode par rapport au BAEL et les sollicitations sont plus importantes selon Eurocode qu'en BAEL donc les ponts conçus selon l'Eurocode devraient supporter des sollicitations plus importantes par rapport à ceux conçu suivant le BAEL.

Mots clés : Etude comparative, Béton précontraint, Eurocode, BAEL

LIST OF FIGURES

LIST OF TABLES

TABLE OF CONTENTS

GENERAL INTRODUCTION

The design of a structure has to satisfy requirements in terms of safety, durability economics and aesthetics. Hence the need to establish a certain organization based on specific rules in order to be able to suit in the best possible way the constraints to be satisfied by the structure. Over the centuries, scientific discoveries have been grouped together in structure calculation codes with variants adapted to each region and French speaking Africa has not been left on the side lines. Indeed, the current calculation code used in Cameroon, is the modified BAEL 99 which is the French code, replaced since March 2012 by the Eurocode 2 which applies to reinforced concrete and prestressed concrete structures.

The problem originates from the knowledge gap in the performance of Eurocode compared to BAEL in the design of prestressed bridges. Considering the need for the harmonisation of the design norms in Cameroon and from the problem just mentioned, the idea of a comparative design between the two norms finds all its interest.

A lot of comparative studies have been done between Eurocode and BAEL but the comparative analysis of the traffic loads by numerical and analytical methods has often been ignored. This is particularly important as the different nature of the traffic loads may produce different responses in the bridge elements depending on the method used.

The main objective of this work is to differentiate the design approaches of Eurocode and BAEL by assessing their performance in terms of number of parameters, sollicitations and design for the prestressed bridge over the Mahe river. This will add to the pool of knowledge available to the bridge designer to obtain an optimum design of prestressed concrete bridges.

This piece of work is articulated in three chapters. In the first chapter, a brief presentation of the state of the art as far as prestressed concrete and bridges are concerned and the fundamental principles inherent in each of these calculation codes will be made. In the second chapter, we will present the methodology used for the comparative design and finally in the last chapter, we will present the various results obtained which will be followed by analysis of these in order to be able to draw out the key points, advantages and disadvantages linked to each of these codes.

CHAPTER 1. LITERATURE REVIEW

Introduction

The design of prestressed concrete bridges has rapidly evolved in the past century since its first application in the 1900s this accounts for the lots of research work in their design and innovations in structural codes. This chapter presents the state of the art in the design of prestressed concrete bridges. To better talk about it, this chapter is divided into five parts. The first part of this chapter presents a brief historical overview of prestressed concrete bridges, the second part talks about the typology of prestressed bridges, the third part talks about the principle governing prestressing ,the fourth part concerns the different methods for the analysis of highway superstructures and the fourth part talks about the various aspects concerning Eurocode and BAEL and the the state of the art as far as comparative design between Eurocode and BAEL are concerned.

1.1. A brief history on prestressed bridges

Prestressing of concrete dates back to the early 1900s, when several engineers experimented with the technique, but it was Eugene Freyssinet (1879-1962) who first applied for a patent in 1928 covering the principle. Freyssinet is reported to have built an experimental arch in 1908, which incorporated Prestressing tendons, and in 1930 he utilized prestressing during the construction of the Plougastel Bridge in France.(Menn, 1986)

1.1.1. Construction of the first prestressed concrete bridge

The first prestressed concrete bridges were built in the mid-1930s with the Oued Fodda Bridge in Algeria (1936), Aux Bridge in Saxony (1936) and the Oella Bridge in Germany (1938) leading the way. Eugene Freyssinet built six bridges across the Marne, France between 1945 and 1950 and firmly established the techniques of prestressed bridge construction. One of these is the Annet bridge, France (figure 1.1). After the Second World War, with a shortage of steel in Europe, the use of prestressed concrete became popular in the reconstruction of bridges across the continent, and the 1950s saw prestressed concrete being used widely for bridgeworks. In this period Eugene Freyssinet continued to design many new prestressed concrete bridges, while Gustave Magnel developed the technique on several notable structure in Belgium. (Menn, 1986).

Figure 1.1. Annet bridge France(Mossot, 2004)

1.1.2. Development of prestressing equipment

In 1939 Freyssinet developed and patented the first conical friction anchor. After 1945 other systems, such as those produced by Magnel-Blaton, BBRV and Lee-McCall, began to appear, as prestressing of concrete became popular. The early prestressing systems used were comprised of wires usually of 5 mm or 7 mm diameter, tensioned and anchored by a gripping device at the ends that transferred the load to the concrete. With the BBRV system, the wires were fitted with button heads at the ends to hold the individual wires against the anchor head, a system that is still used by BBR today (figure 1.2). Towards the late 1950s, more systems using bars were developed; while the use of the wire systems evolved, with larger tendons employing wire-by-wire stressing and wedge anchors. (Menn, 1986)

Figure 1.2. Modern BBRV prestressing system(source : bbrnetwork:com)

1.1.3. The use of high strength steels

The very early attempts at prestressing concrete used normal steel as 'tie rods', and were not very successful as the low level of prestress in the steel was lost due to the shrinkage and creep in the concrete. By the time that prestressing was beginning to be used more widely in bridgeworks, higher strength steel wires were available with ultimate strengths of up to1725 N/mm2 and a yield limit of 1240 N/mm2. Low relaxation grades of steel and higher strength wires, with ultimate strengths of up to 1860 N/mm2, have now become standard in the industry. By the early 1960s the wires were being assembled into strands and anchored by wedges onto an anchor cone cast into the concrete. This led to the development of the standard '7-wire' strand most commonly used today. Also, at this time, large capacity jacks were developed that could tension the large multi-strand cables in one operation, and this type of tendon began to dominate, although bars and wires were still used for more specialist applications. (Menn, 1986)

1.1.4. Development of modern techniques of bridge construction

In the following section modern techniques of bridge construction will be discussed such as precast segmental construction, insitu construction, implementation of the balanced cantilever technique, incrementally launched decks, the use of prestressed concrete in cable stayed bridges.

1.1.4.1. Precast segmental construction

Jean Muller introduced the technique of match-cast precast segmental concrete deck construction on the Shelton Road Bridge, USA, in 1952. In 1962 He went on to use this approach on numerous viaducts and major bridges worldwide, with one of the most notable bridges being the Linn Cove Viaduct, (figure 1.3). This was built by a 'top down' approach to minimize the disruption to the environmentally sensitive area beneath. The deck was cantilevered out using precast segments and when the pier position was reached, the precast substructure was placed from the deck and then used to support the deck as the construction continued. (Menn, 1986)

Figure 1.3. Linn cove viaduct under construction with precast segmental deck (Menn, 1986)

1.1.4.2. In situ construction

In 1948, Nunns Bridge in Lincolnshire became the first in situ post-tensioned concrete road bridge in the UK with a span of 22.5 m. This was followed by several other short-span bridges formed using precast beams and in 1954 the Northam Bridge in Southampton became the first major prestressed concrete bridge in the UK, with a total length of 148 m and spans up to 32 m (Menn, 1986)

1.1.4.3. Implementation of the balanced cantilever technique

The first balanced cantilever bridge was built in reinforced concrete across the Rio de Peixe in Brazil in 1930, and it was not until 1950 that this form of construction was first used with prestressed concrete on the Lahn Bridge at Balduinstein, Germany. When the Medway Bridge in the UK, (figure 1.4), was opened in 1963 it was at the time the longest span in the world constructed as an in situ segmental concrete box girder using the balanced cantilever technique. The central span was 150 m long and included a 30 m-long suspended precast beam section in the centre. The approach spans of this 1000 m-long river crossing were constructed using precast prestressed concrete beams. (Menn, 1986)

Figure 1.4. Medway viaduct under construction with the balanced cantilever method (Menn, 1986)

1.1.4.4. Incrementally launched decks

The technique of incrementally launching a post-tensioned concrete box girder was first used on the bridge over the Rio Caroni in Venezuela in 1962, with the system commonly seen today first used on the Inn Bridge, Kufstein, Austria, in 1965. Both these bridges had the basic design carried out by Fritz Leonhardt and his partner Willi Baur. This technique has since been used on many bridges including several notable viaducts on the motorway systems in Germany, France and Spain, and is especially well suited for crossing over deep valleys or over difficult ground. Dornoch Firth crossing in Scotland, (Figure 1.5), was opened in 1991 and was incrementally launched over the estuary during a ten-month period. With 20 spans it has a total length of 890 m. (Menn, 1986)

Figure 1.5. The bridge of Dornoch firth crossing, Scotland. (Maxwell, 2006)

1.1.4.5. The use of prestress concrete in cable stayed bridges

Prestressed concrete was used in major cable-stayed bridges from the 1960s, with several notable structures built including the Rafael Urdaneta Bridge in Venezuela, with a 235 m main span. Refinements in the design and construction of concrete cable-stayed bridges have led to their common use for spans of up to 500 m. Another early example is the Brotonne Bridge in France. Built in 1976, it has a 320m -long main span formed using a prestressed concrete box girder deck and a single plane of stays, which produced an elegant and striking appearance. (Menn, 1986)

1.2. Types of prestressed concrete bridges

There are many factors affecting the choice of bridge type, span arrangement and general layout. Prestressed concrete decks include a wide range of construction forms with span lengths ranging from 25 m for single spans to over 400 m in cable-stayed bridges. It is important to review the different types of bridges to determine the optimum solution structurally, economically and aesthetically with respect to our site constraints. The different types of prestressed concrete bridges are outlined below

1.2.1. Slab bridges

Solid or voided prestressed concrete slabs are used for short spans and where good access is available for their construction. Using slabs simplifies the formwork and concreting operations, although the decks arc relatively heavy and this makes prestressing inefficient. Slab decks were regularly used in the early period of prestressed bridges and are still used on appropriate projects. The Balbriggan Bridge in Ireland (figure 1.6) is a recent example where this type of deck has been used.

Figure 1.6. Balbriggan Bridge in Ireland
(Menn, 1986)

1.2.2. Beam and slab bridges

Beam-and-slab arrangements are the most common form of prestressed concrete bridge deck and utilize either precast or in situ concrete beams with the deck slab usually cast in situ. This type of deck is well suited for small- or medium-span bridges where the beam weights are small enough to use readily available cranes and for projects where repetition in the construction gives cost savings. However, beam-and-slab arrangements are generally considered less attractive than the box girder form of construction for the longer spans.

1.2.3. In situ multi cell box girder bridges

In situ multi-cell concrete box girder bridges are frequently used in the medium span range from 30 m up to 50 m. They provide a versatile arrangement suitable for simple highway bridges or longer viaducts while able to cope with complex geometry, tight curvature and variable deck widths. The box shape gives a good aesthetic appearance as well as being efficient in its design.

The deck arrangement is similar to a voided slab, but with the voids occupying a larger proportion of the deck area and usually being rectangular in section. A typical multi cell box girder bridge is the Ku un Tong Bypass, Hong Kong (Figure 1.7). The outer webs are often sloped and the side cantilevers made longer to improve the appearance. The web thickness is governed by the shear requirements, but they must be wide enough to provide space for the reinforcement and concrete to be placed around the prestressing ducts

Figure 1.7. The Ku un Tong Bypass Hong Kong (source : honkongthrumeyes.com)

1.2.4. Insitu single cell box girder

Single-cell box girders cast in situ are used for spans ranging from 40 m up to 270 m. The box arrangement is considered to give a good aesthetic appear-ance; with the web of the box in shadow producing a slender appearance when combined with a slim parapet profile. Single box arrangements are efficient for both the longitudinal and transverse designs, and they produce an economic solution for most medium- and long span structures.

A typical single cell box girder section consists of a top slab with cantilever arms, a bottom slab and two webs. Using a constant depth section throughout allows the deck details to be standardized, simplifying the construction. With a haunched profile the shallower deck at mid-span reduces the dead-load bending moments and shears in the deck, while the deeper section at the pier is more efficient resulting in an overall reduction in concrete and prestress quantities.

1.2.5. Precast segmental box girder

These bridges are constituted of precast segments usually match cast in a factory and joined on site with only a thin layer of epoxy between them.

Precast segmental box girder decks usually have single-cell arrangements with side cantilevers and are similar to the in-situ box girder. Top slab widths range typically from 6 m to 16 m with box widths between 3-5 m and 8 m. The Belfast Cross-Harbour Links (figure 1.8), carries both road and rail traffic through the heart of Belfast, and it was built with precast segments using the balanced cantilever technique.

Figure 1.8. Belfast Cross Harbour links(geograph.ie)

1.2.6. Precast full-length box girder

These are bridges where complete spans are precasted in a casting yard and the units transported to the site and placed in position. The Central Viaduct in Fig. 14.2, part of the Vasco da Gama crossing in Portugal, used 77-6 m long precast units weighing 2200 tonnes each to form the deck. The sections were cast on-shore and transported on barges before being lifted into place.

Cross-sections for full-length precast decks are usually similar to the single cell box girder arrangement used for in situ or precast segmental construction. A box section is efficient from the design aspects and provides robust units for moving and erecting. The transverse cross-section arrangement depends on the traffic requirements which dictate the top slab width. The precast deck units have diaphragms at the pier positions, similar to the other forms of box construction

1.2.7. Cable stayed bridges

Many recent major cable-stayed bridges have utilized post-tensioned concrete in the main deck elements. The use of stay cables to support the deck results in a slim section and makes long spans possible. Concrete is a versatile material able to combine efficient deck arrangements with an aesthetically pleasing appearance. As concrete is good in compression it is an ideal material to resist the high compression forces generated in the deck by the stays, especially adjacent to the pylons. Elsewhere, where the compression from the stays is less, the

deck is prestressed to overcome the tension and bending stresses generated by the deck behavior. The stiff concrete section assists in distributing the load along the deck and between the stays, while its high mass and damping characteristics reduce its susceptibility to vibrations or aerodynamic movements. Sunshine Skyway Bridge, Florida, uses a concrete box girder deck to give an elegant cable-stayed arrangement.

Of all the types of prestressed concrete bridges, the cable-stayed form gives the most diverse range of structural arrangement. Concrete cable-stayed bridges are built with one, two or more pylons; span arrangements are symmetrical or asymmetrical; and piers may be used in the back spans. The choice of the final arrangement is often due only to the designer's preference. Concrete cable-stayed decks are either a box or a beam-and-slab arrangement. The beam-and-slab arrangement produces the lightest decks, but it needs two planes of stays for support, while the box girder arrangement provides a stiff deck and is used with either one or two planes of stays. The figure 1.9 illustrate the evolution of bridge decks span.

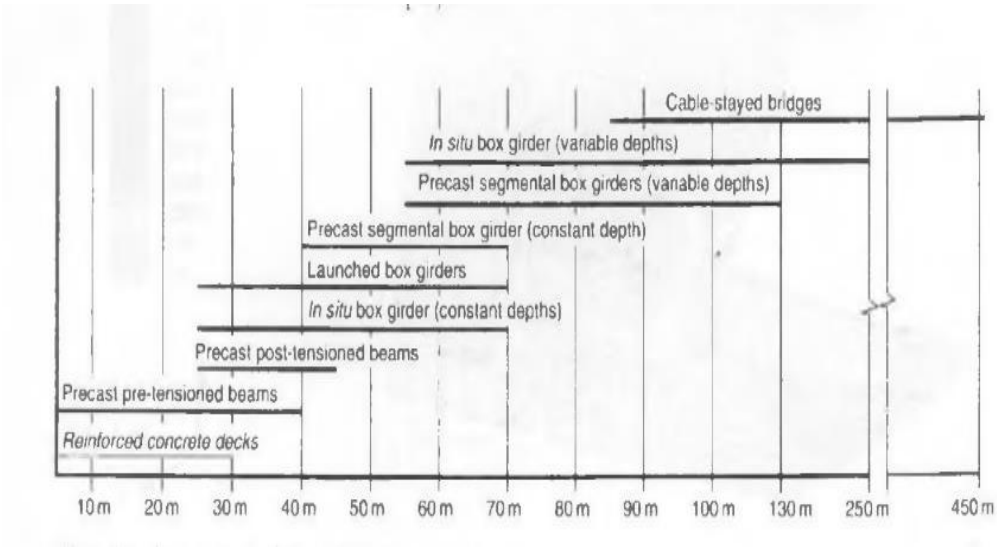

Figure 1.9. Evolution of bridge decks((Gilbert et al., 2013)

Figure 1.10 illustrate the span ranges for different types of deck and choice for span deck type.

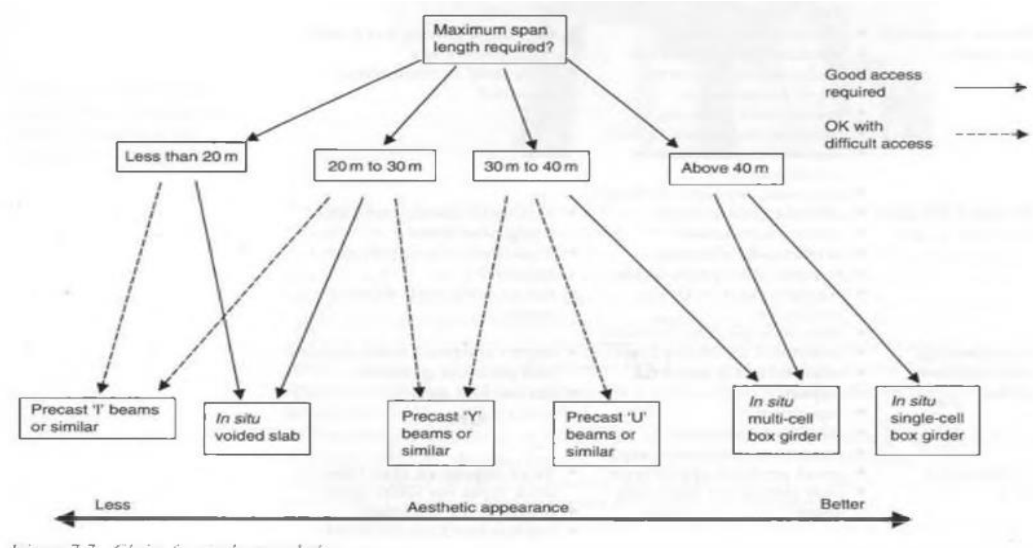

Figure 1.10. Span ranges for different types of deck and choice for span deck type (Gilbert et al., 2013)

1.3. Principle of prestressing

The word prestress created by E. FREYSSINET, means constrained before. Prestressing can be defined as the imposition of internal stresses into a structure that are of opposite character to those that will be caused by the service or working loads. In the design of a reinforced concrete beam subjected to bending it is accepted that the concrete in the tensile zone is cracked, and that all the tensile resistance is provided by the reinforcement. Since concrete is strong in compression and weak in tension the material in a beam will be used most efficiently if it can be maintained in compression throughout. Provision of a compressive force is made with the use of tensioned steel wires anchored to the concrete. Prestressing is primarily used to counteract tension stresses caused by the weight of the members and the superimposed loads. Should these loads cause a positive moment in a beam, it is possible by prestressing to introduce a negative moment that can counteract part or all of the positive moment. An ordinary beam has to have sufficient strength to support itself as well as the other loads, but it is possible with prestressing to produce a negative loading that will eliminate the effect of the beam's weight, thus producing a "weightless beam."(Gilbert et al., 2013)

1.3.1. Method of prestressing

There are two basic techniques commonly employed in the construction of prestressed concrete, Pretensioning and post-tensioning. The main difference between them is that the steel tensioning process is performed before or after the hardening of the concrete. The choice of method will be governed largely by the type and size of member coupled with the need for precast or in situ construction.

1.3.1.1. Pretensioning

Pre-tensioning is used primarily for the prefabrication of concrete components. The pre stressing steel is stressed between fixed abutments, forms are installed around the steel and the concrete is cast. After the concrete has hardened, the prestressing steel is detached from the abutments and the prestressing force is transmitted to the concrete by bond.(Gilbert et al., 2013)

1.3.1.2. Posttensioning

In posttensioned construction, the tendons are stressed after the concrete is placed and has gained the desired strength. Plastic or metal tubes, conduits, sleeves, or similar devices with unstressed tendons inside (or later inserted) are located in the form and the
Concrete is placed. After the concrete has sufficiently hardened, the tendons are stretched and mechanically attached to end anchorage devices to keep the tendons in their stretched positions. Thus, by posttensioning, the prestress forces are transferred to the concrete not
by bond but by end bearing.

1.3.2. Prestress losses

The prestress force at any point in the structure is always less than the force measured at the jack during stressing. The difference between the effective prestress force and the jacking force is called the loss of prestress. Prestress losses can be immediate or time dependent.(Gilbert et al., 2013)

1.3.2.1. Immediate losses

Immediate losses occur when the prestress is transferred to the concrete at time t_0 and may vary along the length of the tendon.

Immediate loss = p_{max}-$p_{m0}(x)$ (1.1)

p_{max} is the force imposed on the tendons by the hydraulic jack.

$p_{m0}(x)$ is the force in the tendon immediately after transfer. The following immediate losses occur in prestressed concrete members:

a. Elastic shortening of the member;

In pretensioned members, the change in strain in the tendon $\Delta\varepsilon_{p,0}$ is equal to the instantaneous strain in the concrete at the stress level $\varepsilon_{cp,0}$

$$\varepsilon_{cp,0} = \frac{б_{cp,0}}{E_{cm,0}} = \Delta\varepsilon_{p,0} = \frac{\Delta б_{p,0}}{E_p}. \quad (1.2)$$

The corresponding loss of stress $\Delta б_{p,0}$ is evaluated using

$$\Delta P_{el} = \frac{б_{cp,0}\, E_p}{E_{cm,0}} \qquad (1.3)$$

In posttensioned members if all tendons are stretched at once there is no loss due to elastic deformation. If there are several tendons stressed sequentially, stressing a tendon causes an elastic shortening loss in all previously stressed tendons. The average loss can be determined using equation 1.4.

$$\Delta б_p = \frac{n-1}{2n} \frac{E_p}{E_{cm,0}} \frac{p}{A} \qquad (1.4)$$

Where:

n is the number of tendons.

b. Friction at the interface of tendon-concrete;

In post tensioned members, friction losses occur along the tendon during the stressing operation. An estimation of the loss of force due to friction in a tendon at a distance x from the jacking end(EN 1992-1-1, 2004) by equation 1.5.

$$\Delta p_u(x) = p_{max}(1 - e^{-\mu(\theta + kx)}) \qquad (1.5)$$

Where:

θ is the sum of absolute values of successful angular deviations;

μ is the coefficient of friction between the tendons and its ducts;

K is the angular deviation.

1.3.2.2. Long term losses

These losses occur during the service life of the prestressed member. They are due to shrinkage and creep mechanisms in the concrete and the relaxation of the steel. The loss in tensile force of the concrete is not equal to the loss in compression of concrete if prestressing reinforcements are present.

The time independent losses often interact with each other and should not be calculated separately. An estimate of these losses, (EN 1992-1-1, 2004) is given by equation 1.6.

$$\Delta P_{C+S+r} = A_p \Delta\sigma_{p,\mathrm{C+S+r}} = A_p \frac{\varepsilon_{CS} E_P + 0,8\Delta\sigma_{\mathrm{Pr}} + \frac{E_P}{E_{Cm}} \phi(t,t_0).\sigma_{C,Qp}}{1 + \frac{E_p}{E_{Cm}} \frac{A_p}{A_C} \left(1 + \frac{A_C}{I_C} Z_{Cp}^2\right) \left[1 + 0,8\phi(t,t_0)\right]} \qquad (1.6)$$

Where:

ΔP_{C+S+r} is the loss of prestressing due to shrinkage, creep and relaxation at time t;

ε_{CS} is the total shrinkage deformation; E_{Cm} =the concrete elastic modulus;

$\Delta\sigma_{\mathrm{Pr}}$ is the loss of stress due to relaxation at time t_0 ;

$\phi(t,t_0)$ is the viscosity coefficient at time t, considering the application of load at t_0 ;

$\sigma_{C,Qp}$ is the stress at the fibre of interest due to quasi-permanent SLS combination including prestressing;

A_p is the Area of the prestressing steel; A_C = area of the concrete section;

I_C is the second moment of area of the concrete section.

1.3.3. Materials properties

The deformation of a prestressed concrete member is a function of the properties of its constituent materials. For adequate structural strength of a member and serviceability, the ultimate strength of the constituent materials as well as the in-service behavior needs to be known.

1.3.3.1. Concrete

Concrete is a mixture of cement, water, aggregates in definite proportions. It may also contain chemical admixtures (MBESSA, 2005). A typical mix used for prestressed concrete by weight might be coarse aggregate 45%, fine aggregate 30%, cement 18% and water 7%. The idealized stress strain relationship for nonlinear analysis of concrete subjected to short term uniaxial loading (figure 1.11) with $б_c$ and ε_c expressed as absolute values, (EN 1992-1-1, 2004).

$$\frac{\sigma_c}{f_{cm}} = \frac{kn-n^2}{1+(k-2)n} \qquad (1.7)$$

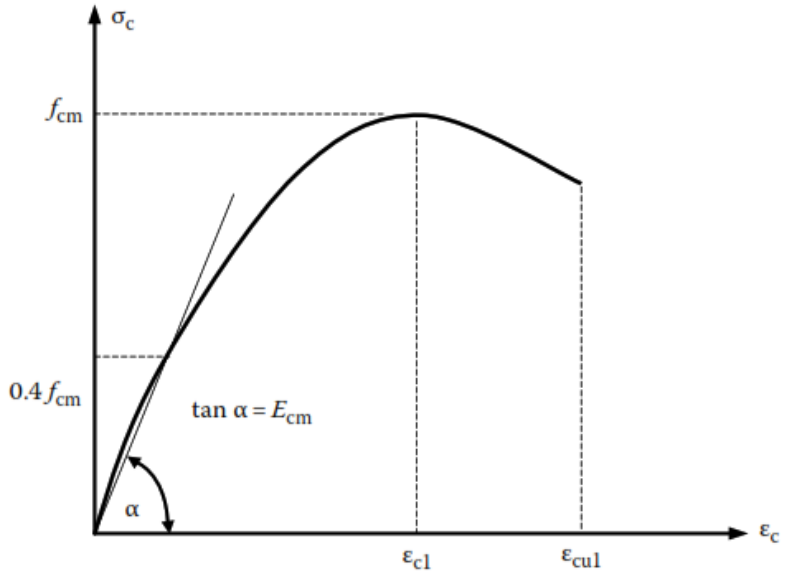

Figure 1.11. Idealised stress–strain relationship for concrete in uniaxial compression (EN 1992-1-1, 2004)

Where:

$$\eta = \frac{\varepsilon_c}{\varepsilon_{cl}}$$

$$k = 1.05\frac{E_{cm}}{E_{cp}}$$

1.3.3.2. Mild steel

Steel reinforcement in prestressed concrete members is used for the same reason as it is used in conventional reinforced concrete structures: to provide strength, ductility and serviceability. It is also strategically placed to reduce short term and long-term deformations. The shape of the stress–strain curve for a typical hot rolled bar is shown in figure 1.12. In design, (EN 1992-1-1, 2004)allows the idealised bilinear relationship (figure 1.13) to be used with a recommended strain limit of $\varepsilon_{ud} = 0.9\varepsilon_{uk}$ and a maximum stress of kf_{yk}/γ_s. Alternatively, an elastic–plastic relationship with a horizontal top branch at $f_{yd}=f_{yk}/\gamma_s$ may be used without the need to check the strain limit.

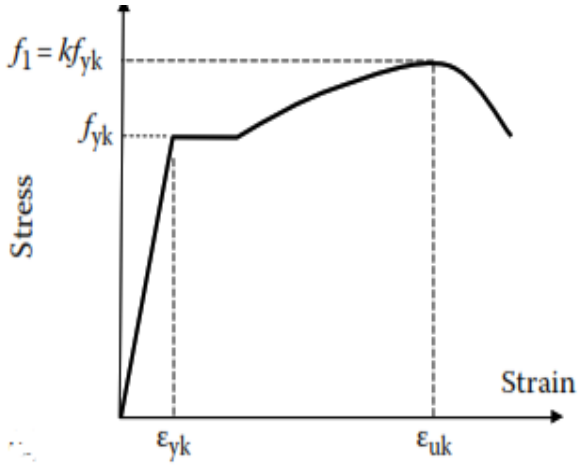

Figure 1.12. Actual stress–strain curve of a hot-rolled bar
(EN 1992-1-1, 2004)

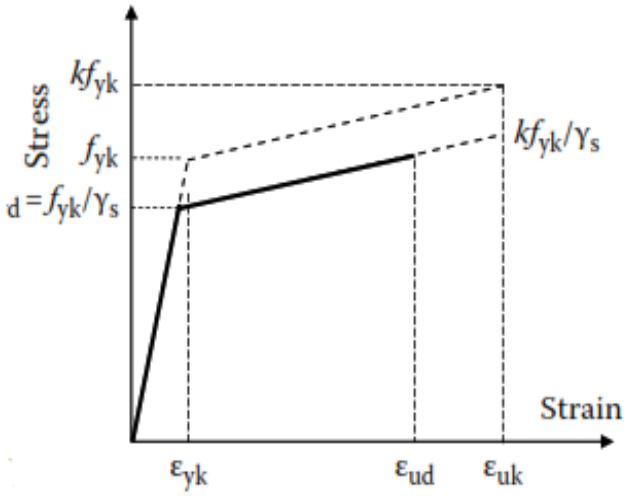

Figure 1.13. Idealised stress–strain curve of a hot-rolled bar
(EN 1992-1-1, 2004)

1.3.3.3. Prestressing steel

The steel used in prestressing should be able to carry a very high initial stress such that the losses due to creep and shrinkage represent a small percentage of the initial prestressing force. Moreover, low relaxation steel should be use to mitigate the losses of prestress due to relaxation. The terms used to define strength and ductility of prestressing steel are illustrated on the stress strain curve of prestressing steel (figure 1.14) In design calculations, the characteristic breaking strength f_{pk} is taken as the strength of the tendon. The strain corresponding to f_{pk} is the uniform elongation ε_{uk}. The yield stress$f_{p0.1k}$ is taken as the 0.1% proof stress and may be determined and may be determined by testing. The design values of the steel strength f_{pd} are taken as $f_{p0.1k}$ /γ_s.

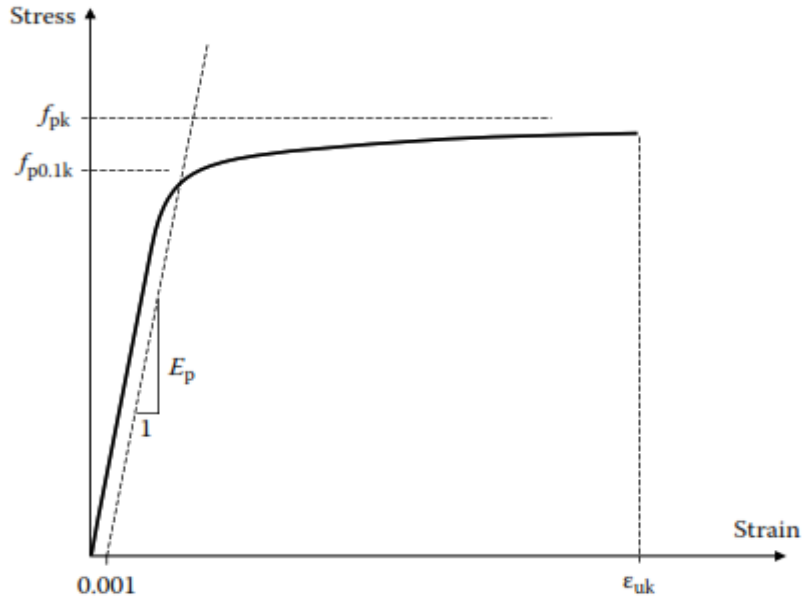

Figure 1.14. Stress-strain curve for prestressing steel.
(EN 1992-1-1, 2004)

For cross-sectional design, (EN 1992-1-1, 2004) allows the stress–strain curve for prestressing steel to be approximated by either of the two bilinear curves (figure 1.15)

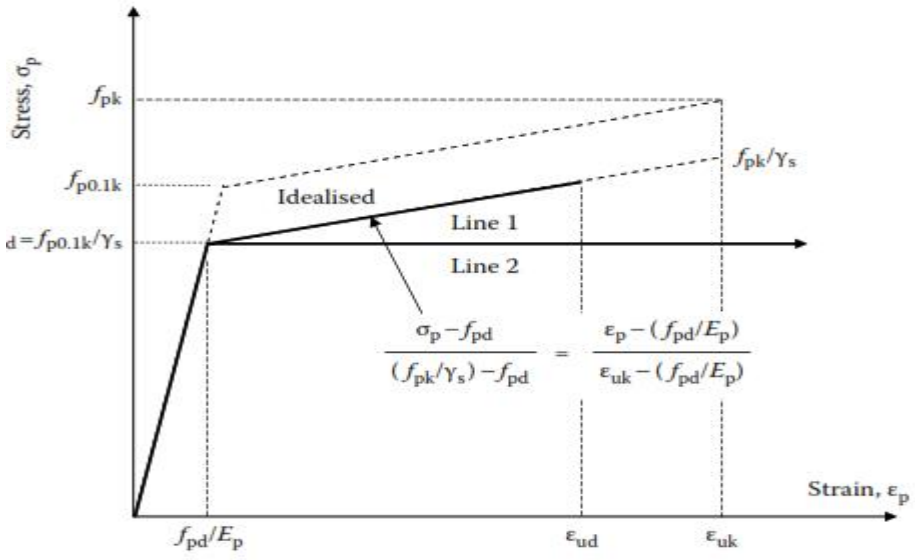

Figure 1.15. Idealised and design stress-strain diagrams for prestressing steel.
(EN 1992-1-1, 2004)

1.3.4. Analysis of a prestressed concrete section

A beam subjected to an eccentric prestress force is subjected to a direct compressive force due to the prestress, a moment due to eccentricity of the prestress and a moment from the

external load and the beam's self-weight (figure 1.16). The resulting stress at any point in the beam caused by these three factors can be written as defined by equation

$$f = \frac{P}{A} \pm \frac{Pec}{I} \pm \frac{Mc}{I} \quad (1.8)$$

Where:

P is the prestressing force;

e is the eccentricity of the prestressing force with respect to the centroidal axis to the extreme fiber.

c is the distance from the centroidal axis to the extreme fiber.

M is the applied moment from unfactored loads at the stage at which the stress is applied.

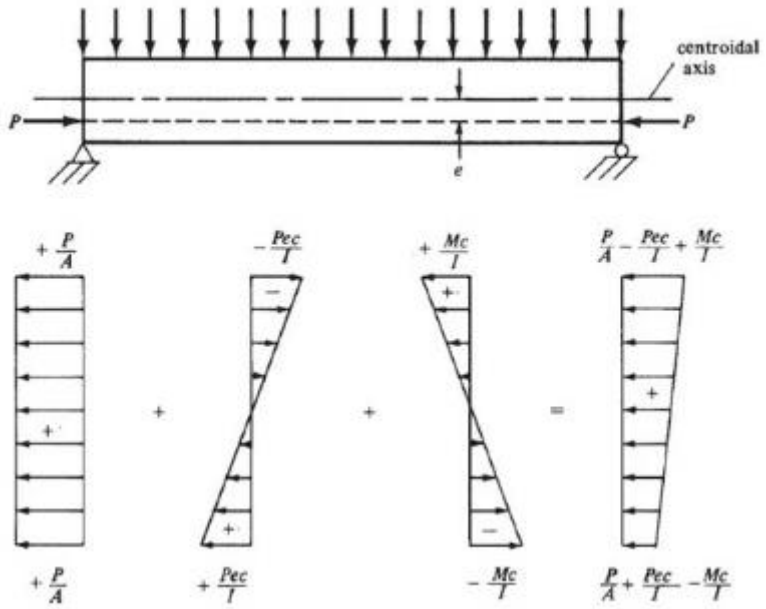

Figure 1.16. Concrete stress distribution from eccentric prestress force and superimposed load (Izzet & Abdulhameed, 2017)

1.4. Deformation

In the following section deformation in concrete will be discussed, instantaneous strain, creep strain and shrinkage.

1.4.1. Deformation of concrete

The Deformation of a loaded concrete specimen is both instantaneous and time dependent. The gradual increase in deformation with time is due to creep and shrinkage. Creep and shrinkage cause an increase in axial deflection, excessive deformation camber, and excessive

shortening of concrete members. Although not strictly correct, the strain in a concrete member at a time t may be expressed as the sum of its different components as defined by equation 1.9.

$$\varepsilon_c(t) = \varepsilon_{ce}(t) + \varepsilon_{cc}(t) + \varepsilon_{cs}(t) \quad (1.9)$$

Where:

ε_{ce} is the instantaneous strain;

ε_{cs} is the shrinkage strain;

ε_{cc} is the creep strain.

1.4.2. Instantaneous strain

Service loads rarely exceed the compressive strength of concrete it is therefore reasonable to assume that the behavior of concrete is linear elastic. The instantaneous strain is given by equation 1.10.

$$\varepsilon_{ce}(t) = \frac{б_c(t)}{E_{cm}} \quad (1.10)$$

1.4.3. Creep strain

Creep is the deformation of concrete under sustained stress. Creep increases at a decreasing rate from the moment of application of the force.

The capacity of concrete to creep is measured in terms of creep coefficient. For a concrete specimen subjected to a constant compressive stress $б_{c0}$,applied at an age t_0,the creep coefficient at a time t is the ratio of the creep strain to instantaneous strain as defined by equation 1.11.

$$\varphi(t, t_0) = \frac{\varepsilon_{cc}(t,t_0)}{\varepsilon_{ce}(t)} \quad (1.11)$$

The creep strain caused by a constant sustained stress $б_{c0}$ first applied at an age t_0, is defined by equation 1.12.

$$\varepsilon_{cc}(t, t_0) = \varphi(t, t_0)\varepsilon_{ce}(t) \quad (1.12)$$

An approach to estimate the creep coefficient is stated in EN 1992-1-1, 2004.

1.4.4. Shrinkage

Shrinkage of concrete is the time dependent strain in an unloaded and unrestrained specimen at constant temperature. Shrinkage is often divided into several components including plastic shrinkage, drying shrinkage, chemical shrinkage. Drying shrinkage is the reduction in

volume caused by the loss of water in the drying process. Drying shrinkage is a function of all the factors affecting drying.

Chemical shrinkage or autogenous shrinkage result from various chemical reactions in the cement paste and include hydration shrinkage which is related to the degree of hydration of the binder in a sealed specimen with no moisture exchange.

Thermal shrinkage is the shrinkage that occurs in the first few hours or days after the heat of hydration starts to dissipate.

The endogenous shrinkage is the sum of the autogenous shrinkage and the thermal shrinkage.

A model for estimating the magnitude of shrinkage strain is defined in EN 1992-1-1, 2004. The total shrinkage can be divided into autogenous shrinkage ε_{ca} and drying shrinkage ε_{cd} as defined by equation 1.13.

$$\varepsilon_{cs} = \varepsilon_{ca} + \varepsilon_{cd} \tag{1.13}$$

The autogenous shrinkage, ε_{ca} at any time t (in days) after casting is defined by equation 1.14.

$$\varepsilon_{ca}(t) = \varepsilon_{ca}(\infty)(1 - e^{0.2t^{0.5}}) \tag{1.14}$$

Where:

$$\varepsilon_{ca}(\infty) = 2.5(f_{ck} - 10) * 10^{-6} \tag{1.15}$$

The drying shrinkage at any time t is defined by equation 1.17.

$$\varepsilon_{cd}(t) = \beta_{ds}(t, t_s) k_h \varepsilon_{cd,0} \tag{1.16}$$

Where:

$$\beta_{ds}(t, t_s) = \frac{t - t_s}{(t - t_s) + 0.04(\sqrt{h_0}^3)} \tag{1.17}$$

k_h is a coefficient that depends on the notional size.

1.5. Methods for the analysis of prestressed concrete bridges

Traffic loads on girder bridges are distributed according to the stiffness, the geometry and boundary conditions of the deck. Different methods for the analysis of girder bridges have been developed over the years. The different methods are briefly reviewed below with particular emphasis on the methods relevant to our study.

1.5.1. Finite Element method

The finite element method seeks to replace a continuous type of structural problem, which is alternatively represented by a set of partial differential equations, by a set of discrete,

simultaneous linear equations which may be readily solved by computer (Johnson, 2000). The discretization is achieved by sub-dividing the surface to be considered into a number of regions and so creating a set of elements and nodes (meshes). The accuracy of the results of a finite element model increases as the element size decreases (Shreedhar & Mamadapur, 2012). The required size of elements is smaller at areas where high loads exist such as location of applied concentrated loads and reactions

1.5.2. Grillage Analogy

Basically, grillage analogy method uses stiffness approach for analyzing the bridge decks (Jaggerwal & Bajpai, 2014). The whole bridge deck is divided into a number of longitudinal and transverse beams (planar grids). In the analysis, the elements of a grid are assumed to be rigidly connected, so that the original angles between elements connected together at a node remain unchanged. Both torsional and bending moment continuity then exist at the node point of a grid (Qaqish et al., 2008). The method has proved to be reliable and versatile for a wide variety of bridge decks.

1.5.3. Orthotropic plate theory Method

Guyon and Massonet respectively made the first attempt to simplify the method of analyzing bridge decks using orthotropic plate theory. They introduced the concept of distribution coefficients which involved the distribution of live loads to a particular beam as a fraction of the total imposed load. Their work led rise to the Guyon Massonet bares method for load distribution reviewed below. This method is suitable in the analysis of short and wide decks with significant rotational stiffness. It transforms the grillage representing the deck into a Kirchhoff Orthotropic plate. The hypotheses of the Massonet method are:

- The actual grillage representing the bridge is replaced with an infinitesimal mesh having the same average bending and torsional stiffnesses.
- The close analytical solution is given only for harmonic analysis in longitudinal direction.

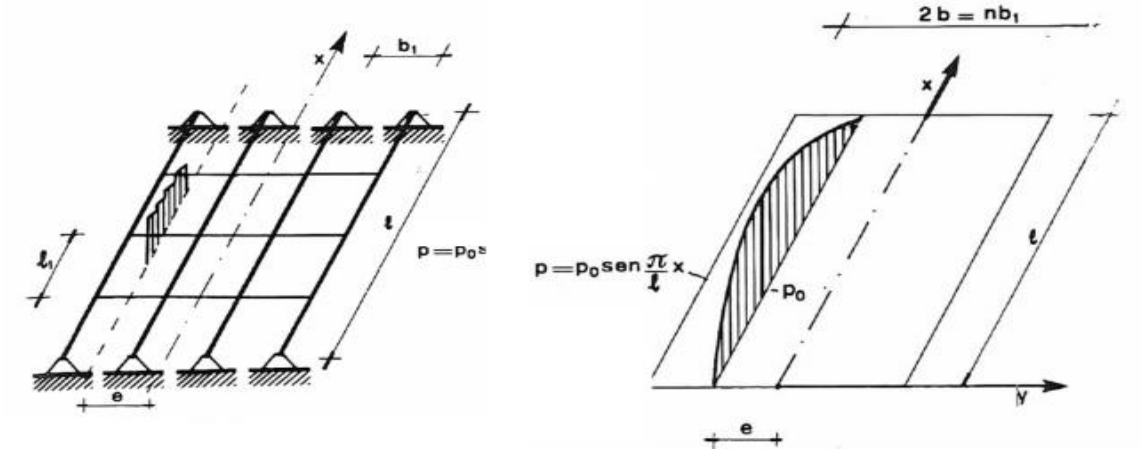

Figure 1.17. Simplification of grillage model to orthotropic plate

1.6. Norms of structural design

The Norms of structural design discussed in the following section are Eurocodes and BAEL.

1.6.1. Eurocodes

The Eurocodes are the ten European standards (EN; harmonized technical rules) specifying how structural design should be conducted within the European Union. These were developed by the European committee for standardization upon the request of the European commission (EN 1990, 2002). The purpose of the Eurocodes is to provide:

- Means to prove compliance with the requirements for mechanical strength and stability in the case of fire established by the European union law.
- Basis for construction and engineering contract specifications
- Framework for creating harmonized technical specifications for building products (CE mark).

By March 2010, the Eurocodes are mandatory for the specification of European public works and are to become the de facto standard for the private sector. The Eurocodes therefore replaced the existing national standard bodies although many countries had a period of co-existence. Additionally, each country is supposed to issue a national annex to the Eurocodes which will need referencing for a particular country. By 2010, ten sections have been developed and published:

- Eurocode 0: Basis of structural design (EN 1990)
- Eurocode 1 : Action on structures (EN 1991)
- Eurocode 2 : Design of concrete structures (EN 1992)
- Eurocode 3: Design of steel structures (EN 1993)

- Eurocode 4: Design of Composite and concrete structures (EN 1994)
- Eurocode 5 : Design of timber structures (EN 1995)
- Eurocode 6: Design of masonry structures (EN 1995)
- Eurocode 7: Geotechnical design (EN 1997)
- Eurocode 8: Design of structures for earthquake resistance (EN 1998)
- Eurocode 9: Design of Aluminium structures.

All the Eurocodes are divided into parts specific aspects of the parts in total there are 58 EN Eurocode parts distributed in the ten Eurocodes.

1.6.2. BAEL

BAEL is an acronym for "Béton Armé aux Etats Limits. "It is a French national standard which defines a set of technical rules for the design of reinforced concrete structures according to the limit states method. The rules of BAEL were adapted as from 1980 and were named BAEL 80. With the advancement in technology and research the rules were revised to BAEL 83 and the final version BAEL 91. The code is divided into two parts: the first part deals with the rules of design, actions, characteristic of materials and verification of materials. The second part deals with the rules pertaining to the reinforcement. The code was then revised for a last time in 1999 leading to it being referred as BAEL 91 modified 99.

Conclusion

The objective of this chapter was to give an overview of prestress bridge design and the state of the art in research work regarding the comparative design of prestressed concrete bridges. This was done by starting with a brief presentation of the historical overview of prestressed concrete bridges. This was followed by an overview of prestress bridge typoogies. The different methods for the analysis of highway superstructures were then outlined. After this, the general aspects regarding Eurocode and BAEL were reviewed. In the following chapter, the methodology used to approach the comparative study will be given.

CHAPTER 2: METHODOLOGY

Introduction

This chapter presents the methodology used to carry out the comparative design of the prestressed bridge. To attain the objective above mentioned, this chapter was divided into six parts. To begin with, a recognition of the site will be carried out to obtain the necessary data relevant to the study, in the second part the conceptual design of the bridge shall be discussed. This was followed by the load analysis according to Eurocode and BAEL. In the fourth part, the analytical and numerical methods of load distribution were discussed. Thereafter, the procedure of the prestressed bars prescribed in Eurocode 2 and BAEL 99 will be outlined. Finally, the criteria used for the comparative study will be stated.

2.1. Site recognition

The site recognition shall be carried out by documentation with the objectif of gathering information on the geographical location of the bridge, data related to the climate, hydrology,topography and also the socio-economic parameters and demography of the region.

2.2. Site visit

The site visit consists of an observation phase carried out on the site and an interview phase where all the information necessary for the project is collected.

2.2.1. Observation

This activity amounts to making careful observations of the activities surrounding the project in order to describe the condition of the old bridge and the changes that the environment will undergo during the construction of the new bridge.

2.2.2. Interview

This phase consists of establishing a questionnaire and submitting them to the project stakeholders (construction company), to local residents, in order to gather more information concerning the bridge and its impact in the region.

2.3. Data Collection

The data relevant to the design will be collected and it consists principally of geometric data of the interchange and the design data defined by the material characteristics.

2.3.1. Geometric characteristics

The geometric characteristics consist essentially of the span of the interchange, the transversal section, the longitudinal section of the bridge, the number of spans of the bridge, the height of superstructure, the loadable width and the traffic width

2.3.2. Design data

Several data were collected for the design among which, the properties of the material (concrete, reinforcing steel, prestressing steel) used, the static scheme adopted and the hypothesis made on traffic

2.4. Predesigning of the bridge

The interchange subject to our study spans an obstacle of about 40m. A proper design of our bridge will imply selecting the appropriate deck geometry, articulation, material characteristics and deck sections properties. The choice of these elements will be based on documentation from previous designs and the constraints imposed by the site.

2.4.1. Deck arrangement

For a deck and slab bridge in prestressed concrete, the economic height of a beam h is given by equation 2.1.

$$\frac{L}{17} \leq h \leq \frac{L}{16} \qquad (0.1)$$

Where:

L is length of the span.

The minimal width of the flange is equal to 0,6h

The following disposition is recommended in Calgaro & Bernard-Gély(1994) and illustrated by figure 2.1.

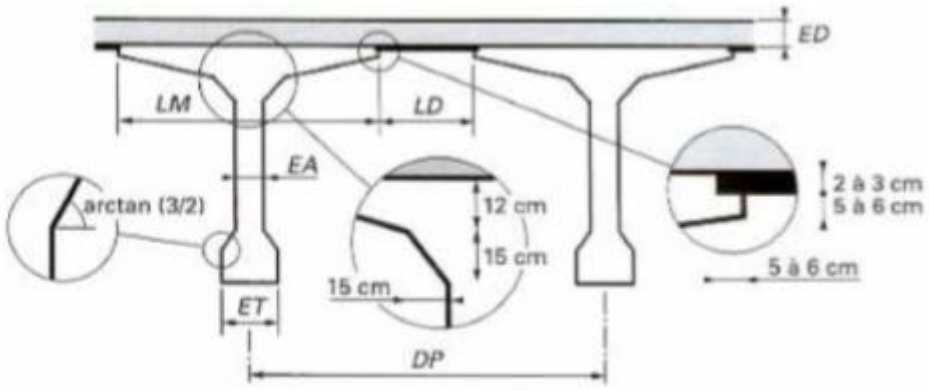

Figure 2.1. Design considerations for the deck

2.4.2. Bridge articulation

The bearings are used to transfer forces from the superstructure to the substructure whilst either tolerating or constraining relative movement. The appropriate type of bearing must be selected for proper functioning of the structure.

2.5. Actions on the bridge

The effects on the bridge can be divided into permanent actions and variable actions. The variable actions differ between both norms but the permanent actions will be considered equal

2.5.1. Permanent actions

These are actions acting during the whole nominal life of the structure with negligible time variation of their intensity (that can be considered as constant in time). The permanent actions will be calculated based on the geometrical characteristics for the structural elements and according guidelines set forth in EN 1991 Action on structure. part 1-1 for the nonstructural elements. The permanent actions applied on the bridge will be identical in both design procedures.

2.5.2. Variable actions on the bridge according to Eurocode

According to UNI EN 1991, the following actions should be considered on bridges: self-weight, thermal actions, traffic loads, Accidental actions, actions during execution. Other actions are foreseen in other Eurocodes but are less relevant compared to the aforementioned. In this section, the traffic loads, thermal actions, shrinkage and wind actions will identified.

2.5.2.1. Traffic loads

According to EN 1991-2 “Actions on structures. Part 2: general actions-Traffic loads on bridges», the first operation consists in determining the width w of the roadway and the number of notional lanes. The number of notional lanes and their size depends on the bridge width as shown by table 2.1.

Table 2.1. Division of cross section into notional lanes

Carriageway width (m)	Number of conventional notional lanes	Width of notional lane(m)	Width of remaining area
w<5.4	$n_1 = 1$	3.00	w-3.00
5.4≤w×< 6	$n_1 = 2$	w/2	0
w≥ 6	$n_1 = Int\left[\frac{w}{3}\right]$	3.00	w-(3.00× n_1)

Eurocode 1, part 2 calls for four separate calculation models, herein only Load Models, LM1 is relevant as LM2 concerns local verifications and Model 3, the transition of special vehicles which is considered only when expressly required. The LOAD MODEL 1 consists of two partial systems: A double -axle concentrated load (Tandem system), each axle having the weight $\alpha_Q Q_K$ where α_Q are adjustment factors; a uniformly distributed loads (UDL system), having the following weight per square meter of notional lane: $\alpha_q q_K$ where $\alpha_q$are adjustment factors (figure 2.2). Regarding Q_K and q_K their values, were calculated as prescribed in including the dynamic amplification coefficients (table 2.2). Transversally, load model 1 can be applied according to different traffic schemes to produce the most unfavourable effect in the element considered.

Table 2.2. Characteristic values of Load model 1

Conventional lane	$Q_K[KN]$	$q_K[KN/m^2]$
Lane 1	300	9.0
Lane 2	200	2.5
Residual area	0	2.5

$\alpha_q and\ \alpha_Q$ are assumed to be equal to unity.

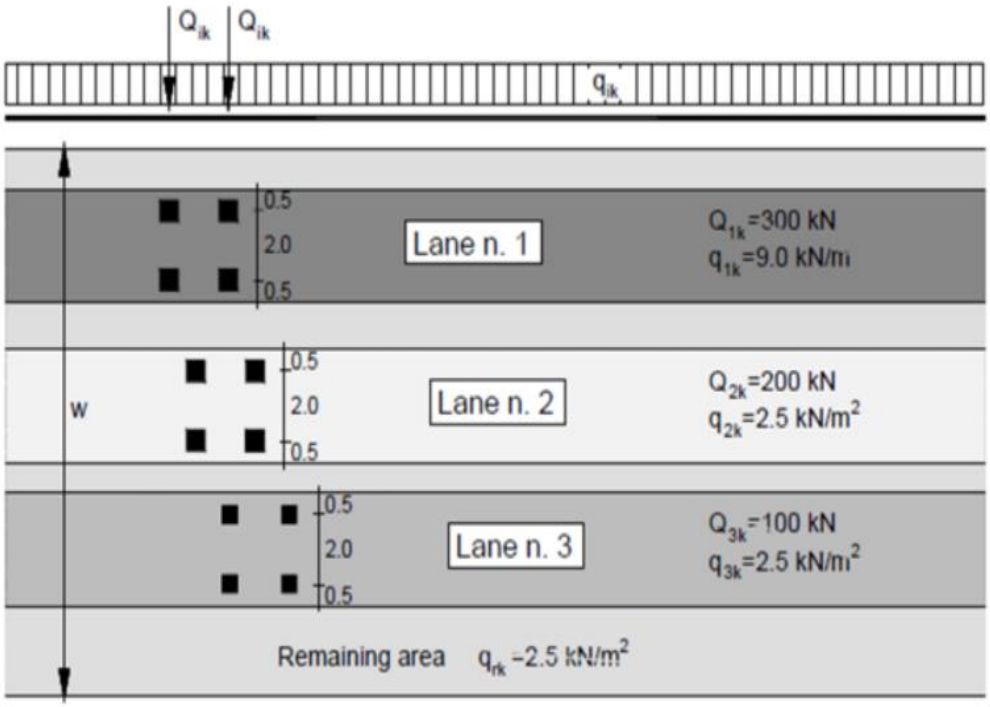

Figure 2.2. Application of Load Model 1

2.5.2.2. Wind action

The action of the wind, was considered as a uniformly distributed horizontal static force. The surface of transiting loads is assimilated as a continuous wall with a height of 3m starting from the road surface. The wind action must be evaluated in the following cases:

- Loading of the bridge. The height on which the wind act is given by H1;
- Unloading of the bridge, the stresses related to the wind action with the bridge unloaded is considered only in combinations for which the concomitant presence of mobile loads is excluded. In this case wind acts on the height of the deck, H2 as illustrated by figure 2.3.

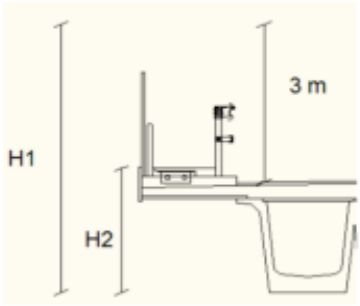

Figure 2.3. Height in loaded and unloaded conditions

According to Eurocode 1, part 1-4 the force acting on the bridge is given by equation 2.2.

$$\boldsymbol{F_{w,x} = C_s C_d q_p(z).C_{f,x}.A_{ref}} \quad (2.2)$$

Where:

$C_s C_d$ is the structural factor;

$C_{f,x}$ is the force coefficient in the x direction;

$q_p(z)$ is the peak velocity pressure at a reference height, z_e;

A_{ref} is the reference area.

To determine the wind actions on the bridge deck, the following steps were followed:

- Determine the basic wind velocity v_b;
- Determine the mean wind velocity $v_m(z)$;
- Determine the Peak velocity pressure $q_p(z)$;
- Determine F_W after evaluating A_{ref} and by choosing $C_{f,x}$ and $C_s C_d$.

2.5.2.3. Thermal action

The stresses induced due to thermal gradients in the cross section resulting from differential heating and cooling of the different parts of the cross section have to be analyzed.

The variation of temperature differences across the cross section due to heating and cooling (figure 2.4) were calculated as prescribed by EN 1991-1-5. Depending on the type of construction, the temperature differentials to be taken into account when determining the stresses caused by these differentials.

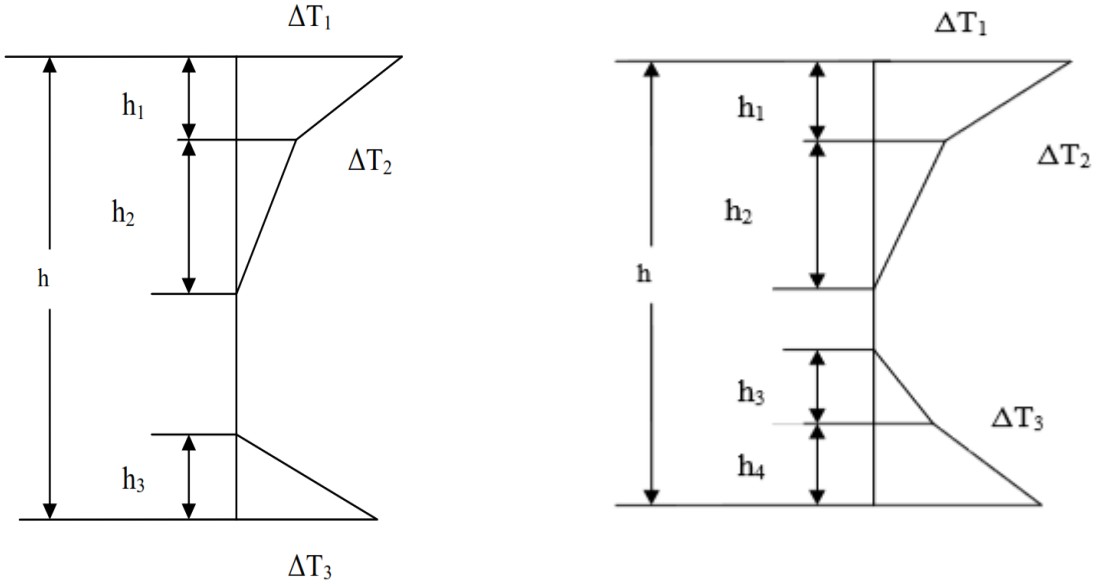

a) Heating b) Cooling

Figure 2.4. Variation of temperature difference due to heating and cooling

The heating parameters are defined following total height of superstructure.

Following figure 2.4(a)

Here:

h_1=0.3h≤150mm

h_2=0,3h≥100mm and ≤250mm

h_3=0,3h but ≤100mm+surfacing depth

The cooling parameters are defined following total height of superstructure.

Following figure 2.4(b).

Here:

$h_1 = h_4 = 0.22h \leq 250mm$

$h_2 = h_3 = 0.25h$ but≥ 200mm

The temperature differentials due to heating are shown on table 2.3 and cooling are shown on table 2.4 assuming there is a 100mm surfacing depth are elaborated in Eurocode 1.

Table 2.3. Temperature differentials due to heating

h, mm	ΔT_1	ΔT_2	ΔT_3
≤ 200	8.5	3.5	0.5
400	12.0	3.0	1.5
600	13.0	3.0	2.0
≥ 800	13.0	3.0	2.5

Table 2.4. Temperature differentials due to cooling

h, mm	ΔT_1	ΔT_2	ΔT_3	ΔT_4
≤ 200	−2.0	−0.5	−0.5	−1.5
400	−4.5	−1.4	−1.0	−3.5
600	−6.5	−1.8	−1.5	−5.0
800	−7.6	−1.7	−1.5	−6.0
1000	−8.0	−1.5	−1.5	−6.3
≥ 1500	−8.4	−0.5	−1.0	−6.5

2.5.2.4. Breaking loads

A breaking force of Q_{lk} is calculated as a fraction of the maximum vertical loads to be applied to lane number 1.It is limited to a maximum value of 900KN for the entire bridge width. The formula 2.3 permits the evaluation of the breaking loads.

$$180\alpha \boldsymbol{Q_1} \leq \{\boldsymbol{Q_{lk} = 1.2 \times [\alpha_{Q_1} \times Q_{1K}] + 0.1 \times [\alpha_{Q_1} \times q_{1K}] \times (W_1 \times L)}\} \leq \boldsymbol{900KN} \quad (2.3)$$

Where:

L is the length of the deck part under consideration

2.5.3. Variable actions on the bridge according to BAEL

The variable actions, as the name goes, vary with respect to time. They consist of actions on the structure (or on the structural element) with instantaneous values which can be significantly different in time: That is, their magnitude is time dependent. The variable actions include traffic loads, wind loads, thermal actions, breaking loads and shrinkage. The variable actions differ with the norms and will therefore be evaluated according to Eurocode and BAEL successively.

2.5.3.1. Traffic loads according to BAEL

Two systems of loads to be taken into account successively for the global verifications of the structural members: System A and system B

Also all classified bridges should permit the circulation of military convoys (article 9)

a. Load System A

It consists of a uniformly distributed load A_l applied on all the surface of the pavement.

$$\boldsymbol{A_l} = 2{,}3 + \left(\frac{\boldsymbol{360}}{\boldsymbol{L+12}}\right) \qquad (2.4)$$

Where:

L is the loaded length in m.

The value of A_l is to be multiplied by the coefficients a_1 and a_2 function of the number of lanes and the class of the bridge. (table 2.5).

Table 2.5. Coefficients $a_1$as a function of bridge class

Number of loaded lanes		Coefficient a_1					Conventional Width V_0
		1	2	3	4	5	
Bridge class	1	1.0	1.0	0.9	0.75	0.70	3.5
	2	1.0	0.9	-	-	-	3.0

Transversally, A_l can be applied on one or two lanes to have the most unfavourable effect for the element considered. The table below summarises the results for A_l.Longitudinally, $A_l$is applied to have the most unfavourable effect in the section under investigation for the effect considered.

The loads in this system are subject to dynamic amplification. This system comprises 3 subsystems

b. Load System B

The loads in this system are divided into three subsystems: system Bc, Br, and Bt. They consist essentially of axle loads and are subject to dynamic application.

i. Load system Bc

The load system Bc is made up of typical 30t trucks. The number of trucks is limited to two per row (2), oriented in the same direction. The distance separating the trucks is determined to produce the most unfavorable effect. The longitudinal loading of the truck is illustrated by

figure 2.5. Transversally, we can have as many trucks as we have traffic lanes. The transversal loading for the truck is illustrated by figure 2.6.The trucks are placed transversally so as to have the maximum effect for the element considered.

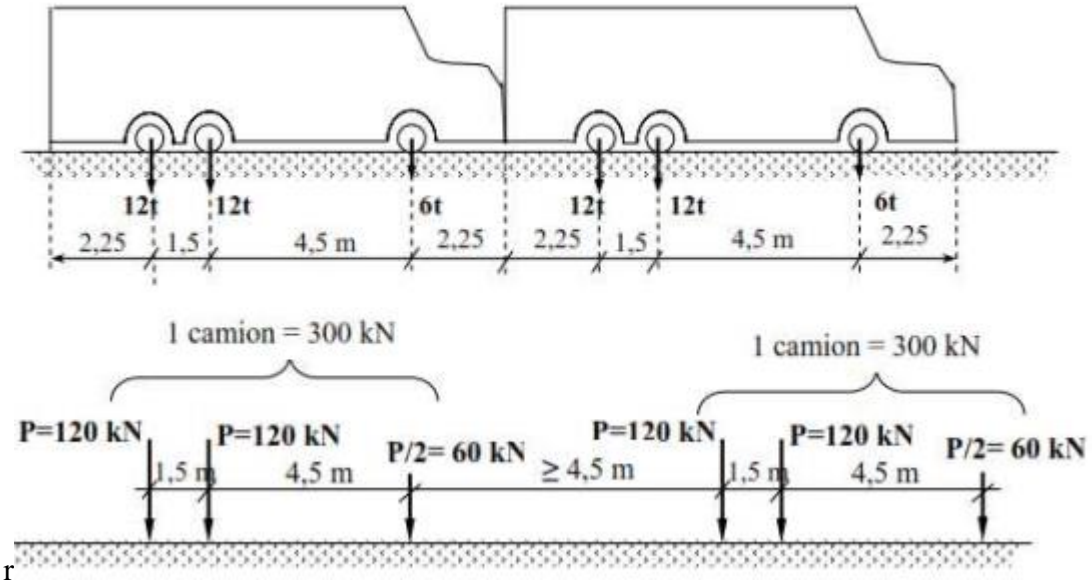

Figure 2.5. Longitudinal disposition of load system Bc. (Bourrel & Gourdou,(2016))

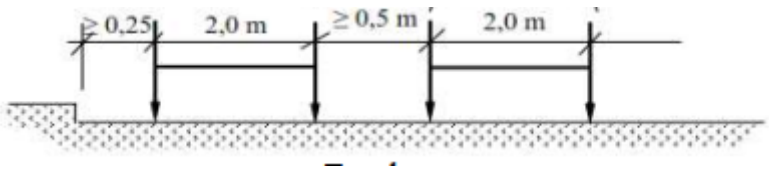

Figure 2.6. Transversal disposition of load system Bc. (Bourrel & Gourdou, 2016)

The load Bc is multiplied by a coefficient bc function of the bridge class and the number of rows of trucks. (table 2.6)

Table 2.6. Recommended values of coefficient Bc

Number of loaded traffic lanes		1	2	3	4	5
Bridge Class	1	1, 2	1,1	0,95	0,8	0,7
	2	1	1			

ii. Subsystem Bt

This subsystem is composed of 2 tandem axles each comprising four (4) isolated wheels. Longitudinally only one tandem is arranged per lane as shown in figure 2.7. Transversally, two tandem axles are disposed on 2 lanes of traffic according to the configuration in figure 2.8. The load Bt is to be multiplied by a coefficient bt function of the class of the bridge defined in table 2.7.

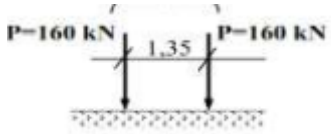

Figure 2.7. Longitudinal disposition of Load system Bt.(Bourrel & Gourdou, 2016)

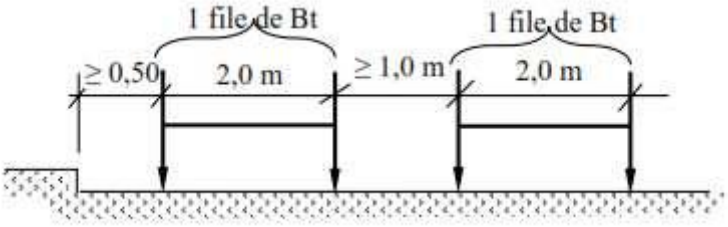

Figure 2.8. Transversal disposition of load system Bt. (Bourrel & Gourdou, 2016)

Table 2.7. Recommended values of coefficient Bt

Bridge class	1	2	3
Coefficient bt	1,0	0,9	

iii. Subsystem Br

This system is composed of a single isolated wheel carrying a load of 100KN placed on the longitudinal axis of the road.

Breaking loads

2.5.3.2. Breaking loads

The loads of system A and Bc can generate breaking loads which can be supposed to be centred on the longitudinal axis of the road pavement.

The Breaking load due to A is defined by equation 2.5.

$$B\ (A) = \frac{A(L)}{20+0{,}0035S} \tag{2.5}$$

The breaking load due to Bc is the weight of a truck breaking.

2.5.3.3. Wind action

According to "fascicule 61 titre 2 article 14: charges du vent" the following simplifying hypotheses are stated to evaluate the action of the wind:

- The action of the wind on a bridge under service is equal to a uniform pressure of 2000 N acting orthogonally on all surfaces;
- For a bridge under execution, this pressure is equal to 1000 for a duration of construction less than one month and 1250 for a greater duration;
- The wind is considered to act in isolation without any traffic load acting simultaneously such that their effect cannot be cumulated.

2.6. Calculation parameters

The method used for the verification of structural elements is the semi probabilistic limit state method. It states that the safety of a structure or part of it must be evaluated in relation to the limit states that can occur during the nominal life. The limit state is the condition beyond which the construction does not satisfy the requisites for which it was designed. Limit state checks must be carried out for all the heaviest load conditions that can act on a structure. The actions acting on the structure must be distributed and combined in the most unfavorable way.

2.6.1. Combination of actions.

The actions on the bridge will occur in different combinations all of which must be considered to determine the most critical condition for the structure. The duration of the actions and their frequencies will also vary therefore; the characteristic actions will not be multiplied by the safety factors but also by a Ψ factor. Different combinations will be used depending on the situation:

The combination of actions for Ultimate Limit State is defined by equation 0.2.

$$F_d = \gamma_g G_k + \gamma_p P_k + \gamma_{Q,1} Q_{k,1} + \sum_{i>1}^{i=n} \gamma_{Q,1} \Psi_{0i} Q_{ki} \tag{2.6}$$

The characteristic load combination of actions for Serviceability limit state is given by equation 0.3.

$$F_d = G_k + P_k + Q_{k,1} + \sum_{i>1}^{i=n} \Psi_{0,i} Q_{k,i} \tag{2.7}$$

The frequent load combination of actions for Serviceability limit state is given by equation 0.8.

$$F_d = G_k + P_k + \Psi_{1,1}Q_{k,1} + \sum_{i>1}^{i=n} \Psi_{2,i}Q_{k,i} \quad (2.8)$$

The Quasi-permanent combination of actions for Serviceability limit state is given by equation 2.9.

$$F_d = G_k + P_k + \sum_{i=2}^{i=n} \Psi_{2,i}Q_{k,i} \quad (2.9)$$

Putting aside the differences in Ψ factors the equations are identical in both Eurocode and BAEL.

The load combinations used for the design at ULS and SLS following Eurocode are defined by equation 2.1 for ULS and 2.11 for SLS

ULS for persistent and transient design situations is defined by equation 2.10.

$$1.35G_{max} + 1.35(\text{Ts} + \text{UDL} + q^*_{fk}) + 1.5 \times \begin{cases} \min(0.6F_{wk}, F^*_{wk} \\ 0.6T_k \end{cases} \quad (2.10)$$

SLS characteristic combination is defined by equation 2.11.

$$G_{max} + (\text{Ts} + \text{UDL} + q^*_{fk}) + \begin{cases} \min(0.6F_{wk}, F^*_{wk} \\ 0.6T_k \end{cases} \quad (2.11)$$

If the traffic load to be considered, Q_r is the maximum value of the Traffic system A and B.

The load combinations used from the design at ULS and SLS following BAEL are defined by equation 2.12 for ULS and equation 2.13 for SLS.

ULS for persistent and transient design situations as defined by equation 2.12.

$$1.35\,G + 1.5 \times (1.07 \times \max(A,B) + (1.5 \times 1.07 \times \text{Tr}) + 1.3 \times 0.6T \quad (2.12)$$

SLS Characteristic combination is defined by equation 2.13.

$$G + 1.2 \times \max(A,B) + \text{Tr} + 0.6\,T \quad (2.13)$$

2.6.2. Transversal load distribution

The transversal load distribution is a critical part of the design of bridges as it determines the solicitations in each beam. Several methods can be used and the choice of the method depends on the bridge type. The transversal load distribution will be carried out using the Massonet method and by using a finite element model.

This method allows us to determine a parameter called the load amplification coefficient. This coefficient makes it possible to proportionally distribute the loads placed on the slab to the beams according to their position in relation to the load. The Massonet method treats the beams, the slab and cross beams no longer as a grid work, but as an equivalent orthotropic plate that behaves differently in the two main directions of the deck. Bares & Massonnet.(1966). Two parameters that characterize the orthotropic bridge deck are determined.

The torsion parameter is evaluated using equation 2.14.

$$\theta = \frac{b}{l}\sqrt[4]{\frac{\rho_p}{\rho_E}} \quad (2.14)$$

The stiffening parameter is evaluated using equation 2.15.

$$\alpha = \frac{\gamma_P+\gamma_E}{2\sqrt{\rho_p*\rho_E}}\sqrt[4]{\frac{\rho_P}{\rho_E}} \quad (2.15)$$

The specific eccentricity of the load, e/b.

The specific ordinate of the point considered, y/b.

Where:

$\gamma_P, \gamma_E, \rho_p, \rho_E$ is the characteristics of the equivalent grid work;

$\gamma_P = \frac{GJ_{t,p}}{b_1}$;

$\gamma_E = \frac{GJ_{t,p}}{b_1}$;

$\rho_P = \frac{EJ_P}{b_1}$;

$\rho_E = \frac{EJ_E}{b_1}$.

The parameters mentioned above are then input into the Massonet table and through linear interpolation of the values, it is possible to obtain the load amplification coefficient of the loads K_α.In particular this coefficient is given by applying the interpolations of sattler which also depend on the value of θ.

Where:

$K_\alpha = K_0 + (K_1 - K_0)\alpha^B$

$\beta = 1\text{-}e^{(0.065-\theta)/0.663}$

If $\theta > 0.3$, we consider the actual stiffness of the cross beams and the most appropriate analytical method for load distribution is Guyon Massonet method.

If $\theta < 0.3$, we can consider the crossbeams as been infinitely rigid which corresponds to $\theta = 0$ and the most appropriate method is Courbon Eingeisser method. Due to the symmetry of the bridge it is sufficient to evaluate the influence line for one edge beam and one inner beam.

2.7. Numerical method

The numerical method adopted for this application is the Finite element method which is used to solve partial differential equations in two or three space variables by subdividing large system into simpler parts called finite elements. The bridge was simulated on a numerical model using CSI bridge on which was performed Numerical analysis.

2.7.1. Numerical modelling of bridge

The Mahe prestressed bridge was modelled using CSI bridge software. CSIBridge offers a single user interface to perform modeling and analysis of our bridge. The bridge models are defined parametrically, using common bridge engineering terms such as layout lines, spans, grid, deck sections, pretension cables, cables abutments, lanes, diaphragms, bearings, restrainers, pavement. The bridge object model is a finite element assemblage of components making up the entire analytical model that is the frame sections, area sections, links, tendons. After entering the bridge parameters into the software by the definition of materials to match with the physical model materials, the different components were modelled and finally the defined materials were assigned to each corresponding frame or shell element. A flexible structure was built by allowed motion at the abutment and pier defined and the global model for analysis was made.

2.7.2. Numerical analysis

The numerical analysis performed on the bridge according to Eurocodes are the dynamic analysis for the control of the structure vibration after modelling and static for the evaluation of solicitation, load distribution and prestress design.

2.7.3. Dynamic analysis

A dynamic modal analysis was first performed using CSI bridge to ensure that the numerical model of the bridge is well modelled. Modal analysis enables the control of vibration of the structure.

2.7.4. Static analysis

Static analysis were performed using CSI bridge and solicitation diagrams and influence lines obtained.

2.8. Prestressed bar design

The design procedures differ between Eurocode and BAEL. In this section the prestressed girders will be designed successively according to the prescriptions in Eurocode 2 and in BAEL 99. The solicitations for the design will be those obtained load repartition using Massonet method following analytical calculations of BAEL and FEM following Eurocode.

2.8.1. Prestressed bar design according to Eurocode

The prestressed bar design was done following 2 limit sates. The serviceability limit state used to verify stresses in the prestressed beam during transfer and service and the deformations. While, the ultimate limit state is used to design for flexure and shear.

2.8.1.1. Serviceability Limit State design

Prestressed structures are generally designed for serviceability first and then checked to verify ultimate limit state. This is because the design requirements are more severe in the former than the latter. The design will be carried out using a Magnel diagram. The Magnel diagram is a powerful design tool which enables to make a safe choice of prestress and eccentricity. Before drawing the Magnel diagram it will be necessary to calculate the permissible stresses in the concrete and come up with the Magnel equations. The concrete compressive stress is limited to the values($0.6f_{ck}$, $0.45f_{ck}$) to control the development of micro cracks, longitudinal cracks and high levels of creep.

Under characteristic loads, the compressive stress is limited to $0.6f_{ck}$.

Under quasi permanent loads, the stress is limited to $0.45f_{ck}$.

The Concrete tensile stress tensile stress is limited to characteristic tensile strength defined in equation 2.16.

$$f_{ctm} = 0.3{f_{ck}}^{2/3} \tag{2.16}$$

Where:

fck is the characteristic concrete compressive strength which varies at transfer and service.

The state of stress due to bending must satisfy the stress limitations described in equation 2.17.

$$\left(-\frac{P_s}{\eta A}+\frac{P_s e}{\eta Z_t}\right)\gamma_{sup}-\frac{M_{selfweight}}{Z_t}\leq f_{tt} \tag{2.17}$$

$$\left(-\frac{P_s}{\eta A}-\frac{P_s e}{\eta Z_b}\right)\gamma_{sup}+\frac{M_{selfweight}}{Z_b}\geq f_{tc}$$

At service, equation 2.18 and 2.19 should be satisfied.

$$\left(-\frac{P_s}{A}+\frac{P_s e}{Z_t}\right)\gamma_{inf}-\frac{M_{selfweight}+M_{slab+formwork}}{Z_t}-\frac{M_{live}}{Comp.Z_{topof\ precast}}\geq f_{sc} \tag{2.18}$$

$$\left(-\frac{P_s}{A}-\frac{P_s e}{Z_b}\right)\gamma_{inf}+\frac{M_{selfweight}+M_{slab+formwork}}{Z_t}+\frac{M_{live}}{Comp.Z_{topof\ precast}}\leq f_{st} \tag{2.19}$$

Where:

P_s is the prestressing force at service;

e is the Eccentricity;

f_{tt} is the permissible stress at transfer in tension;

f_{tc} is the permissible stress at transfer in compression;

f_{sc} is the permissible stress at service in compression.

The Magnel equations for the section are defined at transfer and service.

At transfer, the equations 2.20 and 2.21 should be verified.

$$\left(-\frac{1}{A}+\frac{e}{Z_t}\right) \leq \left(f_{tt}+\frac{M_{selfweight}}{Z_t}\right)\frac{\eta}{\gamma_{sup}P_s} \quad (2.20)$$

$$\left(-\frac{1}{A}+\frac{e}{Z_b}\right) \geq \left(f_{tc}-\frac{M_{selfweight}}{Z_b}\right)\frac{\eta}{\gamma_{sup}P_s} \quad (2.21)$$

At service, the equations 2.22 and 2.23 should be verified.

$$\left(-\frac{1}{A}+\frac{e}{Z_t}\right) \geq \left(f_{sc}+\frac{M_{selfweight}+M_{slab}}{Z_t}+\frac{M_{live}}{Comp.Z_{topof\ precast}}\right)\frac{1}{\gamma_{inf}P_s} \quad (2.22)$$

$$\left(-\frac{1}{A}-\frac{e}{Z_b}\right) \leq \left(f_{st}-\frac{M_{selfweight}+M_{slab}}{Z_b}-\frac{M_{live}}{Comp.Z_b}\right)\frac{1}{\gamma_{inf}P_s} \quad (2.23)$$

The Magnel equations are obtained by substituting the values in the equations above. Any choice of prestress and eccentricity in the feasible region delimited by the inequalities above is a safe choice regarding serviceability.

2.8.1.2. Ultimate Limit State Design

In order to determine the ultimate moment capacity of a section which has been designed to Serviceability Limit State of bending, it is necessary to determine the position of the neutral axis at the ultimate limit state.

a. Design of flexure

The position of the neutral axis will be obtained by trial and error. The ultimate moment is obtained by calculating the moment of all forces tensile and compressive about the soffit.

b. Design for shear

The following procedure will be used for the design of the shear reinforcements:

- The design shear force V_{ED} will be calculated. This is the stress at an effective depth d from the face of the support;
- The shear capacity of the concrete alone V_{RDC} is determined. If $V_{RDC} > V_{ED}$, no shear reinforcement is required but a minimum amount will be provided calculated using equation 2.24.

$$\frac{A_{SW}}{s \times b_w} \geq 0.08\frac{\sqrt{f_{ck}}}{f_{yk}} \quad (2.24)$$

- If $V_{RDC} < V_{ED}$, then all the shear stress is resisted by the shear links;
- Equate the value of V_{ED} to the maximum value of shear force $V_{RD,max}$ and calculate the value of cot θ where 1≤cot θ≤2,5;
- A value for the total area of a shear link is assumed and using the value cot θ we calculate the spacing of the links such that V< $V_{RD,s}$;

- Check that the spacing requirements meets maximum spacing requirements.

2.8.2. Prestressed bar design according to BAEL

The same method used to design the prestressed bars according to Eurocode was used to design the prestress girders according to BAEL, however the permissible stress at transfer and service conditions differs between both norms and have to be recalculated. The "fascicule 61 titre 2" does not make any provisions for the concomitant presence of wind actions and traffic loads and does not consider nonlinear thermal variations so the only variable action is that due to traffic. Also, the design of flexure and shear at ultimate limit state according to BAEL differ from the Eurocode ultimate limit state design.

2.9. Comparative study criteria

The criteria for comparison will permit us to differentiate between the two norms and obtain the norm more suited for our application. For this comparison, we based ourselves on three criteria: number of parameters, sollicitations and design

2.9.1. Number of parameters

The number of parameters taken into consideration to achieve results during the design following Eurocode and BAEL will be compared. This criterion is very important as it is an indication of the time spent on the design.

2.9.2. Sollicitations

The load models in the two norms are representations of the actual vehicular traffic. The load in the beams will be repartitioned analytically and numerically to see which load model produces the most unfavorable response in the structure.

2.9.3. The design

This last criterion will enable us to determine which norm requires a fewer number of strands. This last criterion is very important as it is an indication of the cost of the prestressed bridge

Conclusion

The objective of this chapter was to present the methodology used to carry out the comparative design of the prestressed bridge. To attain the objective above mentioned this chapter was divided into six parts. To begin with a recognition of the site was carried out to obtain the necessary data relevant to the study, in the second part the conceptual design of the bridge was discussed. This was followed by the load analysis according to Eurocode and BAEL. In the fourth part, the analytical and numerical methods of load distribution were discussed. Thereafter, the procedure of the prestressed bars prescribed in Eurocode 2 and BAEL 99 was outlined and finally, Finally, the criteria used for the comparative study was stated. In the next chapter we will be presenting the results obtained after application of the methodology above to our case study.

CHAPTER 3: PRESENTATION OF RESULTS AND INTERPRETATION

Introduction

The last chapter of this research work will be bringing forth detailed description of the results obtained by the application of the methodology to our case study. To begin with, a detailed description of the site and the properties of the bridge and its constituent materials will be given. A load analysis will follow with the resulting sollicitations obtained by load repartition by numerical and analytical methods. The detailing of the prestress girders after design according to Eurocodes and BAELwill be elaborated and the results of the comparative will be given to differentiate the approaches.

3.1. General presentation of site

After documentary research, the Mahe bridge project site characteristics were obtained such as the location, climate, hydrology, temperature.

3.1.1. location

The bridge is an integral part of the Yabassi-Kondjock road way at PK 17+200 and connects the road section interrupted by the MAHE River. A map inserting the bridge in its territorial context is given by figure 3.1

Figure 3.1. Location of the prestressed bridge over the Mahe
(source: http:cvuc-uccc.com)

3.1.2. Climate

The climate is characterized by high humidity. The temperature generally varies between 23 ° C and 29 ° C, the hottest month being February. Like Nkam county, Yabassi district is very rainy. The annual rainfall amounts are between 2900 and 3000 mm. The dry season is from mid-November to March.

3.1.3. Hydrology

The district of Yabassi is densely watered by numerous rivers, the main ones being; the Nkam, the Dibamba; the Mabombé, the Njanga and the Mahé. The Mahe river is quite wide, has a low flow velocity. This river is influenced by the tide. The depth of the river at the level of the bridge is 9m and with a water depth of about 15m.

3.1.4. Socio-economic activities

Officially estimated at around 13,000 inhabitants according to the reports of the 3rd general population census, Yabassi is now home to a population of approximately 14,685 inhabitants according to the estimate of the population of the Yabassi health district in 2011. This population which is unevenly distributed over the entire territory of the Municipality of Yabassi has a few areas of concentration such as Banya I, Sollè, Ndogbélé, Tondè village and to a lesser extent Bonépoupa II. Sociologically, the indigenous ethnic groups are Bassa, Bandem, Banen, Banya, Bonkeng, Mbang, Bodiman and Ewodi. In terms of traditional chiefdom, the Municipality of Yabassi has 08 cantons (2nd degree chiefdom) and 48 villages. The people of Yabassi are deeply rooted in religion. The religions encountered are Christianity (Protestant - UEBC, EE, CEBEC - and Catholic), Muslims and Pentecostal churches.

The principal economic activities are agriculture, (about 60 percent of the active population involved it.) small businesses and fishing. All these activities are mainly for subsistence but the Municipality of Yabassi as a space has a lot of potential and resources which if exploited correctly, can be unifying elements to improve the wellbeing of the populations.

3.2.Physical description of site

An internship was carried out to obtain more information on the project site. From the observations made, the Mahe is one of the main rivers of the Nkam department which waters the arrondissement of Yabassi. To go from Yabassi to Nkondjock, we cross this stream in the village Ndog-bikot. Currently, there is no crossing structure over this river. The villagers use canoes in deep areas of the river and some cross the river on foot in shallow areas. The figures 3.2,3.3, and 3.4 respectively present the condition of the bridge abutments, the debris of the collapsed bridge and the arduous crossing of a road user.

Figure 3.2. State of the two abutments of the old bridge

Figure 3.3. Debris of the previously collapsed bridge on the Mahe river

Figure 3.4. Crossing of the river by a motorcyclist

3.3. Presentation of Project

In the following section the Mahe prestressed bridge conception data, that is geometric data, bridge articulation, material characteristics and deck sections properties will be presented.

3.3.1. Geometric data

The Mahe bridge is made up of conventional reinforced concrete.Introducing prestressing enables us to eliminate the pier,have a larger span, reduce the number of beams and the quantity of concrete hence a more economic design .The total length of the prestressed bridge between abutments is 40m.The Bridge is made up of a single span. The bridge has a symmetrical four prestressed beams structure with a center distance between them of 2,75m and a collaborating reinforced concrete slab of 300mm cast in site. The road section is made of a roadway 7.5 m wide (figure 3.5). The properties of the cross section, as summarized in table 3.1were obtained after calculation on excel.

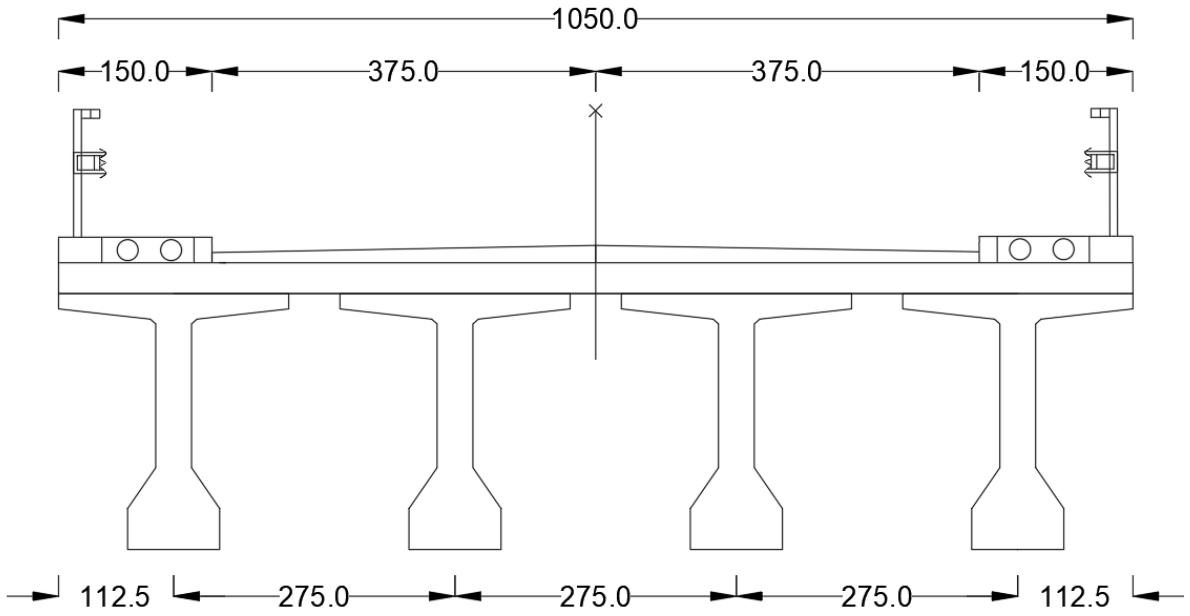

Figure 3.5. Transversal section of the bridge.

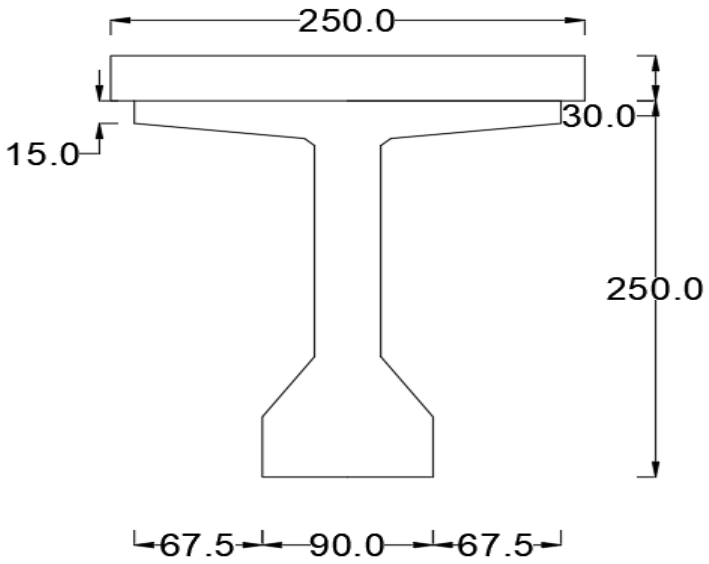

Figure 3.6. Geometrical properties of the bridge girder.

Table 3.1. Geometrical and inertial properties of the beam cross section.

Characteristics of the beam		
F_{ck}	45	MPa
h	2500	mm
A_c	1.54E+06	mm^2
$Y_{G,c}$	1303 ,12	mm
$J_{xx,c}$	1,16E+12	mm^4
$J_{yy,c}$	1,57E+11	mm^4
$i_{x,c}$	863,34	mm
$i_{y,c}$	319.67	mm
E_{cm}	36283,188	MPa

3.3.2. Bridge articulation

Most bridges will require some form of mechanical restraint to resist the horizontal forces and ensure that thermal expansion and contraction occurs in the right direction. This is most easily achieved using pot bearings. The bridge deck is fixed in one corner and horizontal movements are controlled by the use of guided (unidirectional) bearings. A free (multidirectional) bearing is provided for the diagonally opposite corner to the fixed bearing. Figure 3.7 shows the arrangement of the bearings of the bridge.

Figure 3.7. Articulation scheme of the bridge

3.3.3. Materials characteristics

The properties of the materials used in different structural elements are summarized in table 3.2, table 3.3, table 3.4 and table 3.5. The parts of the bridges are subjected to conditions in different exposure classes. The concrete cover was calculated for the different structural elements of the bridge and the results summarized in table 3.5. From the results obtained, a minimum cover of 40mm is assumed everywhere.

Table 3.2. Material properties of concrete for structures cast in situ (slab and cross beams)

Strength class	C35/45
Specific weight of the concrete	25 KN/m^3
Characteristic compressive cubic resistance	$f_{ck,cube} = 45$ MPa
Characteristic compressive cylinder resistance	$f_{ck,cylinder} = 35$ MPa
Cylindrical average resistance	$f_{cm} = f_{ck} + 8$ MPa=43 MPa
Traction average resistance	$f_{ctm} = 0.3 * {f_{ck}}^{2/3} =$ 3.2MPa
Elastic modulus	$E_{cm} = 22000(f_{cm}/10)^{0.3} = 34077$ MPa

Cylindrical design resistance	$f_{cd} = \alpha_{cc} * f_{ck}/\gamma_c = 19.8$ MPa
Traction design resistance	$f_{ctd} = f_{ctk,0.005}/$ γ_c =1.5MPa
Cement type	325
Environmental exposure class	3
Maximum water to cement ratio	0.50
Minimum cement content	320 kg/m^3
Consistency class (slump test)	35mm
Minimum Concrete cover	50mm

Table 3.3. Material properties of reinforcing steel bars

Steel grade	B450C
Characteristic yield strength of reinforcement	f_{tk} =450 MPa
Characteristic tensile strength of reinforcement	f_{yk} =450MPa
Design value of modulus of elasticity of reinforcing steel	E_s =200000MPa
Design value of yielding strain of reinforcement	$\varepsilon_{yd} = 1.96‰$
Design value of ultimate strain of reinforcement ($\varepsilon_{ud} = 0.90\varepsilon_{uk}$)	ε_{ud}=63‰
Partial factor for steel	γ_s =1.15
Design yield strength of reinforcement	f_{yd} =450/1.15=391.3MPa

Table 3.4. Material properties of prestressed bars

Wires (Nominal diameter 15mm)	
Rupture characteristic stress	$f_{ptk} = 1860$MPa
Characteristic stress at 0,1% of residual deformation	$f_{P(0,1)k} = 1670MPa$
Characteristic stress at 1% of total deformation	$f_{P(1)k} = 1670$MPa
Elongation under maximum load	$\varepsilon_{uk} = 0.035$
Elastic modulus	205000

Table 3.5. Concrete cover in different structural elements

Element	**Exposure class**	$C_{min,b}$	$C_{min,dur}$	ΔC_{dev}	**Cover/mm**
Top of slab	XC3	20	10	10	30
Bottom of slab	XC4	20	20	10	30
Elevated structures	XC4	20	25	10	35
Foundation	XC2	20	20	10	30

3.4.Section properties

This section presents the determination of collaborating slab width, slab properties, properties of ideal section and cross beam.

3.4.1. Determination of collaborating slab width

The precast beams and the slab cast in place are composed of concretes of different characteristics which must be homogenised for the calculation of the inertial properties of the ideal section. The homogenisation coefficient n is calculated following equation

$$n = \frac{E_{precast}}{E_{cast}} = \frac{36283}{34077} = 1.06$$

The distribution of the normal stresses in the composite elements must be determined using the effective slab width in the calculation.

Calculations were carried out and the collaborating slab and width of the edge beam and central beam obtained (table 3.6)

At midspan or at an internal support, the total effective width b_{eff},may be determined by equation 3.3.

$$b_{eff} = b_0 + b_{e1} + b_{e2} \tag{3.3}$$

Where:

b_0 is the distance between the connector axes;

$b_{ei} =$ min $(\frac{L_e}{8}, b_i)$ is the value of the collaborate ng width on each side of the section;

b_i is the distance midpoint between the outstand shear connector and adjacent webs.

L_e is the approximate distance between points of zero bending moment.

For the end supports, the formula is defined by equation 3.4.

$$b_{eff} = b_0 + \beta_1 b_{e1} + \beta_2 b_{e2} \quad (3.4)$$

Where:

$$\beta_i = (0.55 + 0.025 L_e / b_{ei}) \leq 1.0$$

Table 3.6. Collaborating slab width of the edge beam and central beam

	Edge beam		**Central beam**		**Unit**
beff	Support	Span	Support	Span	cm
L	4000	4000	4000	4000	cm
Le	4000	4000	4000	4000	cm
bo	0	0	0	0	cm
b1	137,5	137,5	137,5	137,5	cm
b2	112 ,5	112 ,5	137,5	137,5	cm
be1	137,5	137,5	137,5	137,5	cm
be2	112,5	112,5	137,5	137,5	cm
β1calc	1,27	1	1,27	1	
β2calc	1,43	1	1,27	1	
β1	1	1	1	1	cm
β2	1	1	1	1	
beff	250	250	275	275	cm

3.4.2. Slab properties

The properties of interest are the Area (A), centre of gravity, (Y_G), moment of inertia about the bending axis (J_{xx}),torsional constant (J_t) and the section moduli (Z_t and Z_b) .These parameters were evaluated for the collaborating slab and the results summarised in table 3.7 .

Table 3.7. Geometrical and inertial properties of the collaborating slab

SLAB PROPERTIES		
h	300	mm
b	2500	mm
A	750000	mm^2
$Y_{G,slab}$	2300	mm
$J_{xx,slab}$	5 ,62E+09	mm^4
$J_{yy,slab}$	3,394E+11	mm^4
$I_{x,slab}$	86,60	mm
$I_{y,slab}$	721,687	mm
E_{cm}	34077,1462	Mpa
f_{ck}	35	Mpa
f_{cm}	43	Mpa

3.4.3. Ideal section propreties

The properties of interest are the height, ideal centre of gravity,($Y_{G,i}$), ideal moment of inertia about the bending axis ($J_{xx,i}$), ideal moment of inertia about the y-axis($J_{yy,i}$),torsional constant (J_t) and the section moduli (Z_t and Z_b). These parameters were evaluated and the results summarised in table 3.8.

Table 3.8. Properties of the Ideal section

PROPERTIES OF THE IDEAL SECTION(t=0)		
h	2800	mm
n	1,06	
A_i	2,25 E+06	mm^2
$Y_{G,i}$	1725.33	mm
$J_{xx,i}$	2,04 E+12	mm^4
$J_{yy,i}$	5,42E+11	mm^4
$I_{x,i}$	954,15	mm
$I_{y,i}$	438.14	mm
Z_t	1,90E+09	mm^3
Z_b	1,19E+09	mm^3
J_t	8,30E+10	mm^4

3.4.4. Cross beam properties

The properties of interest are the width, height, area, center of gravity, centre of gravity, (Y_G), moment of inertia about the bending axis (J_{xx}), moment of inertia about the y-axis(J_{yy}),torsional constant (J_t) These parameters were evaluated and the results summarized in table 3.9

Table 3.9. Properties of the crossbeam

CROSS BEAM		
b	500	mm
B	1100	mm
h	1500	mm
H	1800	mm
A	1080000	mm2
A1	750000	mm2
A2	3,3E+05	mm2
Yg	1025	mm
Jxx	3,29E+11	mm4
Jyy	4,89E+10	mm4
Jt	5,67E+10	mm4

3.5. Load analysis

The actions to consider in the design of road bridges are the permanent actions, and variable actions (thermal variations, wind). The load analysis was performed according to Eurocode and BAEL

3.5.1. Permanent load analysis

The self-weight of the beams, crossbeams and the slab were calculated based on their geometrical properties and the results obtained are summarised in table 3.10

Table 3.10. Self weight of structural elements

Self-weight of the precast beam		
Ac	1 ,54	m^2
γ_{cast}	25	KN/m^3
G1beam	38,57	KN/m
Self-weight of the cross beam		
Ac	1,05	m^2
γ_{cast}	25	KN/m^3
G1 transversal	18,75	KN/m
Self-weight of the slab		
Predalle thickness	0,06	m
Effective slab thickness	0,24	m
Slab total thickness	0,3	m
Effective width	2,5	m
Aslab	0,75	m^2
γ_{cast}	25	KN/m^3
G_1	18,75	KN/m
G1	83,57	KN/m

The superimposed dead loads are those applied to the structure when the concrete of the slab has reached sufficient strength. They constitute non-structural elements among which we find the pavement, protection railing, safety barrier, sidewalk jet. The weights of these elements are evaluated according to guidelines set forth in EN 1991 Action on structure part 1-1 and the results obtained were summarised in table 3.11. The total weight of the deck was evaluated and the results summarised in Table 3.12 as it is useful in the calculation of the load amplification coefficients.

Table 3.11. Permanent actions of deck finishes

Sidewalk in concrete		
Height	0,2	M
Width	1,5	M
Number	2	
Gamma concrete	25	KN/m3
G1	15	KN/m
Road pavement		
Height	0,17	M
Width	7,5	M
G, pavement	20	KN/m3
G1'	25,5	KN/m
Protection railing		
G	1,5	KN/m
Number	2	
G1''	3	KN/m

Table 3.12. Calculation of the total weight of the deck

Nature	**area**	**γ**	**length**	**number**	**Load**	
Crossbeams	0.75	25	10.5	2	393.75	KN
Slab	3.15	25	40	1	3150	KN
Beam	1,54	25	40	4	6170.8	KN
Guardrails	1	1.5	40	2	120	KN
Pavement	1.275	22	40	1	1122	KN
Sidewalk	0.3	25	40	2	600	KN
Total permanent					11162.8	KN

3.5.2. Variable load analysis according to Eurocode

In this section, the traffic loads, thermal actions, shrinkage and wind actions will be evaluated according to Eurocodes.

3.5.2.1. Traffic loads

The traffic loads analyzed are the load model 1 and breaking loads.

a. Load analysis for Load Model 1

The first operation consists in determining the number of notional lanes and their size.

$$n_1 = Int\left[\frac{w}{3}\right] = Int\left[\frac{10.5}{3}\right] = 3$$

From the notional lanes, the width (w_r) of the residual area is evaluated.

w_r =W-(3.00× n_1) =10.5-(3.00× 3)=1.5m

The road section is divided into 2 notional lanes and the remaining area. The bridge is loaded transversally to produce the most unfavourable effect for the element considered. The Intensity of traffic loads for traffic scheme M0 (table 3.13), M1 (table 3.14), M2 (table 3.15) were evaluated.

Table 3.13. Intensity of traffic loads for traffic scheme M0

Intensity of traffic loads for different lanes of the traffic scheme M0				
DISTRIBUTED LOADS		[KN/m^2]	Width m[m]	q_{tot} [KN/m2]
Lane no1	q_1	9	3	27
Lane no2	q_2	2,5	3	7,5
Remaining part	q_3	2,5	1,5	5
Total				39,5
Tandem loads		KN	Axles no	F_{tot}
Lane no1	F_1	300	2	600
Lane no2	F_2	200	2	400
Remaining part	F_3	0		0
Total				1000

Table 3.14. Intensity of traffic loads for traffic scheme M1

Intensity of trafic loads for different lanes of the traffic scheme m1				
DISTRIBUTED LOADS		$[KN/m^2]$	Width m$[m]$	q_{tot} [KN/m2]
Lane no1	q_1	9	3	27
Lane no2	q_2	2,5	3	7,5
Right sidewalk	q_3	2,5	1,5	3,75
Left sidewalk	q_4	2,5	1,5	3,75
Remaining part	q_5	2,5	1,5	5
Total				47
Tandem loads		KN	Axles no	F_{tot}
Lane no1	F_1	300	2	600
Lane no2	F_2	200	2	400
Remaining part	F_3	0		0
Total				1000

Table 3.15. Intensity of traffic loads for traffic scheme M2

Intensity of trafic loads for different lanes of the traffic scheme M2				
DISTRIBUTED LOADS		$[KN/m^2]$	Width m$[m]$	q_{tot} [KN/m2]
Lane no1	q_1	9	3	27
Lane no2	q_2	2,5	3	7,5
Left sidewalk	q_3	2,5	1,5	3,75
Total				38,25
Tandem loads		KN	Axles no	F_{tot}
Lane no1	F_1	300	2	600
Lane no2	F_2	200	2	400
Remaining part	F_3	0		0
Total				1000

b. Effect of breaking loads

The effect of breaking loads is a fraction of the maximum loads applied to lane number one and is calculated using equation 2.3.

$$Q_{lk} = 1{,}2 \times (1 \times 300) + 0{,}1 \times (1 \times 9) \times (3 \times 40) = 468 \text{ KN}$$

3.5.2.2.Wind actions

The effect of the wind was evaluated after following the steps in section 2.4.2.2.The bridge subject of this study is in a suburban milieu so it is classified as terrain category 3.The fundamental value of the basic wind velocity $v_{b,0}$ in the region is assumed to be equal to be 25 m/s. The bridge is designed for a period of 100 years. The mean probability of occurrence of the extreme event p=0.01.

The basic wind velocity v_b is defined as a function of the wind direction and time of year at 10m above the ground of terrain category 2 and calculated using equation 3.5.

$$v_b = C_{prob} C_{dir} C_{season} v_{b,0} \qquad (3.5)$$

Where:

C_{dir} is the directional factor;

C_{season} is the Seasonal factor;

C_{prob} is the probability factor.

$$C_{prob} = \left(\frac{1-KLn(-Ln(1-p))}{1-KLn(-Ln0{,}98)}\right)^n = \left(\frac{1-0{,}2\times\ln(\ln(1-0.01))}{1-0{,}2\times\ln(-\ln(0.98))}\right)^{0{,}5} = (1{,}98/1{,}78)^{0.5} = 1{,}04$$

$$v_b = 1{,}04 \times 1{,}0 \times 1{,}0 \times 25 = 25{,}96 \text{ m/s}$$

The mean wind velocity at a height z above the ground was calculated using the formula 3.6.

$$v_m(z) = C_r(z) C_O(z)\, v_b \qquad (3.6)$$

Where :

$C_O(z)$ is the orography factor;

$C_r(z)$ is the roughness factor;

$C_O(z)$ can be assumed to be equal to be equal to 1.

The roughness factor $C_r(z) = \begin{cases} k_r \ln\left(\frac{z}{z_0}\right) & for\ z_{min} \le z \le z_{max} \\ C_r(z_{min}) & for\ z < z_{min} \end{cases}$

k_r is the terrain factor;

Z is the bridge intrados.

From table $z_0 = 0{,}3$ for terrain category III,

$$k_r = 0{,}19\left(\frac{z_0}{z_{0,II}}\right)^{0{,}07} = 0{,}19\left(\frac{0.3}{0{,}05}\right)^{0{,}07} = 0{,}21$$

The bridge intrados is equal to 10,2 therefore,

$$C_r(z)=0{,}2\times ln\left(\frac{10{,}2}{0{,}3}\right)=0{,}76$$

$$v_m(z) = 0{,}76\times 1 \times 25{,}96=19{,}72 \text{ m/s}$$

The turbulence intensity at a height (z) is defined as the standard deviation of turbulence divided by the mean wind velocity calculated using equation 3.7.

$$I_v(z) = \begin{cases} \frac{k_l}{C_0(z)\ln\left(\frac{z}{z_0}\right)} & for\ z_{min} \le z \le z_{max} \\ I_v(z_{\min}) & for\ z < z_{min} \end{cases} \quad (3.7)$$

The recommended value for k_l is 1.

$$I_v(z) = \frac{1}{1\times\ln\left(\frac{10{,}2}{0.3}\right)} = 0{,}28$$

The peak velocity pressure was obtained as a function of the mean and short term fluctuations.

$$q_p(z)=\frac{1}{2}\rho v_m^2(z)[1+7I_v(z)]=0{,}5\times 1{,}25\times(19{,}72)^2[1+7\times 0{,}28]=725.45 \text{ N}/m^2$$

Two situations are very important in our design, one with the beam only and one with the loaded bridge. The loaded height for both situations was obtained as summarized by table 3.16 and table 3.17 and the force coefficients determined graphically according to figure 3.8.

Table 3.16. Loaded height and force coefficients for the slab and beam

Slab and beam		
Slab	0,3	m
Beam	2,5	m
Pavement	0,17	m
Shape	3	m
dtotload	5,97	m
b	10,5	m
b/dtot	1,75	
$C_{f,x}$	1,9	

Table 3.17. Loaded height and force coefficients for the beam.

Only beam		
Height of Beam	2,5	m
Shape	0	m
Pavement	0	m
dtotload	2,5	m
b	10,5	m
b/dtot	4,2	
$C_{f,x}$	1,3	m

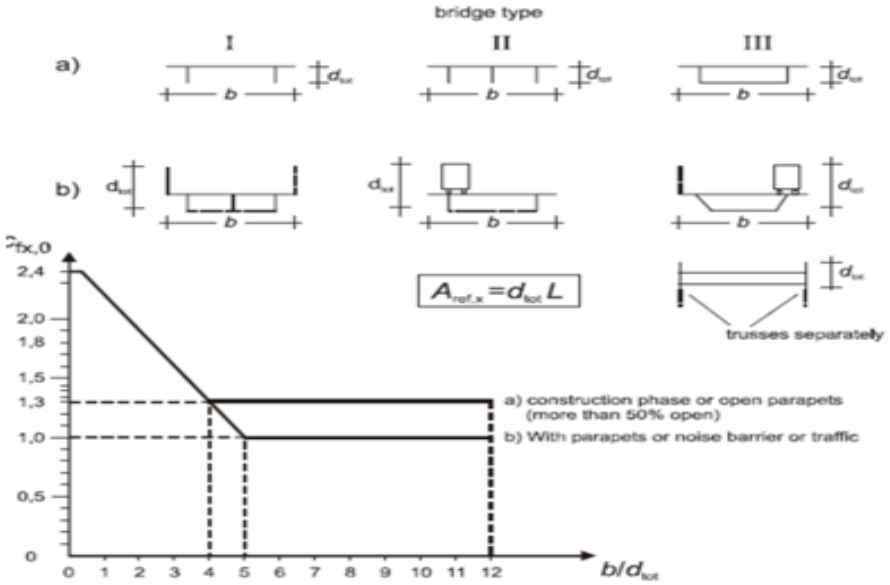

Figure 3.8. Force coefficients evaluation graph

The effect of the wind was considered as a force acting at an eccentricity to the center of gravity of the deck producing a torsion on the deck. The torsion for the deck is subdivided down into a couple of forces applied to the edge beams and results are summarized in table 3.18.

Table 3.18. Division of the wind torsion into a couple.

Phase	F_{beam}**(kN)**	**b(m)**	**Mt(kN)**	**e(m)**	$F_{w,x}$**(KN/m)**
Bridge under construction (only beams)	0,15	8,25	1.19	0.5	2,36
Loaded bridge (Beam +slab)	1,22	8,25	10,09	1.23	8,23

3.5.2.3.Shrinkage

The first operation consists in determining the free shrinkage. For cement class N and a relative humidity of 75%,the shrinkage strain was calculated and the results summarized in table 3.19.

Table 3.19. Calculation of shrinkage strain

Ac	2.52E+06	mm^2
U	11600	mm
h_0	434.48	mm
$\varepsilon_{ca(\infty)}$	6.25E-05	
$\varepsilon_{cd,0}$	3.0 E-04	
kh	0.711	
ε_{cd}	2.13 E-04	
ε_{cs}	2.76×10^{-4}	

3.5.2.4. Thermal stress

The first step consists in evaluating the restraining stresses at various levels of the cross section. Considering the height of the superstructure, H=2800mm.

h_1=150mm, h_2=250mm, h_3=270mm

From table 2.3, $\Delta T_1 = 13$,$\Delta T_2 = 3$,$\Delta T_3 = 2.5$

The corresponding restraining stresses are:

σ=-$\alpha_t \times \Delta T \times E_c$

σ=-0.34$\times \Delta T$= (-4.42, -1.02, -0.85)

The restraining stresses at various levels of the cross section were then evaluated as summarized by table 3.20.

Table 3.20. Restraining stresses at various levels of the cross section due to differential heating

Level from top	**б(Mpa)**
0	-4.43
150	-1.02
300	-0.40
400	0
2530	0
2800	-0.85

Having obtained the restraining stresses, the forces in the different segments of the cross section were obtained by multiplying restraining stresses by the area and the results are summarized in table 3.21

Table 3.21. Forces at different levels of the cross section due to differential heating

б top	**б bot**	**Area**	**F, KN**
-4.43	-1.02	375000	-1024.3
-1.02	-0.40	375000	-268.89
-0.40	0	225000	-46.095
0	-0.85	243000	-103.71

The moment due to the restraining forces about the centroidal axis of the beam shows the details to calculate the moment due to force, F. The resultant due to a trapezoidal stress distribution as shown in figure 3.6 is at a distance c from the top given by equation 3.8.The resultant due to a trapezoidal stress distribution is illustrated by (figure 3.6)

$$c = \frac{D}{3} \times \frac{(2\sigma_{bottom} + \sigma_{top})}{(\sigma_{bottom} + \sigma_{top})} \qquad (3.8)$$

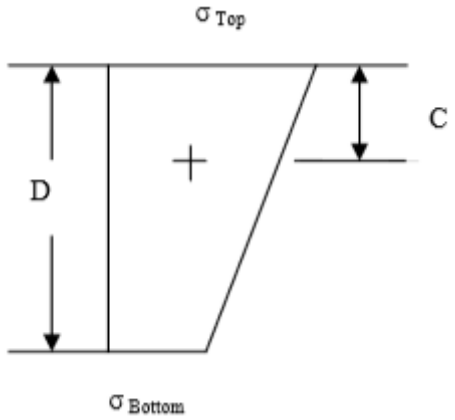

Figure 3.6. Position of force resultant due to a trapezoidal stress distribution

The moment due to restraining forces arising from differential heating is summarized in table 3.22.

Table 3.22. Moment due to restraining forces arising from differential heating

F(KN)	D (mm)	C (mm)	Lever arm (mm)	Moment(KNm)
-1024.33	150	59.37	1015.29	-1040
-268.89	150	64.28	860.381	-231.34
-46.1	100	33.33	741.334	-34.172
-103.71	270	180	-1635.3	169.605
-1443.0197				--1135.9

Having obtained the moment due to the restraining forces, the final stress in the cross section is obtained as the sum of the initial restraining stress plus the stress due to axial force and moment in order to produce a self-equilibrating stress system. The final stress in the cross section due to differential heating is summarized in table 3.23 and its distribution in the cross section is given by figure 3.10.

Table 3.23. Final stress calculation due to differential heating

Position from top	б(Mpa)	∑F/A	y	(∑M/I)y	final stress
0	-4,44	0,64	1074,67	0,60	-3,20
150	-1,02	0,64	924,67	0,51	0,13
300	-0,41	0,64	774,67	0,43	0,66
400	0,00	0,64	674,67	0,37	1,02
1074,667206		0,64	0,00	0,00	0,64
2530	0,00	0,64	-1455,33	-0,81	-0,17
2800	-0,85	0,64	-1725,33	-0,96	-1,17

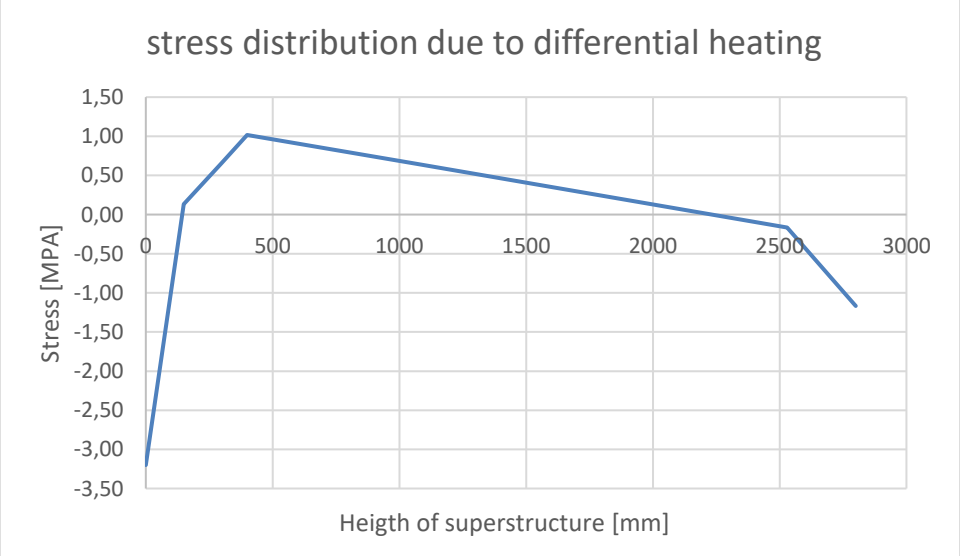

Figure 3.10. Stress distribution in cross section due to differential heating

The procedure adopted to evaluate the thermal stress due to cooling is similar to that already mentioned in calculating the thermal stress due to heating. The temperature differentials due to cooling are applied and the stress distribution across the section due to cooling is obtained as shown in figure 3.11

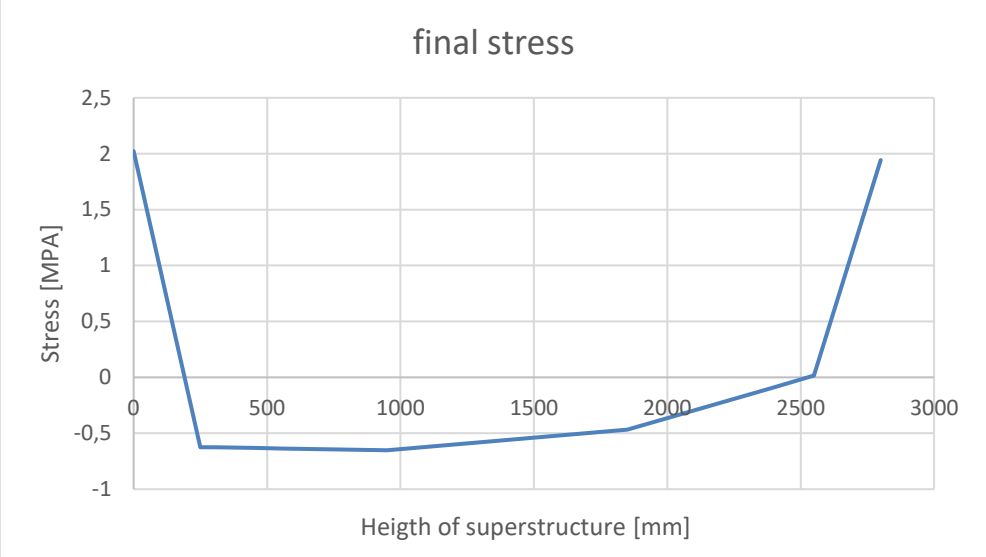

Figure 3.11. Stress distribution due to differential cooling

3.5.3. Load analysis according to BAEL

The load analysis was done for traffic loads, wind loads.

3.5.3.1.Traffic loads

Bridges with pavement width greater than 7 m are classified as first-class bridges. W=7.5m therefore our bridge can be considered as a first-class bridge. The code distinguishes the loadable width , L_W from the traffic width , L_{tr}. The traffic loads discussed in the following section are the load system A, Bc, Bt, Br, pedestrian loads and braking loads.

a. Load system A

The traffic width is the width of the pavement allocated to the movement of vehicles. The loadable width is obtained from the traffic width by removing 0.5 m from each safety barrier.

The Traffic width =7.5m.

Safety barriers are not available; therefore, loadable width is equal to traffic width.

Number of notional lanes=whole number part of $\left[\frac{L_W}{3}\right]$.

Whole number part of $\left[\frac{7.5}{3}\right] = 2$.

Width of notional lanes=$\left[\frac{loadable\ width\ ,L_W}{number\ of\ notional\ lanes}\right]$=$\frac{7.5}{2} = 3.75$.

The load system A is defined as a uniformly distributed loadA_L applied on all the pavement surface.

$A_L = 2{,}3 + \frac{360}{L+12}$ =$2{,}3 + \frac{360}{40+12}$ = 9, 22 KN/m^2.

The load A_L is applied transversally so as to have the maximum effect for the element considered.

One lane charged

$a_1 = 1$

$A_1 = \max\left(a_1.\left(2{,}3 + \frac{360}{40+12}\right), (4 - 0{,}002 \times 40)\right)$=9, 22 KN/$m^2$

This value of $A_1$is multiplied by the coefficient a_2

$a_2 = \frac{v_0}{v}$ Where v is the width of a lane

$a_2 = \frac{3{,}5}{3{,}75}$ = 0, 93

$A_2 = a_2 \times A_1 = 0{,}93 \times 9{,}22 = 8{,}57$ KN/m^2

Table 3.24 summarises the results for the two lanes

Table 3.24. Calculation of traffic load system A

Number of loaded lanes	a_1	a_2	$A_1 \times a_1 \times a_2$	**Width of lane**	A_L/KNm^{-1}
1	1	0.93	8,57	3.75	32,28
2	1	0.93	8,57	7.5	64,56

For uniformly distributed load, the maximum bending moment at the right of any section situated at a distance x from the left support as shown in figure 3.9 ,is obtained by loading entirely the span. This corresponds to the influence area evaluated using equation 3.9. Table 3.25 summarises the maximum bending moment at every section for load system A.

$$S=\frac{L}{2}\left(x - \frac{x^2}{L}\right) \quad (3.9)$$

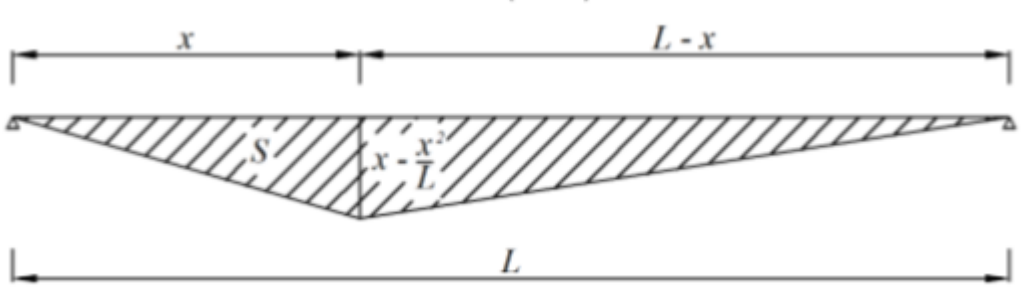

Figure 3.12. Influence line for maximum bending moment at the right of a section x

Table 3.25. Maximum bending moment at every section for load system A

Section	0	support	L/10	2L/10	L/4	3L/10	4L/10	L/2
X(m)	x(m)	0	4	8	10	12	16	20
Mmax(KN)	1 Lane	0	2324.2	4131.9	4842.1	5423.2	6197.9	6456.2
	2 Lanes	0	4648.4	8263.9	9684.2	-10846.	12395	12912.3

The maximum shear force at the right of a section situated at a distance x ($x \leq \frac{L}{2}$) from the left support is obtained by loading the section on the right of the section, which corresponds, to the influence area defined by equation 3.10. Figure 3.13 illustrates the influence line for maximum shear at the right of a section x.

$$S=\frac{(L-x)^2}{2L} \tag{3.10}$$

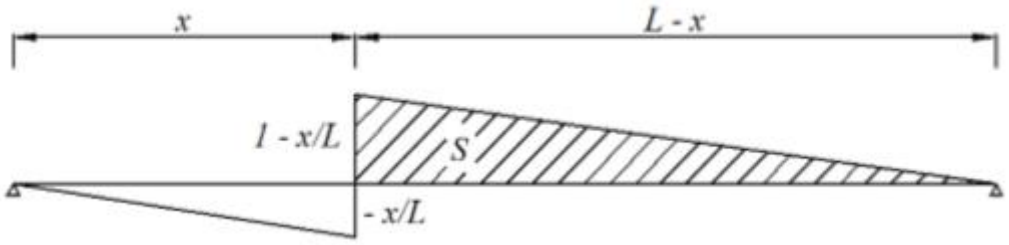

Figure 3.13. Influence line for maximum shear at the right of a section x

The maximum shear force is given by equation 3.11.

$$V^{+}=q.S^{+}=q\frac{(L-x)^2}{2L} \tag{3.11}$$

The minimal shear force is calculated in the same manner but the left of the section is loaded in this case. The minimum shear force is evaluated using equation 3.12.

$$V^{-}=q.S^{-}=\frac{(L-x)^2}{2L}=-q\frac{x^2}{2L} \tag{3.12}$$

b. Load system Bc

For a particular section, the maximum moment is obtained by placing at the right of the section one of the heaviest axles. The trucks are displaced along the bridge so as to produce the maximum effect in each section. The calculations are programmed on excel. As an example, taking the section situated at L/4(x=10 m) illustrated by figure 3.14.

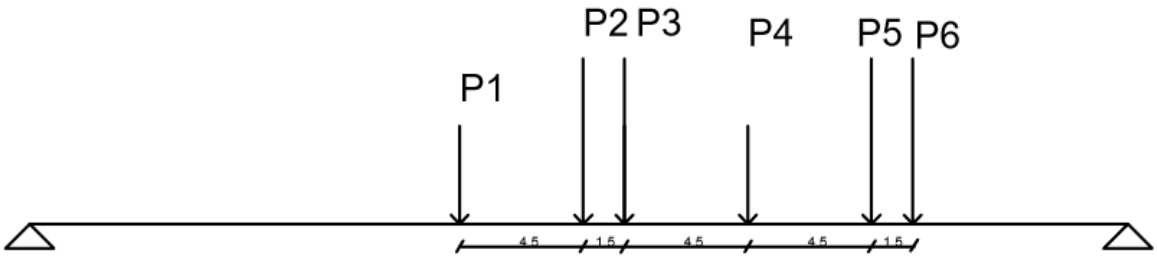

Figure 3.14. Positioning of axles of the load system Bc

The axles are placed successively at the section under investigation and the moment is obtained using equation 3.13.

$$M = \sum_i P_i y_i \qquad (3.13)$$

y_i is the ordinate of the influence line for bending moment at the position of the load.

P_i is the axle load.

The axles are placed successively at x and the position of the axles from the support evaluated (table 3.26) .For each position of the loads, the ordinates of the influence lines were calculated and the results are summarized in table 3.27.The moment due to an axle load is calculated using equation 3.13 and the resulting moment due to each position of the loads is obtained by summing the moment produced by the different axles and the results are summarized in table 3.28. The configuration producing the highest bending moment for the section under investigation is then retained

Table 3.26. Positions of the axle load for moving load analysis

Axle case	**Position of the axle n from the left support**					
	α1	α2	α3	α4	α5	α6
no 1 at x	10	14.5	16	20.5	25	26.5
no 2 at x	5.5	10	11.5	16	20.5	22
no 3 at x	4	8.5	10	14.5	19	20.5
no 4 at x	-0.5	4	5.5	10	14.5	16
no 5 at x	-5	-0.5	1	5.5	10	11.5
no 6 at x	-6.5	-2	-0.5	4	8.5	10

Table 3.27. Ordinates of the influence line at different sections

Case	**Ordinate of the influence line for bending moment at the right of axle**					
	y1	y2	y3	y4	y5	y6
no 1 at x	7.5	6.375	6	4.875	3.75	3.375
no 2 at x	4.125	7.5	7.125	6	4.875	4.5
no 3 at x	3	6.375	7.5	6.375	5.25	4.875
no 4 at x	0	3	4.125	7.5	6.375	6
no 5 at x	0	0	0.75	4.125	7.5	7.125
no 6 at x	0	0	0	3	6.375	7.5

Table 3.28. Maximum moment produced by different axles at x

Case	**Moment due to the axles**						
	y1	y2	y3	y4	y5	y6	Mmax (kN)
no 1 at x	900	1530	1440	585	900	810	6165
no 2 at x	495	1800	1710	720	1170	1080	6975
no 3 at x	360	1530	1800	765	1260	1170	6885
no 4 at x	0	720	990	900	1530	1440	5580
no 5 at x	0	0	180	495	1800	1710	4185
no 6 at x	0	0	0	360	1530	1800	3690

For x=L/4, the maximum moment is obtained by placing the axle number 3 at x=L/4. The procedure above was repeated for several points along the length of the bridge and the maximum shear and moment were obtained. The maximum positive shear is obtained by loading the portion to the right of the influence line for shear of the section x investigated. The maximum negative V^{-}shear is calculated the same manner as the maximum positive shear except for the fact that the former is obtained by loading the portion to the left instead. As a result, the position of the first axle is at the right of x. considering again for x= L/4, the calculation of maximum positive shear and negative shear is summarized in table 3.39.

Table 3.29. Calculation of maximum shear for the load system Bc

	n6	n5	n4	n3	n2	n1
αk	10	11.5	16	20.5	22	26.5
1-x/L	0.75	0.75	0.75	0.75	0.75	0.75
L-x	30	30	30	30	30	30
L-α	30	28.5	24	19.5	18	13.5
yα	0.75	0.7125	0.6	0.4875	0.45	0.3375
V^+(KN) 2 lanes	180	171	72	117	108	40.5
V^+(KN) 1 Lane	90	85.5	36	58.5	54	20.25

The loads of system Bc are to be multiplied by the coefficient bc and the dynamic amplification coefficient δ. (Bourrel & Gourdou, 2016)

From Table 2.6 , for a first-class bridge

$$bc = \begin{cases} 1.2 : 1 lane\ charged \\ 1{,}1 : 2\ lanes\ charged \end{cases}$$

$$\delta = 1 + \alpha + \beta = 1 + \frac{0{,}4}{1+0{,}2L} + \frac{0{,}6}{1+4\frac{G}{S}} = \begin{cases} 1{,}053 : 1\ lane\ charged \\ 1{,}062 : 2\ lanes\ charged \end{cases}$$

Where:

L is the span of the bridge;

G is the total weight of the deck for the span considered excluding the cross beams, G=11556.55KN;

S is the Maximum load applicable on a span;

$$S = nbc \times 600\ KN = \begin{cases} 720 : n = 1 \\ 1320 : n = 2 \end{cases}$$

n is number of loaded lanes;

The moment and shear are obtained following equations 3.14 and 3.15 and the results for the maximum shear produced by load system Bc is summarized in table 3.30 and the maximum shear in table 3.31

$$M = \delta bc M_{max} \quad (3.14)$$

$$T = \delta bc T_{max} \quad (3.15)$$

The table 3.30 summarizes the maximum shear produced by the load system Bc.

Table 3.30. Maximum shear produced by the load system Bc

Section			0	L/10	2L/10	L/4	3L/10	4L/10	L/2
x(m)			0.1	4	8	10	12	16	20
$V^+(KN)$	1 lane		494.25	434.25	374.25	344.25	314.25	254.25	194.25
	2 lanes		988.5	868.5	748.5	688.5	628.5	508.5	388.5
$V^-(KN)$	1 lane		0	-19.5	-46.5	-61.5	-81	-135	-194.2
	2 lanes		0	-39	-93	-123	-162	-270	-388.5

Table 3.31. Maximum moment produced by the load system Bc

Section		support	L/10	2L/10	L/4	3L/10	4L/10	L/2
x(m)		0	4	8	10	12	16	20
M(KNm)	1 lane	0	1620	2976	3487.5	3879	4392	4425
	2 lanes	0	3240	5952	6975	7758	8784	8850

c. Load system Bt

A tandem of system Bt consists of two axles spaced 1.35m apart each carrying a mass of 160KN. A similar procedure as that used to calculate the sollicitations due to load system Bc is followed and the sollicitations are obtained as summarized Table 3.2.

The coefficients considered are bt, δ $\begin{cases} bt = 1: first\ class\ bridges \\ \delta = \begin{cases} 1.05 : 1\ lane\ charged \\ 1{,}053 : 2\ lanes\ charged \end{cases} \end{cases}$

Table 3.32. Maximum moment and shear at each point for the load system Bt

Section	0	support	L/10	2L/10	L/4	3L/10	4L/10	L/2
	x(m)	0	4	8	10	12	16	20
M(KNm)	1 lane	0.0	1186.0	2103.4	2461.4	2752.3	3132.5	3244.1
	2 lanes	0.0	2382.6	4225.7	4944.8	5529.²1	6293.0	6517.2
$V^+(KN)$	1 lane	330.1	296.5	262.9	246.1	229.4	195.8	162.2
	2 lanes	663.1	595.7	528.2	494.5	460.8	393.3	325.9
V^-**(KN)**	1 lane	5.7	-27.9	-61.5	-78.3	-95.1	-128.6	-162.2
	2 lanes	11.4	-56.1	-123.5	-157.2	-191.0	-258.4	-325.9

d. Load system Br

The isolated wheel that constitutes the Load System Br carries a mass of 100KN.

The Coefficients considered are br, δ $\begin{cases} br = 1 \\ \delta = 1.04 \end{cases}$.

The calculations are also similar to that in load system Bc and the resulting sollicitations are summarized in table 3.33.

Table 3.33. Maximum moment and shear obtained at each point for load system Br

Section	support	L/10	2L/10	L/4	3L/10	4L/10	L/2
x(m)	0	4	8	10	12	16	20
M(KNm)	0.00	376.54	669.40	784.45	878.59	1004.10	1045.94
(+)V(KN)	104.59	94.13	83.68	78.45	73.22	62.76	52.30
(-)V(KN)	0.00	-10.46	-20.92	-26.15	-31.38	-41.84	-52.30

e. Pedestrian loads

Unlike Eurocodes, the pedestrian loads are not considered in the traffic loads and have to be calculated separately. According to fascicule 61 titre, 2 the pedestrian load to be taken into account for the justification of the beams is a uniformly distributed load of 1,5KN/m. A similar procedure as that used to calculate the sollicitations due to Load System A is followed and the sollicitations are obtained (Table 3.34).

Table 3.34. Maximum moment and shear due to pedestrian loads

Section	0	support	L/10	2L/10	L/4	3L/10	4L/10	L/2
X(m)	X(m)	0	4	8	10	12	16	20
M(KNm)	1 Sidewalk	0	162	288	337.5	378	432	-450
$V^{+}(KN)$	1 Sidewalk	45	36.45	28.8	25.3125	22.05	16.2	11.25
V^{-}**(KN)**	1 Sidewalk	0	-0.45	-1.8	-2.8125	-4.05	-7.2	-11.25

f. Breaking loads

The breaking loads due to load system A and Bc are calculated.

B (A) $= \frac{64.56 \times 40}{20 + 0.0035 \times (7.5 \times 40)} = 122KN$

B (Bc) =30 KN

3.5.3.2. Effect of the Wind

The pressure action of the wind is different between construction and execution.

$$q = \begin{cases} 2000\ \text{Nm}^{-2} \text{ during construction} \\ 1250\ \text{Nm}^{-2} \text{ during execution} \end{cases}$$

The effect of the wind was calculated as torsion effect on the deck as summarized in table3.35 and later on distributed on the edge beams.

Table 3.35. Calculation of the effect of the wind for BAEL

Phase	F_{beam}**(KN)**	**b(m)**	**Mt(KN)**	**e(m)**	$F_{w,x}$**(KN/m)**
Bridge under construction (only beams)	0,19	8,25	1.59	0.51	3.125
Loaded bridge (Beam +slab)	0.19	8,25	1.62	0.27	5.94

3.6. Analytical Load distribution

The Analytical load distribution was carried out using the Guyon Massonet method to obtain the sollicitations in the edge beam.

3.6.1. Transversal load distribution following Guyon Massonet

The first step is to determine the characteristics of the equivalent grid work. In order to do so, the two spans (lateral and central) are analyzed to determine the flexural and torsional stiffnesses of the beams and cross beams.

The flexural and torsional rigidities were then calculated.

Span length, l = 40 m

Number of beams = 4 beams, Distance between beams: 2,75m $\Longrightarrow$ b = n/2b_1=5,5m.

For the mixed section beam, the parameters ρ_P and γ_P are calculated.

$$\rho_P = \frac{EJ_P}{b_1} = \frac{36283 \times 2.04 \times 10^{12}}{2750} = 2.699\text{E+13 Nmm}$$

$$\gamma_P = \frac{GJ_{t,p}}{b_1} = \frac{15775.2 \times 8.3 \times 10^{10}}{2750} = 4.763\ \text{E+11 Nmm}$$

For the cross beam the parameters ρ_E and γ_E are calculated.

$$\rho_E = \frac{EJ_E}{L_1} = \frac{34077.1462 \times 4.49 \times 10^{11}}{40000} = 3.79\text{E+11Nmm}$$

$$\gamma_E = \frac{GJ_{t,E}}{L_1} = \frac{14816.15 \times 6.6 \times 10^{10}}{40000} = 3{,}551\text{E+11Nmm}$$

Having obtained the characteristics of the equivalent grid work, the Massonet parameters were calculated.

Torsional parameter $\alpha = \frac{\gamma_P + \gamma_E}{2\sqrt{\rho_p * \rho_E}} = 0,25$

Stiffness parameter $\theta = \frac{b}{l} \sqrt[4]{\frac{\rho_p}{\rho_E}} = 0,39$

Since $\theta = 0,39 > 0,3$ the Massonet method is appropriate for this application.

The numerical tables established by Massonet (Annex I), permit us to determine through successive interpolations, the values of the functions k_0 and k_1 as a function of the torsional parameter for the different eccentricities of the load(Annex V). Due to the symmetry of the bridge it is sufficient to find the influence lines for the edge beam and the inner beam. The value of k_α is obtained from the interpolation on θ. Where k_α *is* defined by equation 3.16.

$$k_\alpha = k_\alpha(\theta_1) + \frac{k_\alpha(\theta_2) - k_\alpha(\theta_1)}{\theta_2 - \theta_1}(\theta - \theta_1) \qquad (3.16)$$

These values obtained (Table 3.36) will permit the tracing of the influence line of the edge beam and the inner beam. The loads are positioned to have the maximum response $K_{\alpha,max}$ for the edge beam (figure 3.15) and inner beam (figure 3.16) and the maximum load repartition coefficients are obtained for the different loads (Table 3.37)

Table 3.36. Load amplification coefficients of the edge beam and inner beam

e	-b	-3b/4	-b/2	-b/4	0	b/4	b/2	3b/4	b
y=3b/4	2.242	1.924	1.5896	1.2665	0.948	0.6614	0.3970	0.1488	0.0912
y=b/4	1.291	1.259	1.221	1.160	1.056	0.929	0.795	0.661	0.532

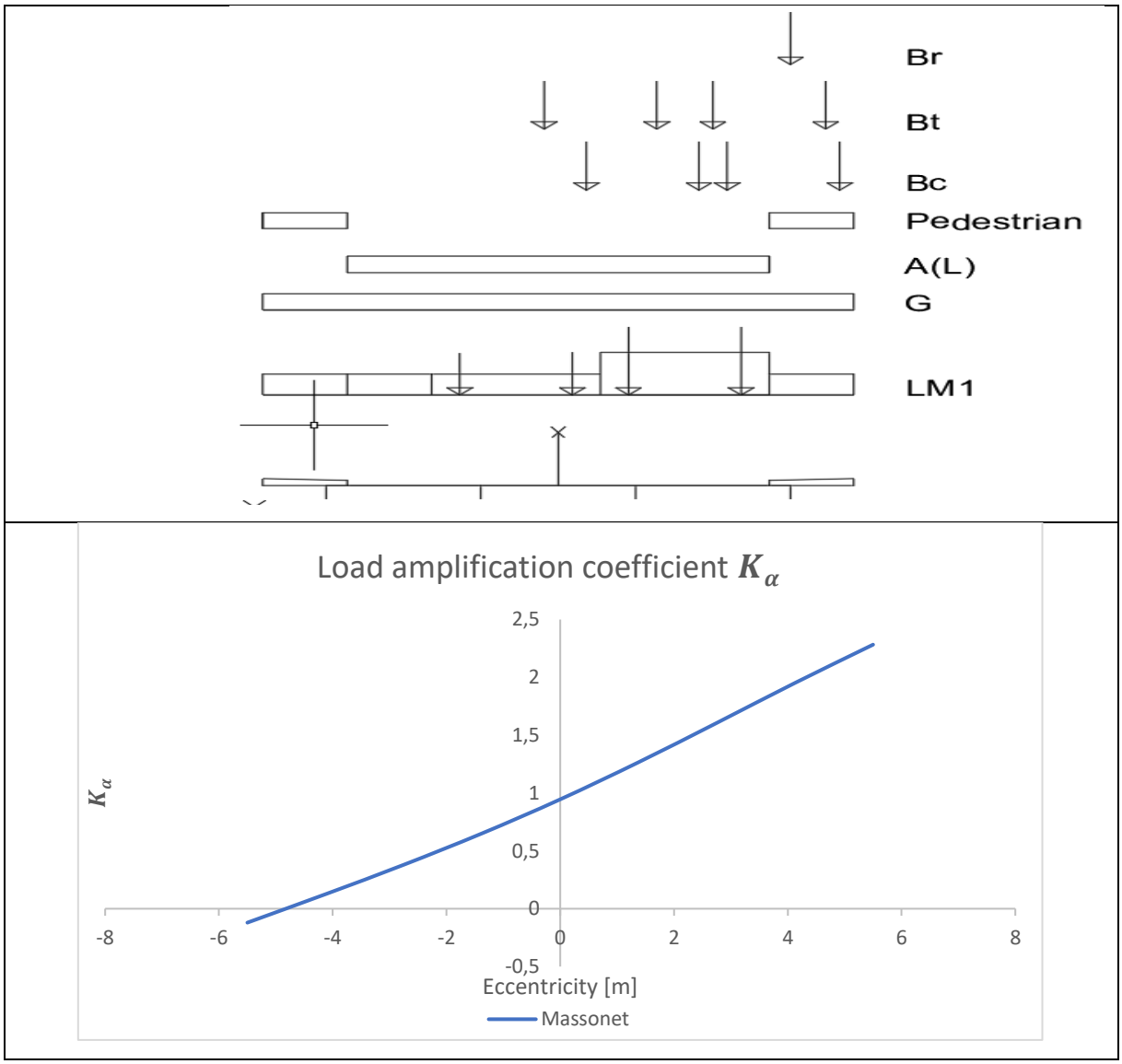

Figure 3.15. Spatial distribution of loads and Influence lines of the edge beam for the different methods

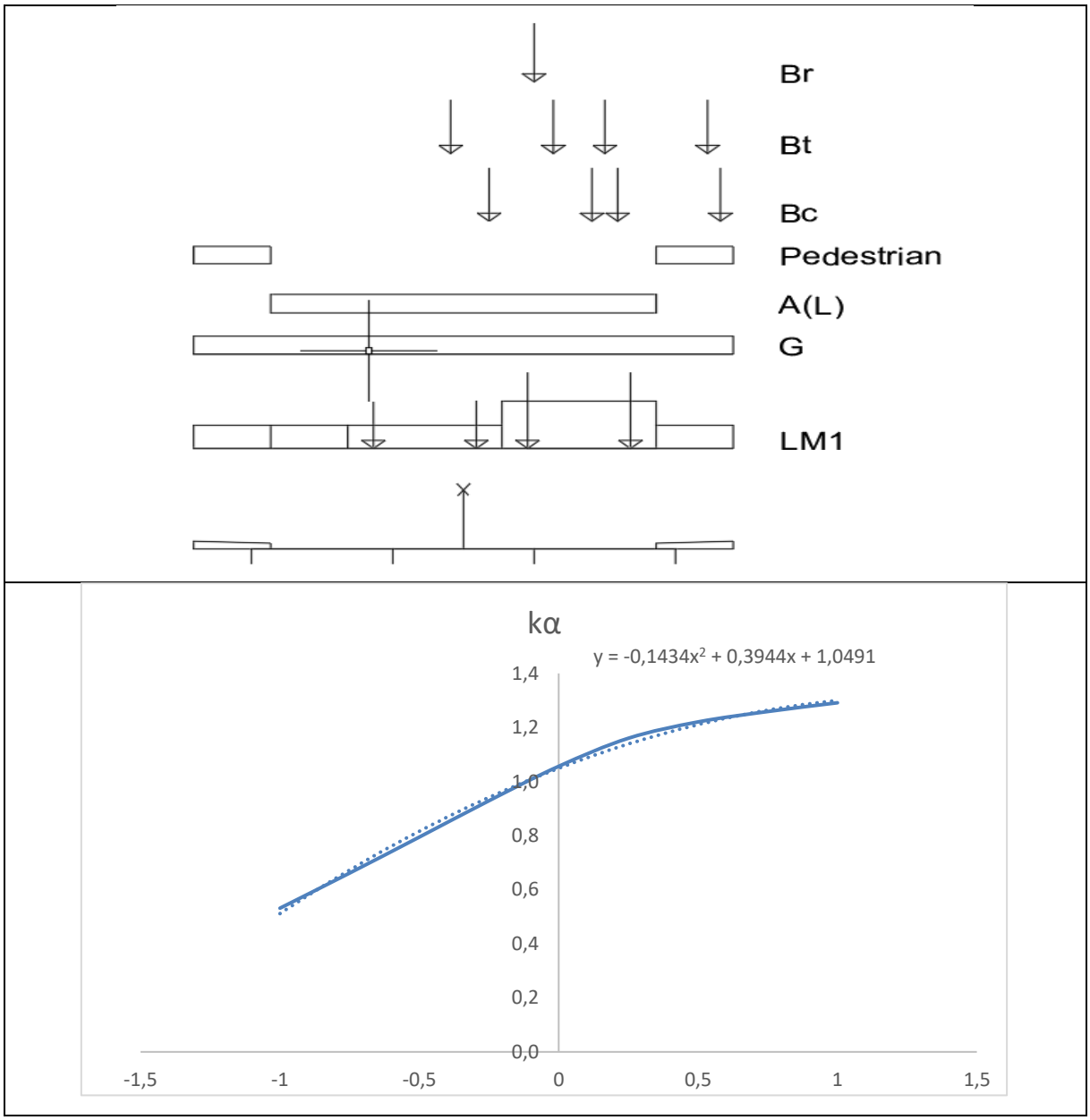

Figure 3.16. Influence lines for the inner beam and spatial distribution of loads

Table 3.37. Maximum load repartition coefficients $k_{\alpha max}$ for the edge beam

Loads	Traffic scheme	Massonet
G	Pavement	0,97
G	All the width	0,99
A(l)	2 lanes	0,97
Bc	2 lanes	1,25
Bt	2 lanes	1,14
Br	isolated wheel	1,94
pedestrian	Right	2,03
	Left	0,05
LM1	Lane 1	1,48
	Lane 2	0,80
	remaining Area	0,33
	1,Sidewalk	2,03
	2 sidewalk	0,05

The bending moment in every beam under the load considered is given by:

$$M_i = K_{\alpha i} \frac{M_0}{n} \tag{3.17}$$

Where:

$K_{\alpha i}$ is the load repartition coefficient for the beam considered;

n is number of beams;

M_0 is the total moment sollicitating the span due to the load considered.

The shear force is calculated similarly defined by equation 3.18.

$$T_i = K_{\alpha i} \frac{T_0}{n} \tag{3.18}$$

Where:

T_0 is the total shear force sollicitating the span due to the load considered.

3.6.2. Analytical solicitations

After the load distribution, the sollicitations diagrams on the edge beam due to the application of the various loads on the structure were obtained. The results of the solicitations on the edge beam only will be represented for simplicity.

Figure 3.14. illustrates the moment due to the self-weight of the precast beam

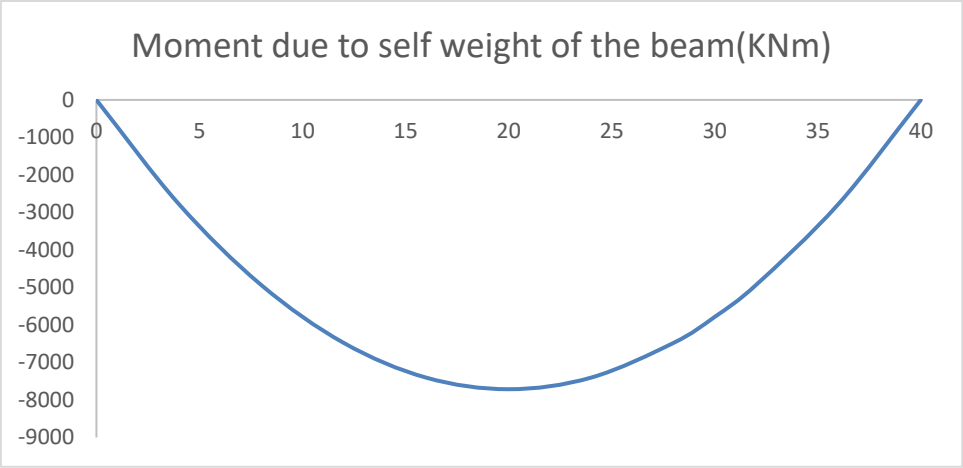

Figure 3.17. Moment due to the self-weight of the beam

Figure 3.15. illustrates the shear due to the self-weight of the precast beam

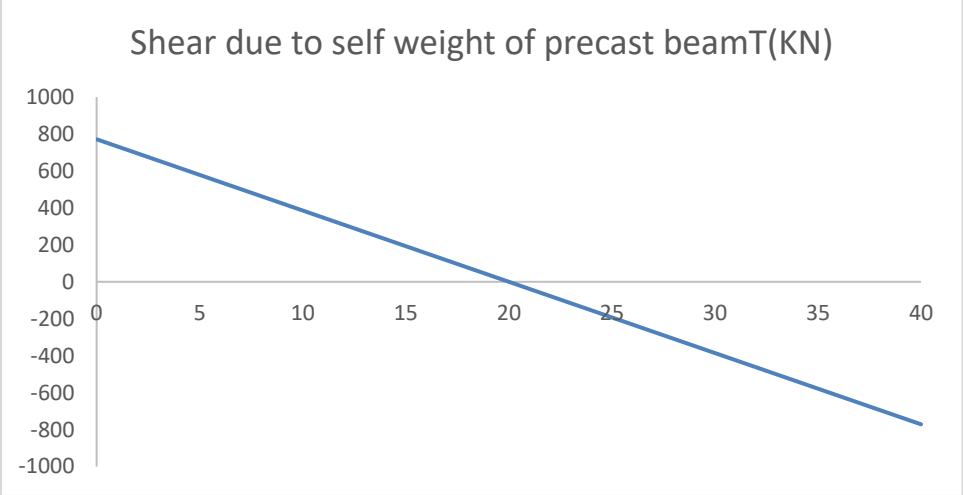

Figure 3.18. Shear due to the self-weight of the precast beam

Figure 3.16 illustrates the bending moment due to the self-weight of the beam and precast insitu elements.

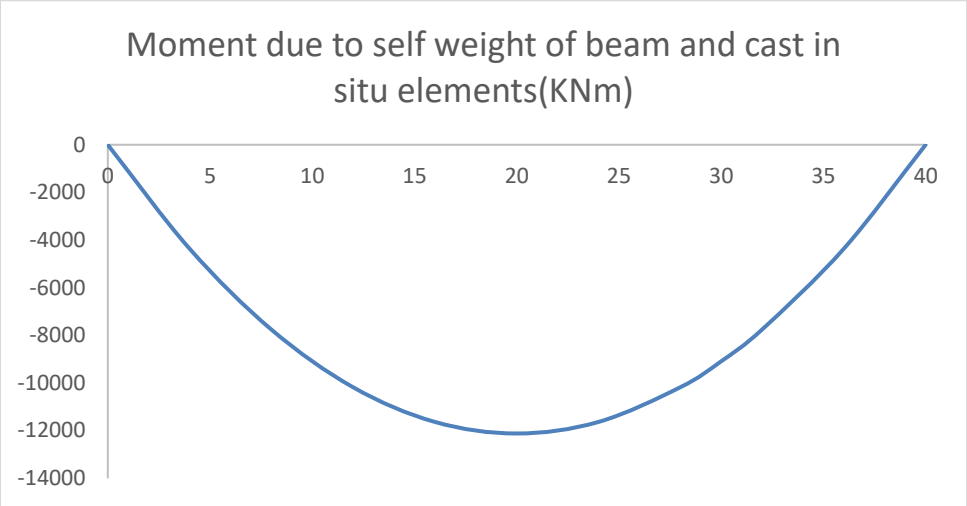

Figure 3.19. Moment due to the self-weight of the beam and the cast in situ elements

Figure 3.17 illustrates the shear due to the self-weight of the beam and precast insitu elements.

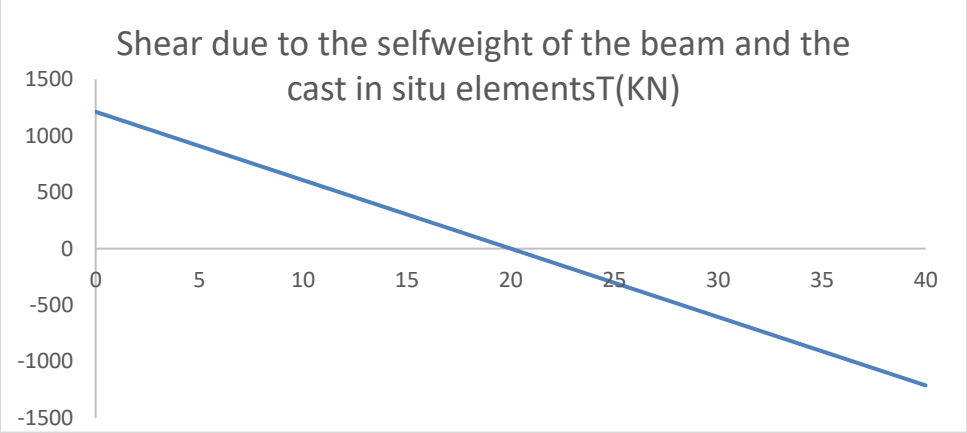

Figure 3.20. Shear due to the self-weight of the beam and the cast in situ elements

Figure 3.18 illustrates the bending moment curve due to load system A.

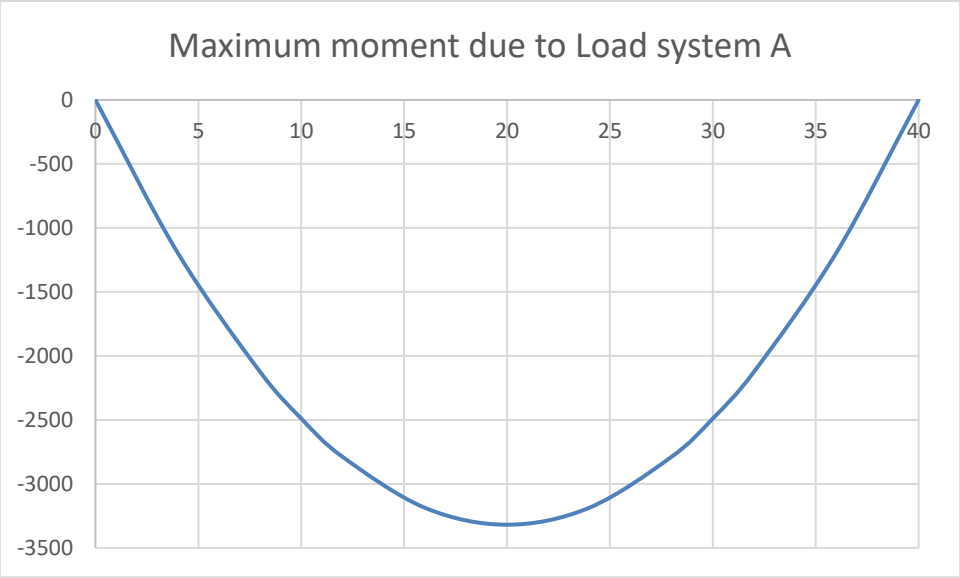

Figure 3.21. Maximum moment due to Load system A

Figure 3.19 illustrates the shear due to load system A.

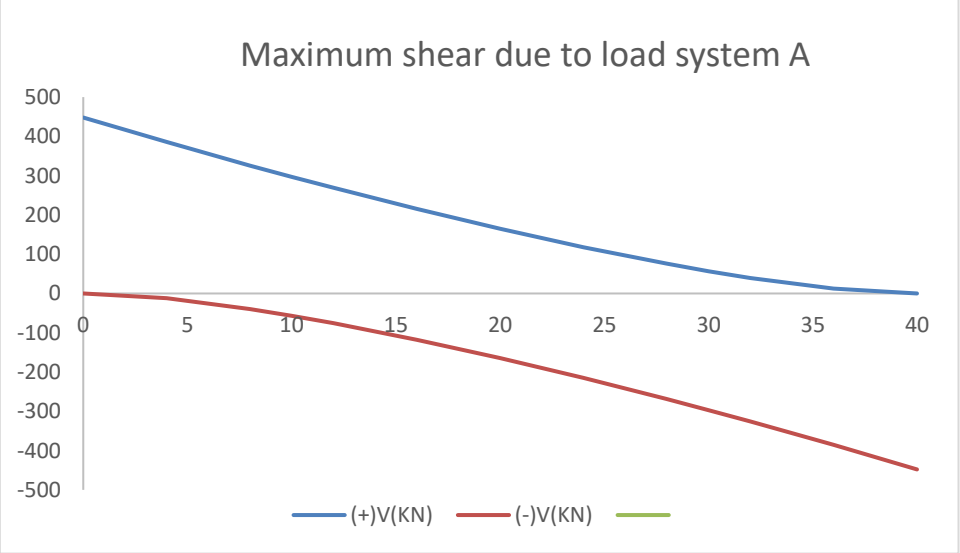

Figure 3.22. Maximum shear due to load system A

Figure 3.20 illustrates the bending moment due to load system Bt.

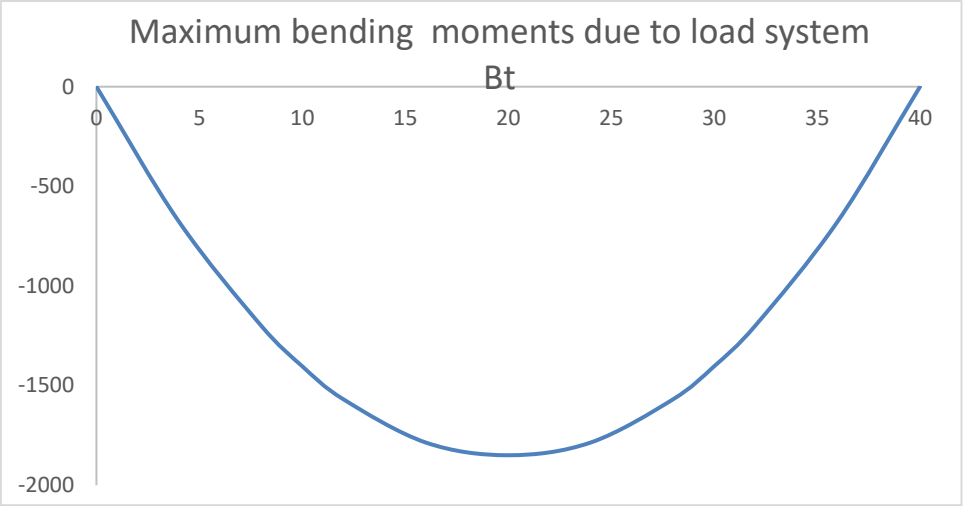

Figure 3.23. Maximum bending moments due to load system Bt

Figure 3.21 illustrates the shear variation due to load system Bt.

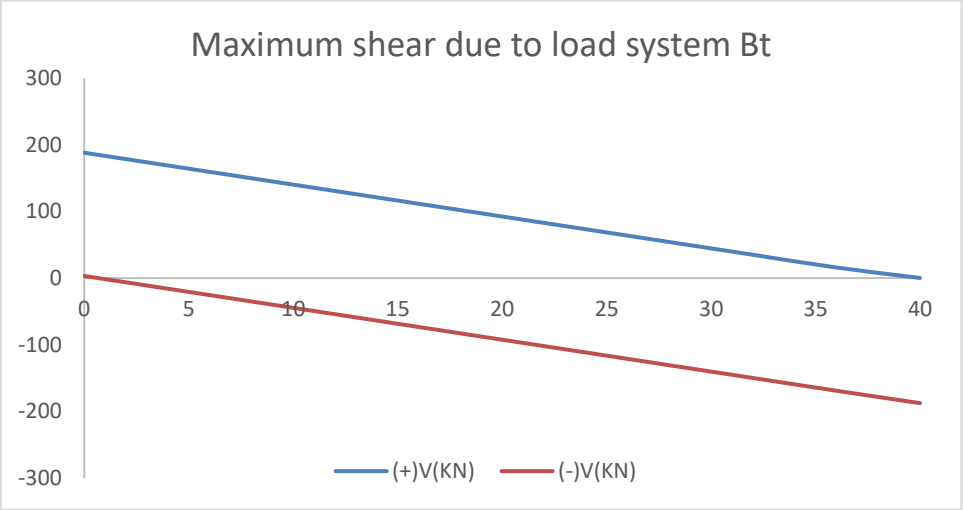

Figure 3.24. Maximum shear due to load system Bt

Figure 3.22 illustrates the bending moment variation due to load system Br.

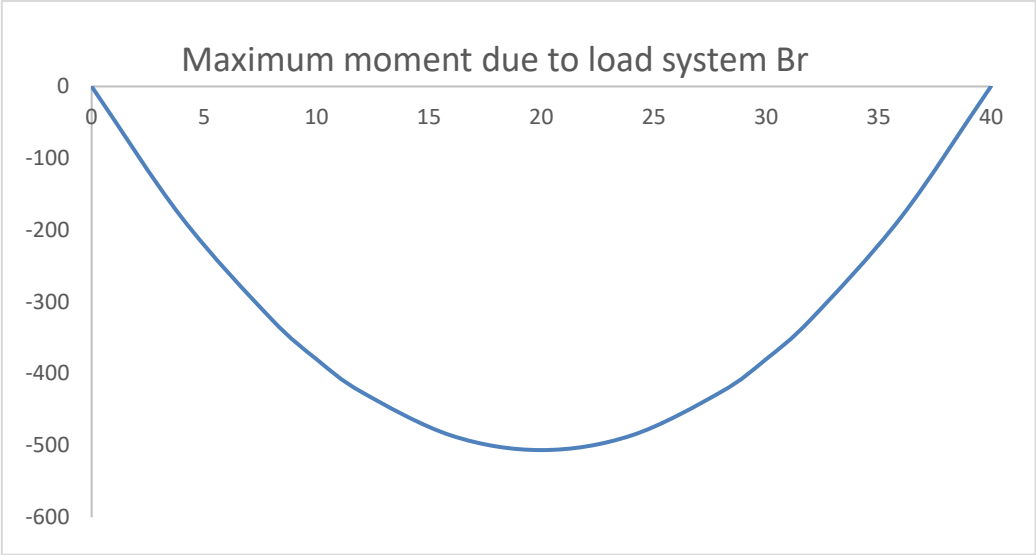

Figure 3.25. Maximum moment due to load system Br

Figure 3.23 illustrates the shear variation due to load system Br.

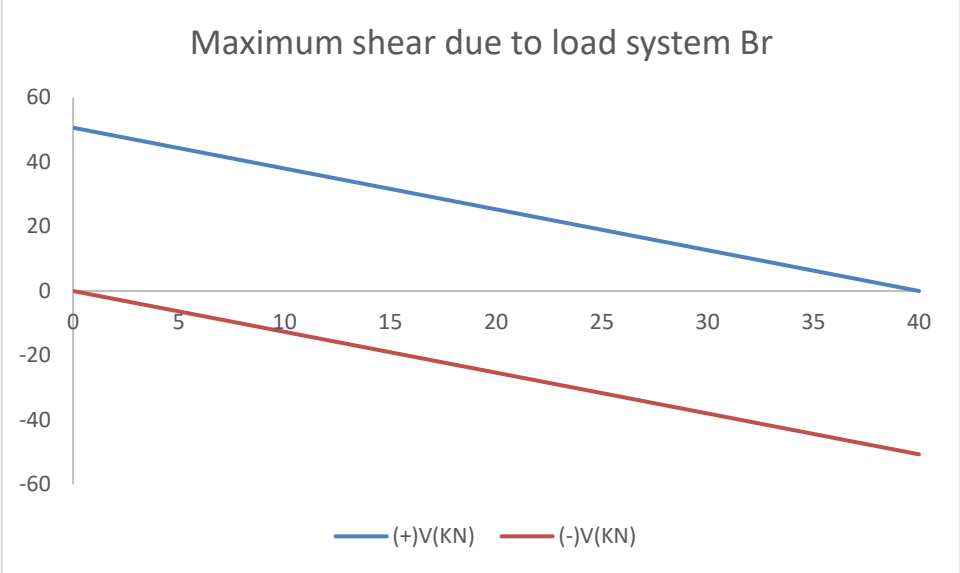

Figure 3.26. Maximum shear due to load system Br

Figure 3.24 illustrates the bending moment variation due to load system LM1.

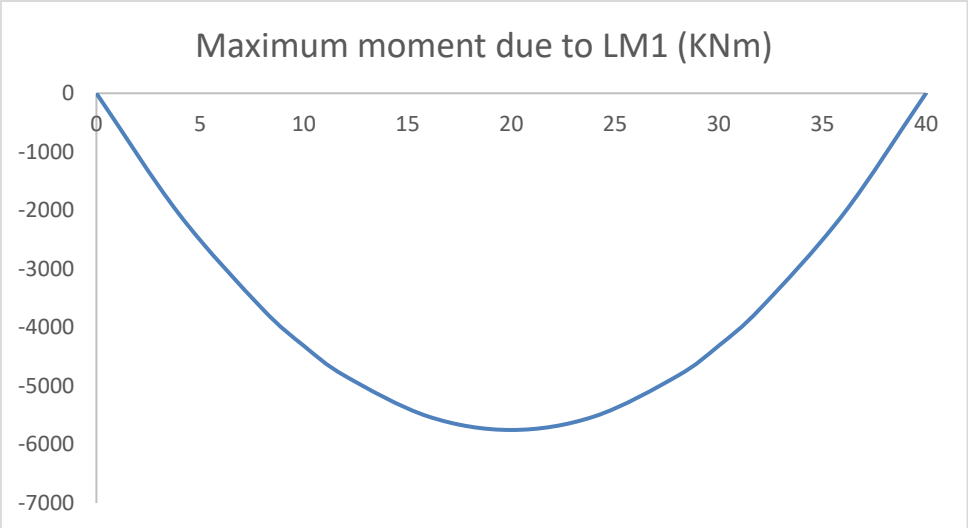

Figure 3.27. Maximum moment due to Load model 1

Figure 3.25 illustrates the shear variation due to load system LM1.

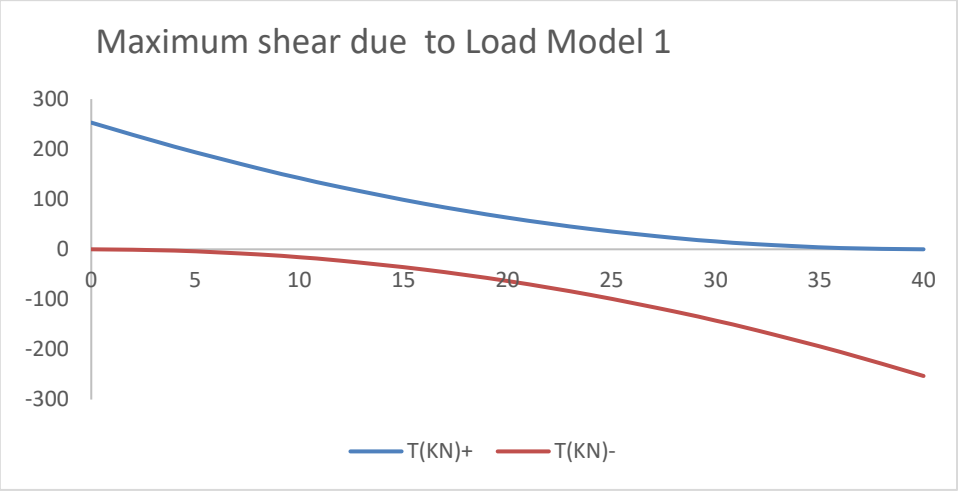

Figure 3.28. Maximum shear due to Load Model 1

The sections of interest are midspan for the bending moment and the support for shear. The unfactored sollicitations are summarized in table 3.39.

Table 3.38. Moment at midspan and shear at support for different loads.

Load	**M(KNm)**	**T(KN)**
LM1	5751.68	260.27
A	4318.11	447.94
Pedestrian loads	233.75	21.48
Beam	7713.5	771.35
Slab +crossbeam precast beam	12120.2	1212.0
Super dead load	3247.37	324.74
Wind Eurocode	244	24.40
Wind BAEL	176.64	17.66

3.6.3. Analytical load combinations

Manual load combinations were done following BAEL and Eurocodes for the calibration of the numerical model.

3.6.3.1. Analytical load combinations following BAEL

The table 3.40 presents the load combination values for manual calculations following Eurocodes.

Table 3.49. Combination values of actions according to BAEL

Moment and shear due to external loads (BAEL)				
SLS Moment midspan (KNm)			ULS Midspan(KNm)	
Traffic+superdead	Selfweight	Selfweight+slab	Selfweight+slab	Traffic+superdead
8664.11	7713,50	12120.22	16362.30	11691.70
SLS Shear at supports (KN)			ULS Shear at supports (KN)	
898.53	771,35	1212.02	1636.23	1215.54

3.6.3.2. Analytical Load combinations Eurocode

The table 3.41 presents the load combination values for manual calculations following Eurocodes.

Table 3.40. Combination values of actions according to Eurocode

Moment and shear due to external loads (Eurocode)				
SLS Moment midspan (KNm)			ULS Midspan(KNm)	
Traffic+superdead	Selfweight	Selfweight+slab	Selfweight+slab	Traffic+superdead
8926.19	7713,50	12120.22	16362.30	12050.36
SLS Shear at the supports (KN)			ULS Shear at the supports (KN)	
585.00	771,35	1212.02	1636.23	789.75

3.7.Numerical results.

3.7.1. Simulation of the bridge

After numerical modelling of the bridge using CSI bridge software the following model given by figure 3.29 was obtained representing the simulation of the Mahe prestressed bridge.

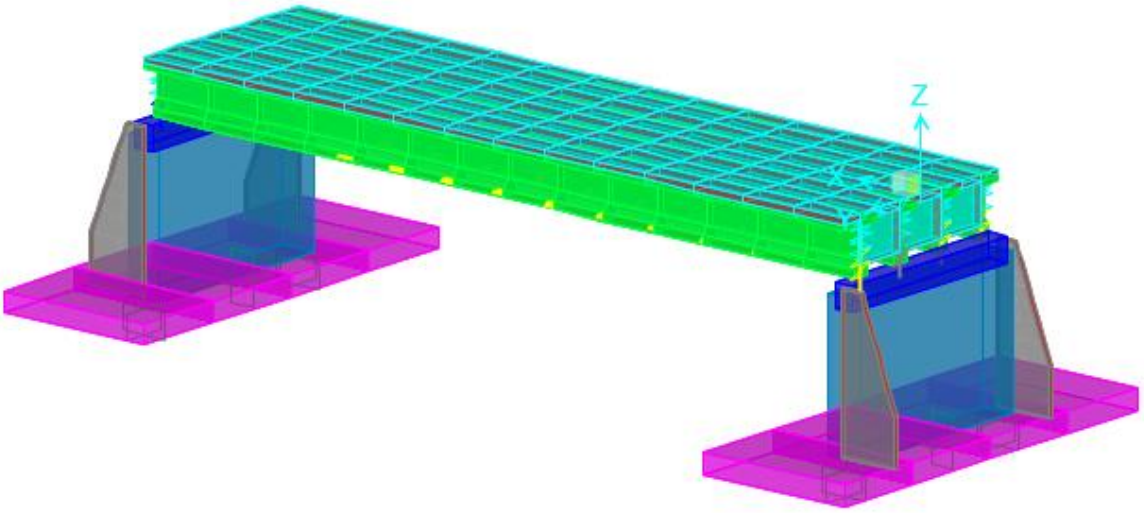

Figure 3.29. Simulation of the Mahe prestressed bridge

3.7.2. Analysis results

The analysis results are the vibration modes from dynamic modal analysis, sollicitation diagrams and load distribution from static analysis.

3.7.2.1. Vibration modes

Six vibration modes were recorded for the bridge. The first mode is translational with a period of 0.42 seconds (figure 3.30). The second mode is vertical with a period of 0.3 seconds

(figure 3.31). The third mode is rotational with a period of 0.28 seconds (figure 3.32).The fourth mode is torsional with a period of 0.25 seconds (figure 3.33).The fifth mode is torsional with a period of 0.16 seconds (figure 3.34) and the sixth mode is transversal flexure with a period of 0.11 seconds (figure 3.35)

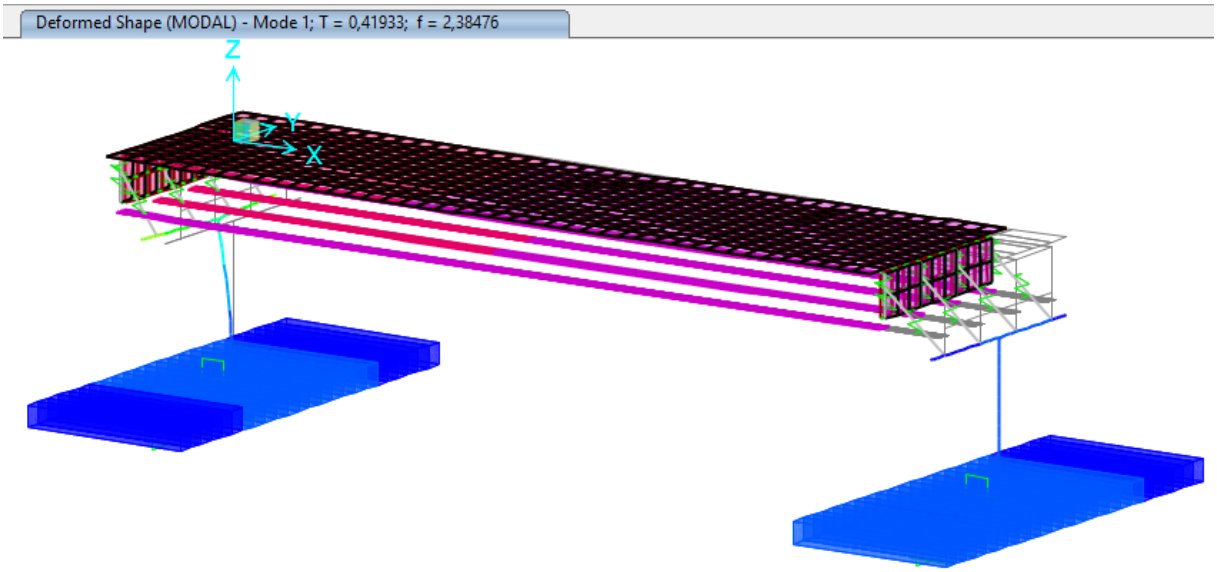

Figure 3.30. First translation vibration mode

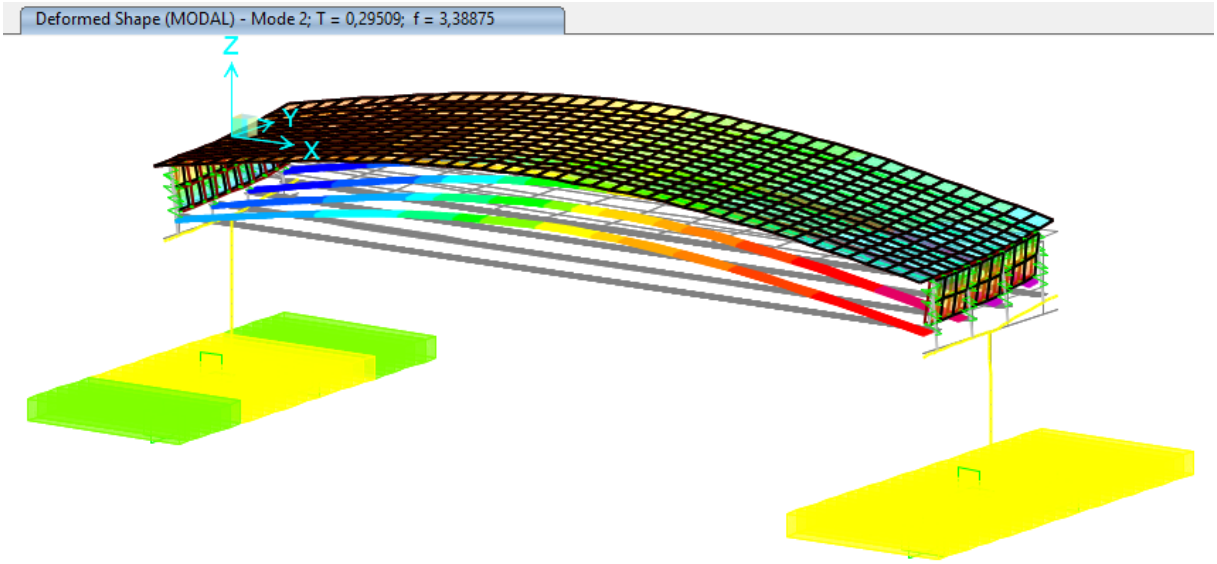

Figure 3.31. First vertical vibration mode

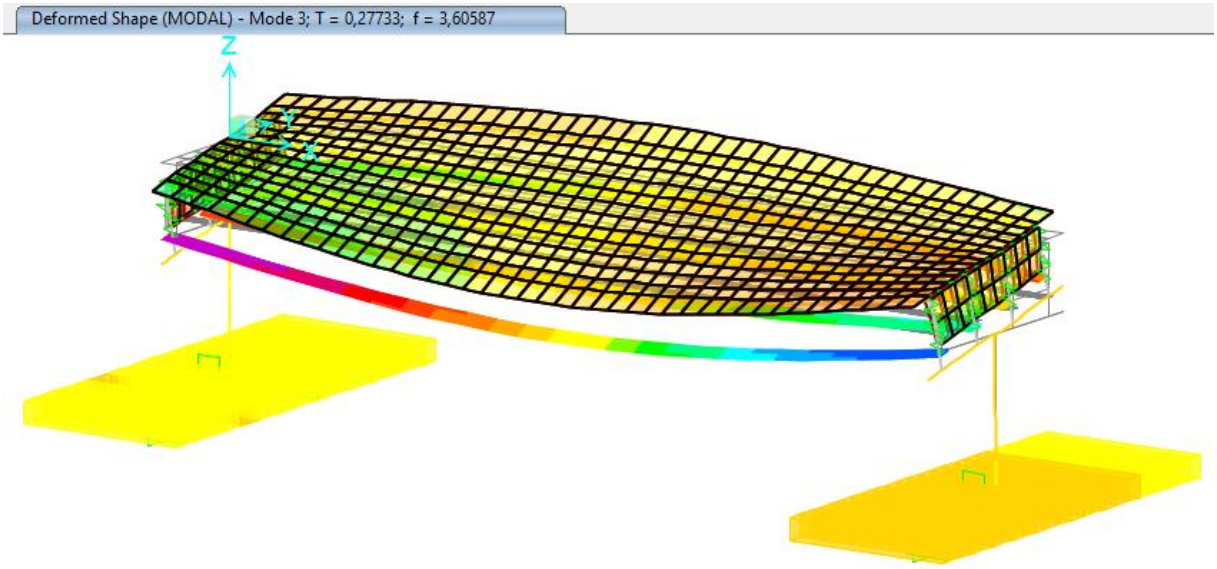

Figure 3.32. First rotation vibration mode

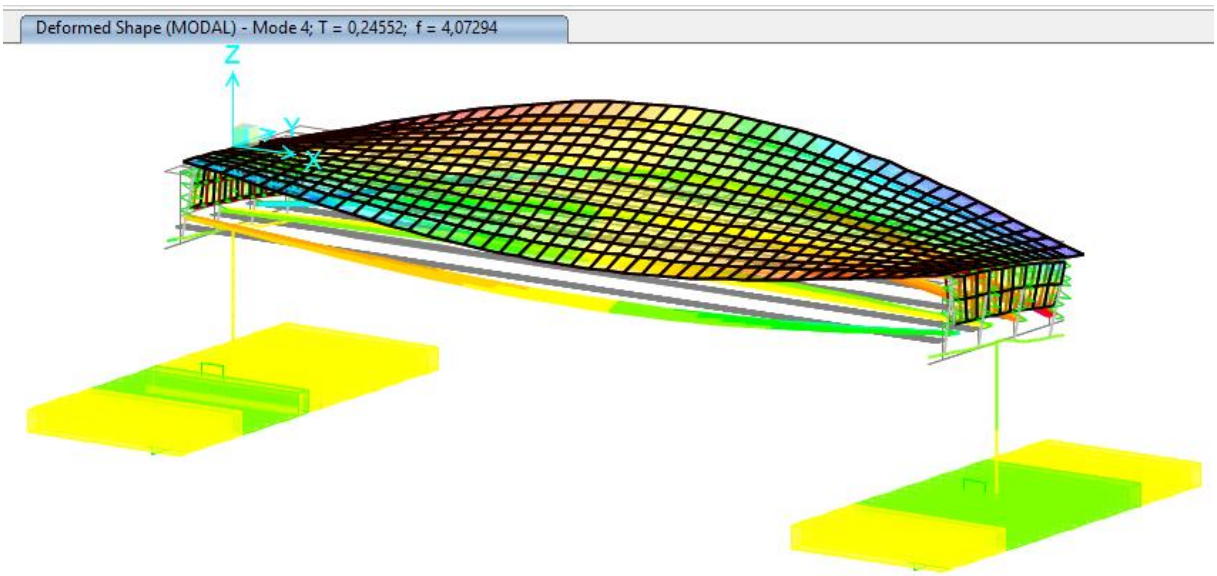

Figure 3.33. First torsion vibration mode

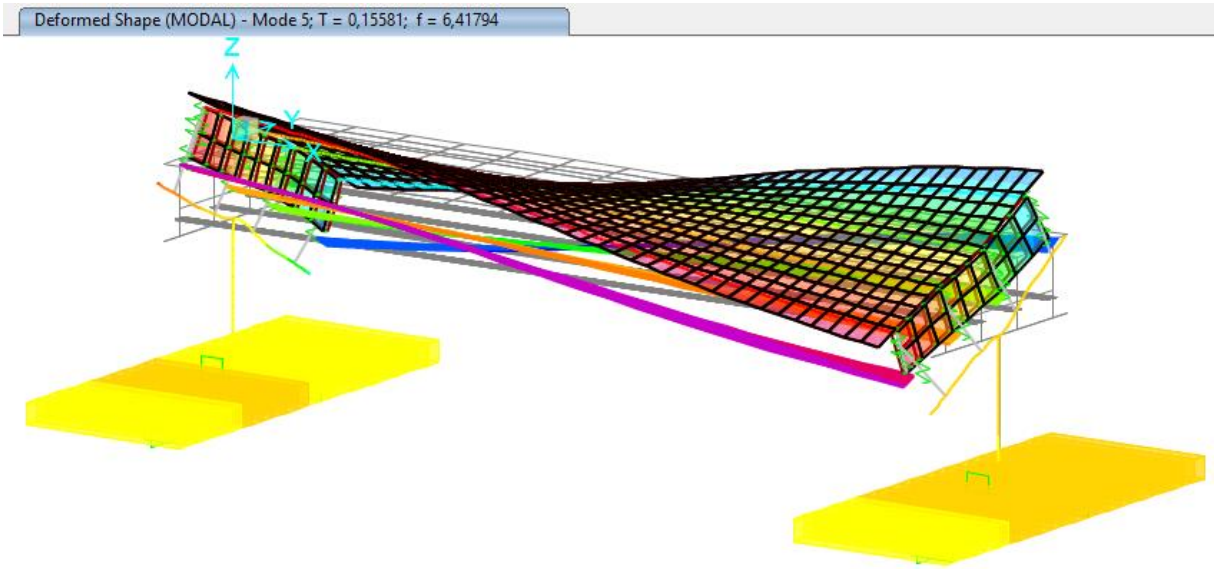

Figure 3.34. Second torsion vibration mode

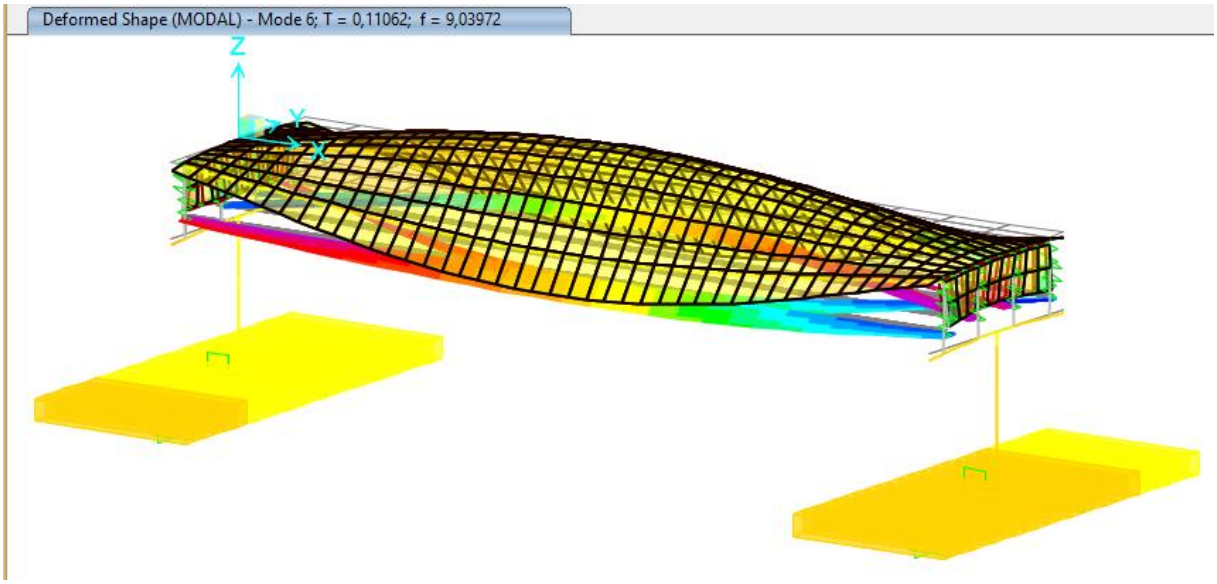

Figure 3.35. First transversal flexure vibration mode

3.7.2.2.Static analysis results

After static analysis the sollicitations in the different beams were obtained .The following diagrams of sollicitations in the edge beam only were represented for simplicity :The moment due to the self-weight of the precast beam (figure 3.36),the shear due to the self-weight of the precast beam(figure 3.37),the moment due to the self-weight of the beam and cast in situ elements (figure 3.38),the shear given by the the self-weight of the beam and cast instu elements (figure 3.39),the moment due to Load model 1(figure 3.40) and the shear due to load model 1(figure 3.41).

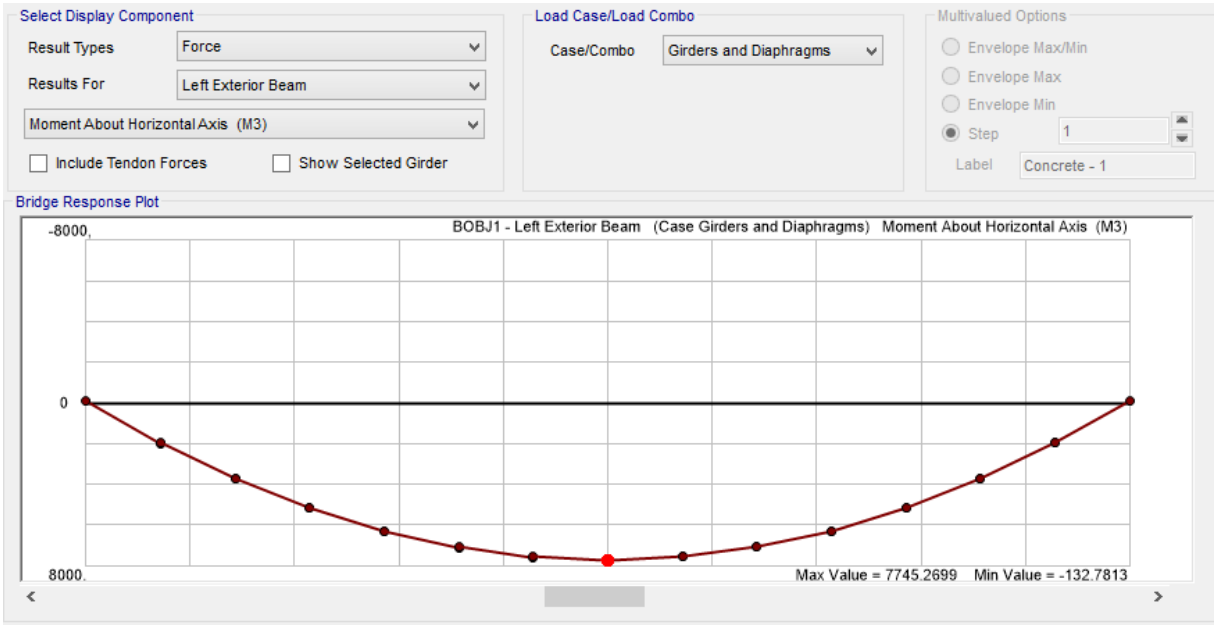

Figure 3.36. Moment due to the self-weight of the precast beam

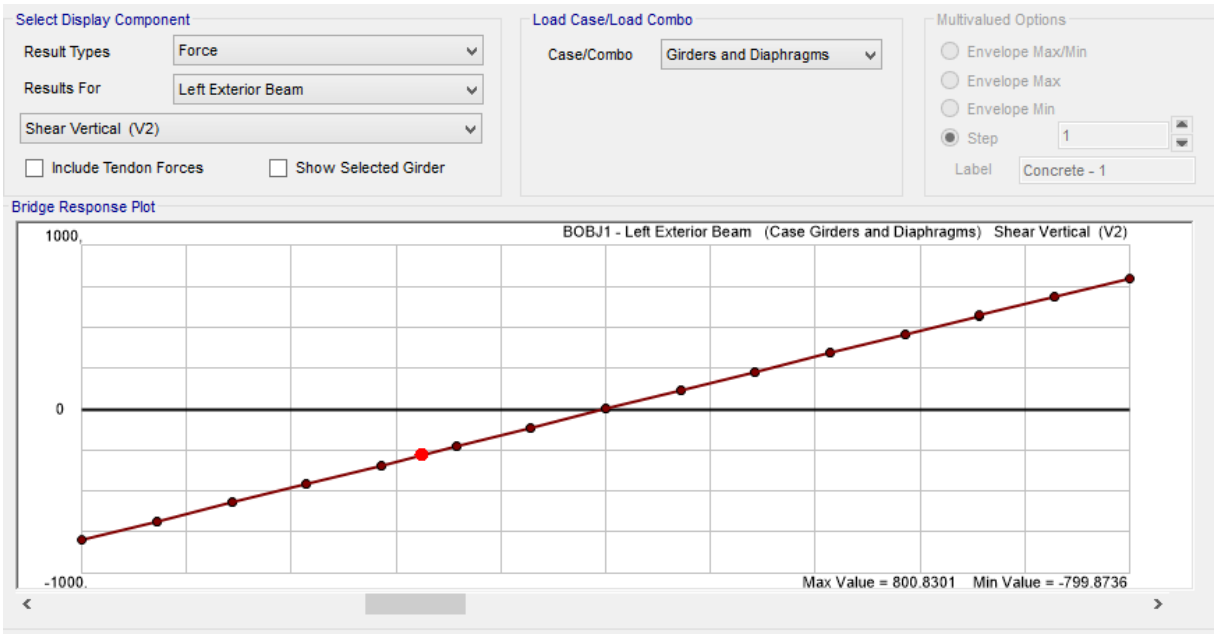

Figure 3.37. Shear due to the self-weight of the precast beam

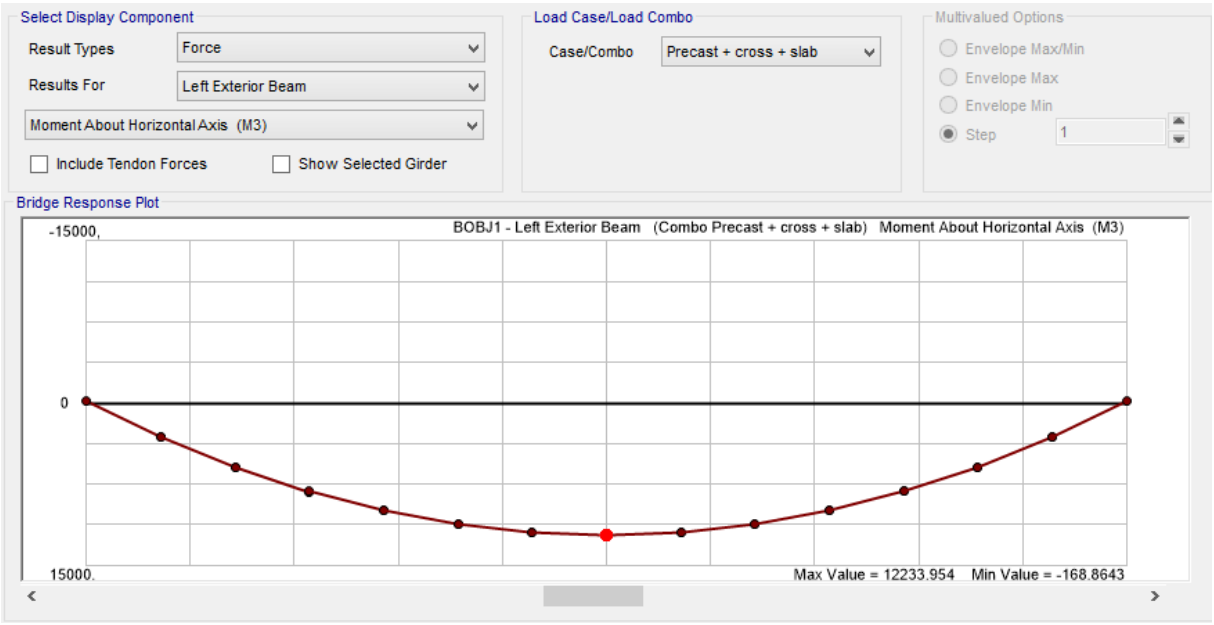

Figure 3.38. Moment due to the self-weight of the beam and the cast in situ elements

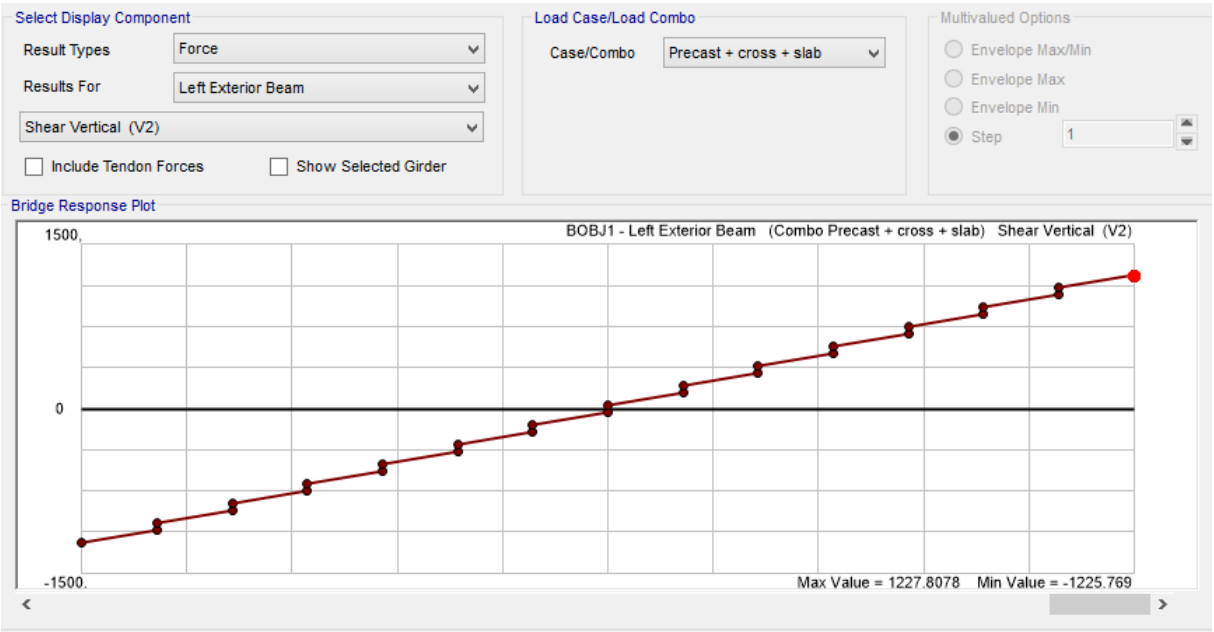

Figure 3.39. Shear due to the self-weight of the beam and the cast in situ elements

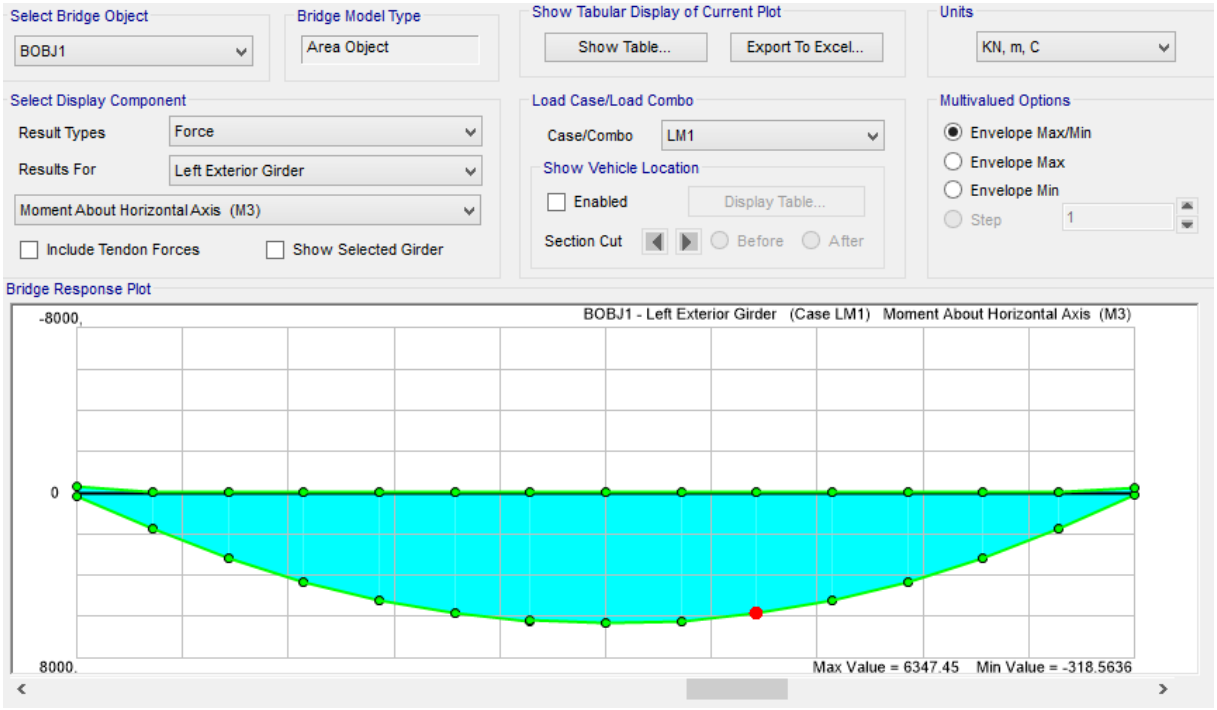

Figure 3.40. Bending moment diagram due to Load model 1

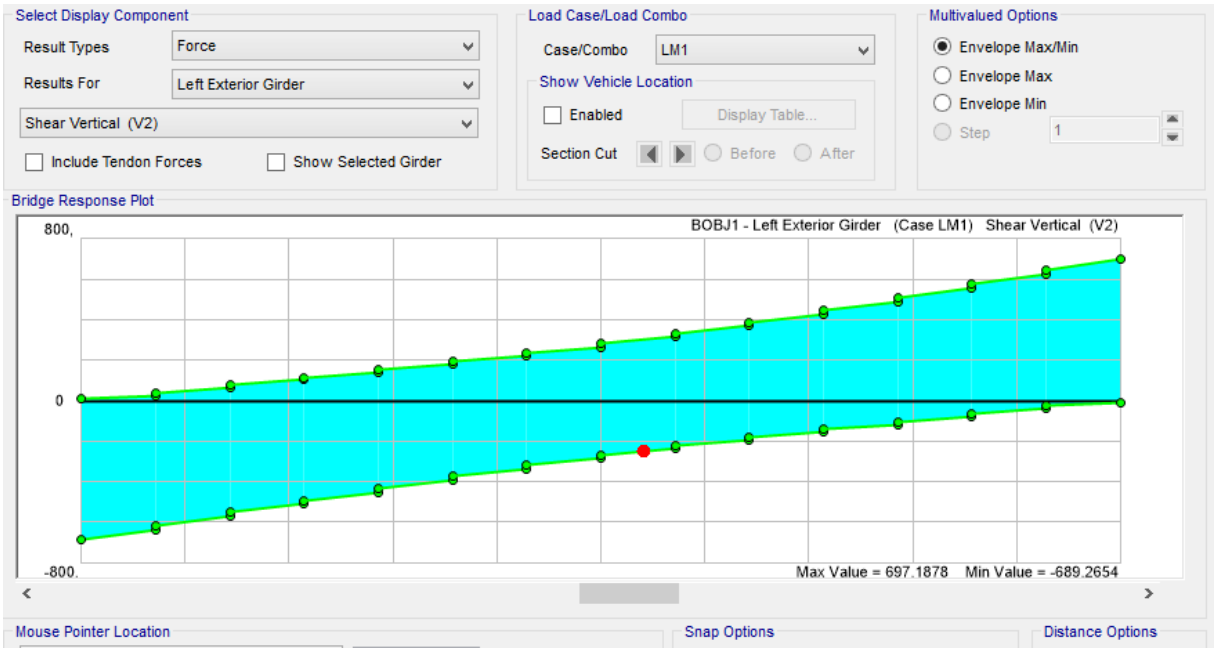

Figure 3.41. Shear diagram due to Load Model 1

The sections of interest are midspan for the bending moment and the support for shear. The unfactored analytical and numerical sollicitations are compared for the calibration of the numerical model of the bridge as summarized in table 3.41. The software obtained moment and shear by finite elements were compared to the manually obtained moment and shear by the Massonet method with the help of histograms given by figure 3.42 and figure 3.43 respectively.

Table 3.42. Moment at midspan and shear at support following Eurocode

Load	**Graph id n°**	**Moment(kNm)** Manual calculation	**Shear(KN)** Manual calculation	**M(kNm)** Software calculation	**T(kN)** Software calculation
LM1	1	5751.68	260.27	6347.45	697.19
Beam	2	7713.50	771.35	7745.27	800.83
Slab +crossbeam precast beam	3	12120.20	1212.00	12233.95	1227.81
Super dead load	4	3247.37	324.74	3532.91	369.73
A	5	4318.11	447.94	3866.39	360.59
Bt	6	1800.00	199.19	2319.59	275.43
Br	7	485.25	52,23	909.71	111.33

Figure 3.39. illustrates the histogram for the comparison of moment values.

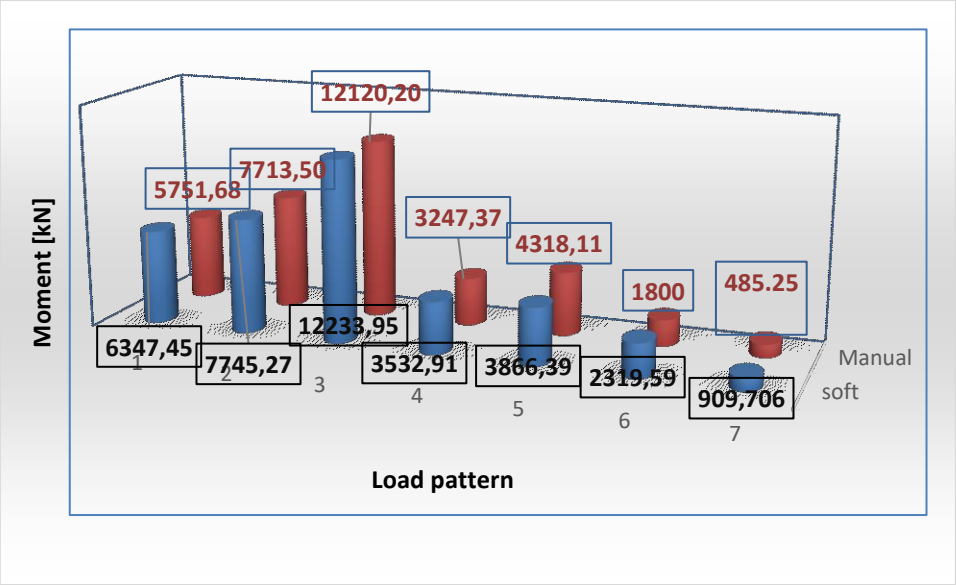

Figure 3.42. Comparison between software and manual calculated moment values

The results show that the software was well calibrated because the software calculated values were followed by manual calculated values.

Figure 3.40 illustrate the histogram for the comparison of shear values.

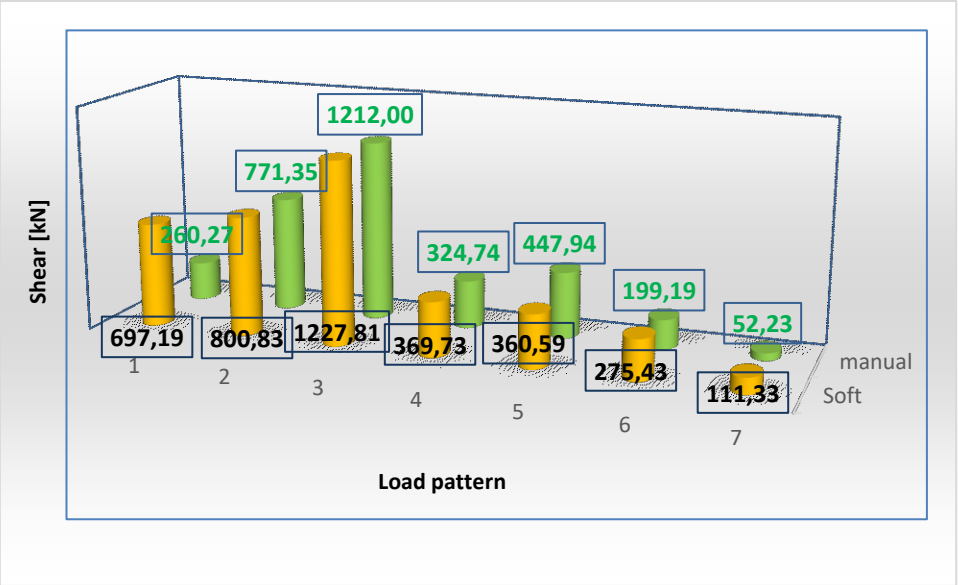

Figure 3.43. Comparison between software values and manual calculated shear values

There is a slight difference between the shear values of the LM1 because of the flexible finite element model support (articulations) compared to the analytical model(restrains). This tends to the increase the sollicitations at support for the structure to resist the actions due to dynamic loading. The results show that the software was well calibrated because most of the software calculated values were confirmed by the manually calculated values.

3.8. Prestressed bar design

In the following section, the prestress bar design will be discussed. Prestressed bar design was done following Eurocode and BAEL norms respectively.

3.8.1. Prestressed bar design according to Eurocode

The prestressed bar design according to Eurocode was done following serviceability limit state and ultimate limit state design.

3.8.1.1. Serviceability limit state design of the prestressed beam

Assuming a loss of prestress of 5 % at transfer and 20% at service, and substituting the necessary parameters in equations 2.20 to 2.21 equations 3.19 and 3.20 are obtained which enable the plot of the Magnel diagrams given by figure 3.44 and figure 3.45.

At the support region only the transfer condition is critical.

$$\text{Line 1: } -64.82 + 0.103e \leq (2.62)\frac{10^8}{P_s} \qquad (3.19)$$

$$\text{Line 2: } -64.82 - 0.112e \leq (-16.81)\frac{10^8}{P_s} \qquad (3.20)$$

At the midspan region, both the transfer condition and service condition are critical.

At transfer equation 3.23 and 3.24 must be satisfied.

$$\text{Line 3: } -64.82 + 0.103e \leq (9.29)\frac{10^8}{P_s} \quad (3.21)$$

$$\text{Line 4: } -64.82 - 0.112e \leq (-24.09)\frac{10^8}{P_s} \quad (3.22)$$

At service equation 3.23 and 3.24 must be satisfied.

$$\text{Line 5: } \leq 64.82 + 0.103e(-10.747)\frac{10^8}{P_s} \quad (3.23)$$

$$\text{Line 6: } 64.82 + 0.103e \leq (-18.54)\frac{10^8}{P_s} \quad (3.24)$$

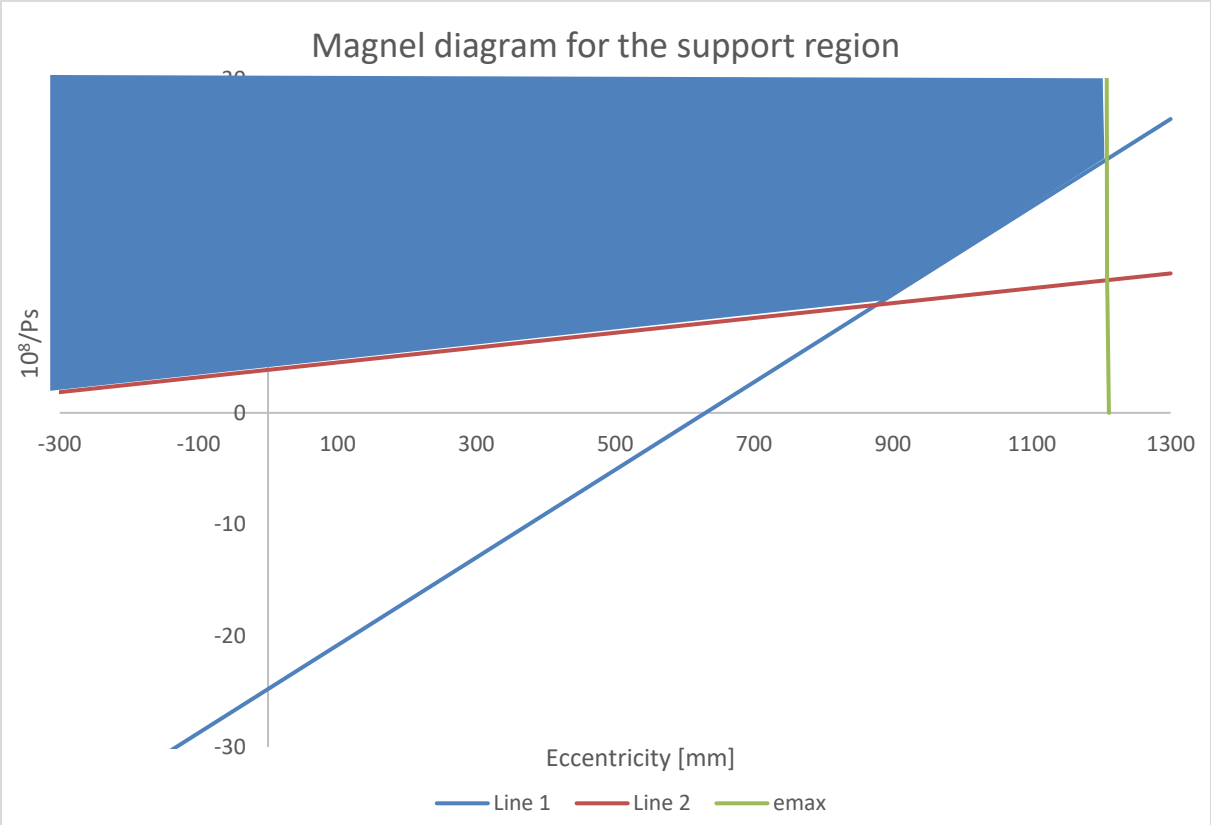

Figure 3.44. Support region Magnel diagram for the beam designed according to Eurocode

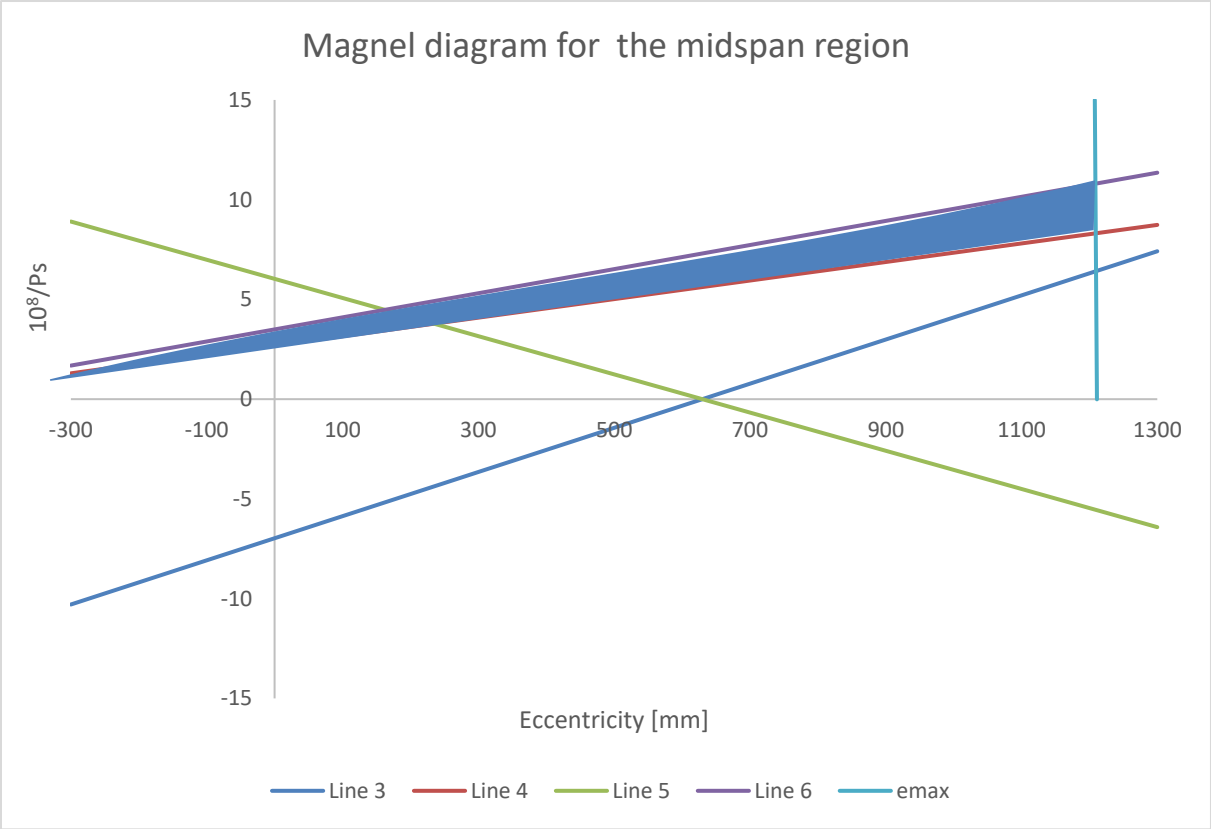

Figure 3.45. Midspan region Magnel diagram for the beam designed according to Eurocode

As for the choice of prestress and eccentricity at midspan region, the design requirements are more critical at midspan than at the supports therefore the prestressing force and eccentricity are determined from the Magnel diagram for the midspan section and debonding is carried out if necessary, at the support. From the Magnel diagram for the midspan section(figure 3.45), the highest value of $\frac{10^8}{P_S}$ is 11 .

The maximum eccentricity $e_{max} = Y_G$ −concrete cover = 1303-40 =1263 mm. An allowance is made for the stirrups and longitudinal reinforcement. So we take $e_{max} = 1200\ mm$.

$$P_S = \frac{10^8}{11} \times 10^{-3} = 9090.91 \text{ kN}$$

Assuming losses of prestress of 20 % at service, prestressing force at Jacking.

$$P_{jack} = \frac{P_S}{0.8} = 11363.6 \text{ kN}$$

For a 15mm unit diameter 7 wire strand with nominal area of $150mm^2$, the maximum permissible load at jacking is about 80 % of the breaking load.

$P_{max} = 0.77 \times P_{break} = 0.77 \times 150 \times 1860 \times 10^{-3} = 214\ kN$

Maximum number of strands $= \frac{P_{jack}}{P_{max}} = \frac{11363.6}{214} = 53.1$ strands $\Longrightarrow$ 54 strands

Prestressing force at jacking per strand $= \frac{P_{jack}}{number\ of\ strands} = \frac{11363.6\ KN}{54} = 210.48$ kN $< P_{max}$

Assuming 54 strands will be provided in the bottom 4 rows in the order 16, 16, 10, 12 the net eccentricity is then calculated.

$e = y_G - \frac{16\times100+16\times150+12\times200+10\times250}{15+15+15+9} = 1138.31$ mm

As for the choice of prestress and eccentricity at the support region from the Magnel diagram for the support section (figure 3.44), the point corresponding to $\frac{10^8}{Ps} = 11$ and e = 1136.46 mm is out of the feasible region. Therefore, debonding is necessary. As a trial if 24 cables are removed from the four layers, 7 from the bottom three and 3 from the top layer,

$e = y_G - \frac{8\times100+8\times150+8\times200+5\times250}{24} = 1135.89$ mm

For 29 cables, $P_S = 4882.15$ KN $\Rightarrow \frac{10^8}{P_s} = 20.48$ the point (1135.89, 20.48) lies in the feasible region of the Magnel diagram at the support.

The prestress force and eccentricity obtained in the previous calculations were obtained based on the assumption that a 5 % loss of prestress occurs at transfer and 20 % at service. It is necessary to evaluate the actual loss of prestress before carrying out the stress verifications. The prestressing force and eccentricity vary between the supports and midspan so we evaluated the prestress losses at both sect ions. From the results obtained in table 3.46 and table 3.47, the assumed loss of prestress is not exceeded at any section.

The percentage debonding exceeds the 15 percent limit but with the formation of cracks can be avoided by terminating the debonding at sections one debonded length apart(Okumus & Oliva, 2014). Having obtained the number of debonded strands at the support, the variation of fibre stress along the girder was plotted before debonding to determine the points where debonding can be terminated as shown in figure 3.46.

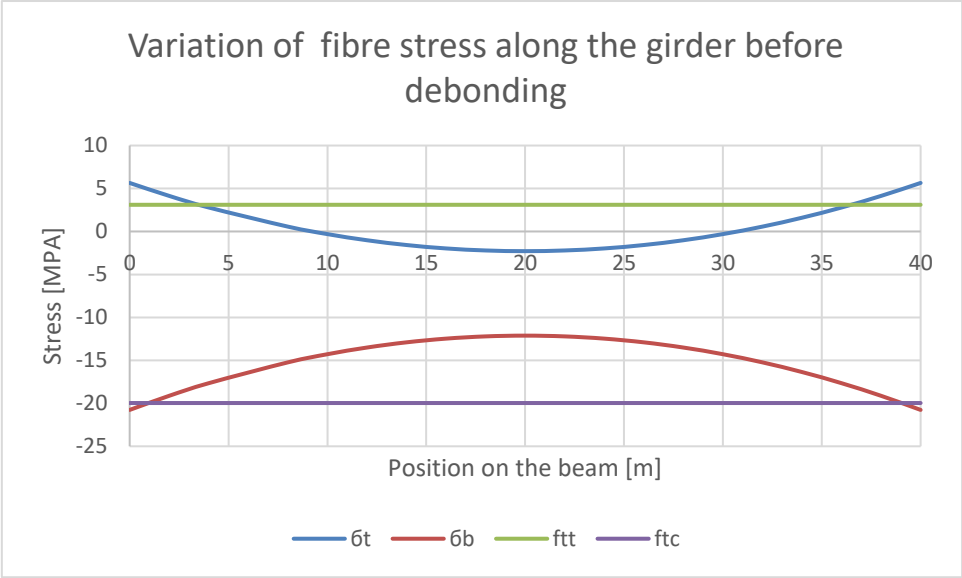

Figure 3.46. Variation of fibre stress along the girder for the transfer condition

The debonding length was determined using equation 3.25

$$l_{pt} = \alpha_1 \alpha_2 \phi \sigma_{pm0} / f_{bpt} \quad (3.25)$$

Where:

α_1 is a coefficient that depends on the method of release of the tendon. α_1=1for gradual release

α_2 is a coefficient that depends on the type of strands. α_2=0.19 for seven wire strands

ϕ is the nominal diameter of the tendon

σ_{pm0} is the tendon stress just after release

f_{bpt} is the bond stress

$f_{bpt} = \eta_{p2} \eta_1 f_{ctd}$

$f_{bpt} = \eta_{p2} \eta_1 f_{ctd}$ = 3.2× 1× 1.88 =6.045 MPa

$l_{pt} = \alpha_1 \alpha_2 \phi \sigma_{pm0} / f_{bpt}$ = (1× 0.19 × 15 × 1332.77)/6.045 =502.6 mm

By terminating the debonding 6 of the strands at 0.5 m intervals from the support, the stress obtained at the different sections now satisfies the stress limitations as detailed in (table 3.42) Having obtained a debonding pattern the effective prestressing force has to be determined and to be determined and to do so,the immediate prestress losses and the long term prestress losses at support and midspan sections were computed as given in table 3.43 and 3.44 respectively.

Table 3.42. Variation of fibre stress along the girder after debonding

Distance from support	0,0	1,0	2,0	2,5	3,0	3,5	4,0
Prestress axial(Mpa)	-3,6	-3,6	-4,4	-5,2	-5,4	-6,2	-7,0
Prestress top (Mpa)	6,6	6,6	8,0	9,4	9,8	11,2	12,6
Prestress bottom (Mpa)	-7,1	-7,1	-8,7	-10,2	-10,7	-12,2	-13,8
$M_{selweight\ top}$ (Mpa)	0,0	-0,8	-1,5	-1,9	-2,2	-2,5	-2,9
$M_{selweight\ bottom}$ (Mpa)	0,0	0,8	1,6	2,0	2,4	2,8	3,1
Бt (Mpa)	2,9	2,2	2,0	2,3	2,2	2,5	2,8
Бb (Mpa)	-10,8	-9,9	-11,4	-13,4	-13,8	-15,7	-17,7

Table 3.43. Immediate losses at the support and midspan sections

Immediate losses			
	Support	midspan	Units
$E_{cm,0}$	33661,4915	33661,4915	MPa
P_s	5797.56	10795.45	KN
e	1135,89	1138.31	mm
A_p	4350	8100,00	mm2
$M_{Selfweight}$	-	7713,5	KNm
σ_{cp}	-10,19	-11,47	Mpa
ΔP_{el}	-263.33	-552.24	KN
Required P_{jack}	6060.89	11347.7	KN
Prestress loss	**-4,32**	**4,86**	%

Table 3.44. Long term losses at the support and midspan sections

	Support	Midspan	Units
E_{cm}	36283,19	36283,19	Mpa
P_{jack}	6094.13	11347.7	KN
σ_{pi}	1400,95	1400,95	KN
f_{pk}	1860,00	1860,00	MPa
μ	0,75	0,75	
t	500000	500000	hours
ρ1000	2,50	2,50	
$\Delta\sigma_{cp,r}$	-69,21	-69,21	Mpa
M_{slab}	-	4406,72	
$M_{superdead}$	-	3247,37	
σ_{cQP}	-10,	-5,34	MPa
$\Delta\sigma p_{c+s+r}$	-152	-140,79	MPa
Long term loss	-661.2	-1140.38	kN
Ps after losses	5136.36	9655.07	kN
percentage loss	15,25	14,91	%

To confirm the results obtained with the Magnel diagram, the resulting stresses due to the prestressing force after losses, traffic loads, self-weight and super dead loads in every section were computed and the total stress verified not to exceed the permissible stresses at transfer and service conditions as summarized by table 3.46 and table 3.47

Table 3.46. Stress verification at transfer

Section	**Stress**	**Prestress (KN)**	**Eccentricity (mm)**	**Prestressing(Mpa)**		**Selfweight (Mpa)**	**Total (Mpa)**
				Axial	Moment		
support	Ϭt	5797.56	1135.89	-3,76	6,78	0,00	3,02
	Ϭb	5797.56	1135.89	-3,76	-7,38	0,00	-11,14
Midspan	Ϭt	10795,45	1138.31	-7,00	12,64	-7,94	-2,29
	Ϭb	10795,45	1138.31	-7,00	-13,77	8,64	-12,12

Table 3.47. Stress verification at service

Section	Stress	Prestress (KN)	Eccentricity (mm)	Prestressing(Mpa)		Selfweight (Mpa)	Traffic (Mpa)	Total (Mpa)
				Axial	Moment			
Support	Ϭt	5136.36	1135.89	-3,33	6,00	0,00	0,00	2,75
	Ϭb	5136.36	1135.89	-3,33	-6,54	0,00	0,00	-10,18
Midspan	Ϭt	9655.07	1138.31	-6,26	11,31	-12,47	-7,59	-15,01
	Ϭb	9655.07	1138.31	-6,26	-12,31	13,58	7,59	2.60

For the characteristic combination,

σ = -15.01+ (0.6 × −0.63) =-15.388 Mpa $< 0.6f_{ck}$ = 27 Mpa

For the quasi permanent condition,

σ = -15.01+ (0.5 × −0.63) =15.325 Mpa $< 0.45f_{ck}$ = 20.25 Mpa

3.8.1.2. Ultimate limit state design for bending

The ultimate limit moment capacity of the beam shall be determined as discussed in section by the strain compatibility method. Due to the complex geometry of the section the position of the neutral axis was be determined by a trial and error procedure. Table 3.48 shows the calculation of the resisting moment of the section.

Using a rectangular stress block ,λ=0.8 ,ε_{cu3}=3.5 × 10^{-3} for $f_{ck} \leq$ 50Mpa

$f_{cd} = \frac{45}{1.5}$= 30 MPa.

ηf_{cd}=30 MPa.

For steel, the prestressing force, P_s = 9655 kN

f_{pd}= 1424 Mpa

Area of steel =150 mm^2

The stress due to the prestressing force in the strands, P_s/Area of 54 strands =1332.77 Mpa

For the slab λ=0.8, ηf_{cd}= 23.3 MPa, ε_{cu3}=3.5 × 10^{-3}

The table 3.48 summarizes the calculation of resisting moment of the girder section.

Table 3.48. Calculation of resisting moment of the girder section

Young modulus of steel	Es	200000	Mpa
Width of Collaborating slab	bf	2500	mm
Height of slab	hf	300	mm
Total tensile force	T	11528,77	kN
Neutral axis	x	247,04	mm
Effective depth	d	2635,19	mm
Lever arm	z	2536,37	mm
Resisting moment	**Mu**	**29241,18**	**kNm**

From table 3.40, $M_{ED} = 28\,,632\ kNm <$ 29,241.18 kNm so the section verifies at ULS

3.8.1.3. Ultimate limit state design for shear

The resistance of the section to shear without reinforcement and with reinforcement are detailed in table 3.49 and table 3.50 respectively. From the results obtained,12 mm shear links can be provided at a spacing of 130 mm to resist shear at the support.

Table 3.49. Calculation of resistance of section without shear reinforcement

Resistance of section without reinforcement		
f_{ctd}	1,77	Mpa
Y_{comp}	1725,33	mm
Y_{beam}	1303,13	mm
σ_{cp}	1,21	MPa
τ	2,05	MPa
V_{dead}	1636,23	kN
τ_{dead}	1,23	MPa
V_{live}	811,71	KN
τ_{live}	1,99	MPa
α	0,41	
V_{ED}	2125,41	KN
$V_{RD.c}$	1970,64	KN

Table 3.50. Resistance of section with reinforcement

Resistance of section with reinforcement		
θ	6,8	°
z	2536,4	mm
σ_c	18,5	MPa
b_w	350,0	mm
V_{rdmax}	7341,1	KN
f_{ywk}	355,0	MPa
f_{ywd}	308,7	MPa
Φ	12,0	mm
A_{sw}	226,3	mm2
s	130,0	mm
S_{max}	1976,4	mm
V_{rds}	2194,2	KN

The deflection at transfer and at service were calculated using the curvature of the beam. Table 3.51 summarizes the calculation of the deflection at transfer and at service.From the results obtained,a deflection of 25 mm is obtained at transfer which is tolerable for most applications and the deflection under quasi permanent conditions does not exceed L/250 =160 mm,hence the deflection is verified.

Table 3.51. Calculation of deflection at transfer and at service

At transfer		
$K_{support}$	-1,7E-07	mm-1
$K_{midspan}$	-1,2E-07	mm-1
Y_t	-2,5E+01	mm (↑)
At service		
Support		
$K_{support}$	-7,9E-08	mm-1
$K_{cc,s}$	-1,1E-07	mm-1
K_{st}	-1,9E-07	mm-1
midspan		
$K_{midspan}$	3,3E-07	mm-1

$K_{cc,m}$	4,2E-07	mm-1
K_{mt}	7,5E-07	mm-1
Ys	119,4561924	mm (↓)

3.8.2. Prestressed bar design according to BAEL

The same method used to design the prestressed bars according to Eurocode was used to design the prestress girders according to BPEL however the permissible stress at transfer and service conditions differ between both norms and have to be recalculated.

3.8.2.1.Serviceability limit state design of the prestressed beam

The serviceability limit state design is done by plotting Magnel diagrams and by choosing an appropriate point in the feasible region of the Magnel diagram. From the Magnel equations and considering the stress limitations we obtained the Magnel diagram for the prestressed beam at the support and midspan region given by figure 3.47 and 3.48 respectively.

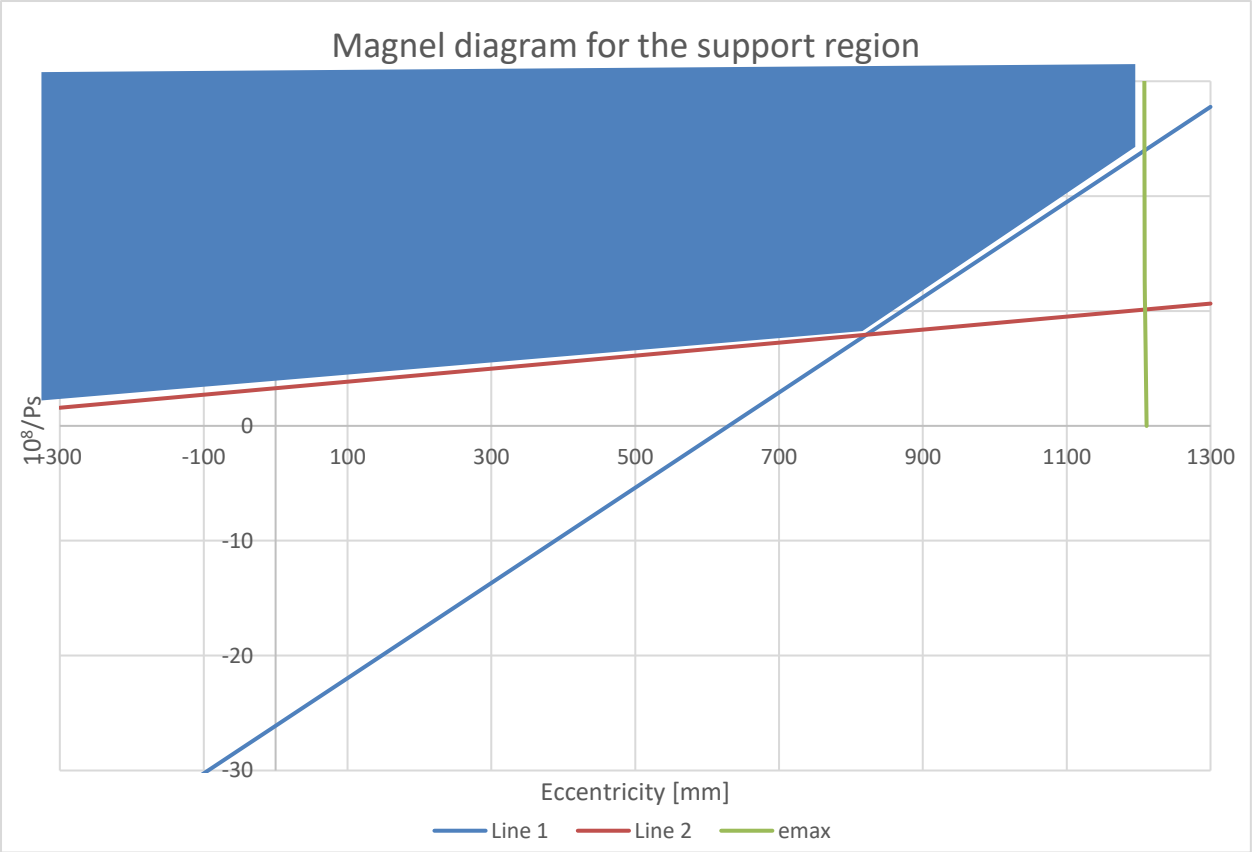

Figure 3.47. Support region Magnel diagram for the beam designed according to BAEL

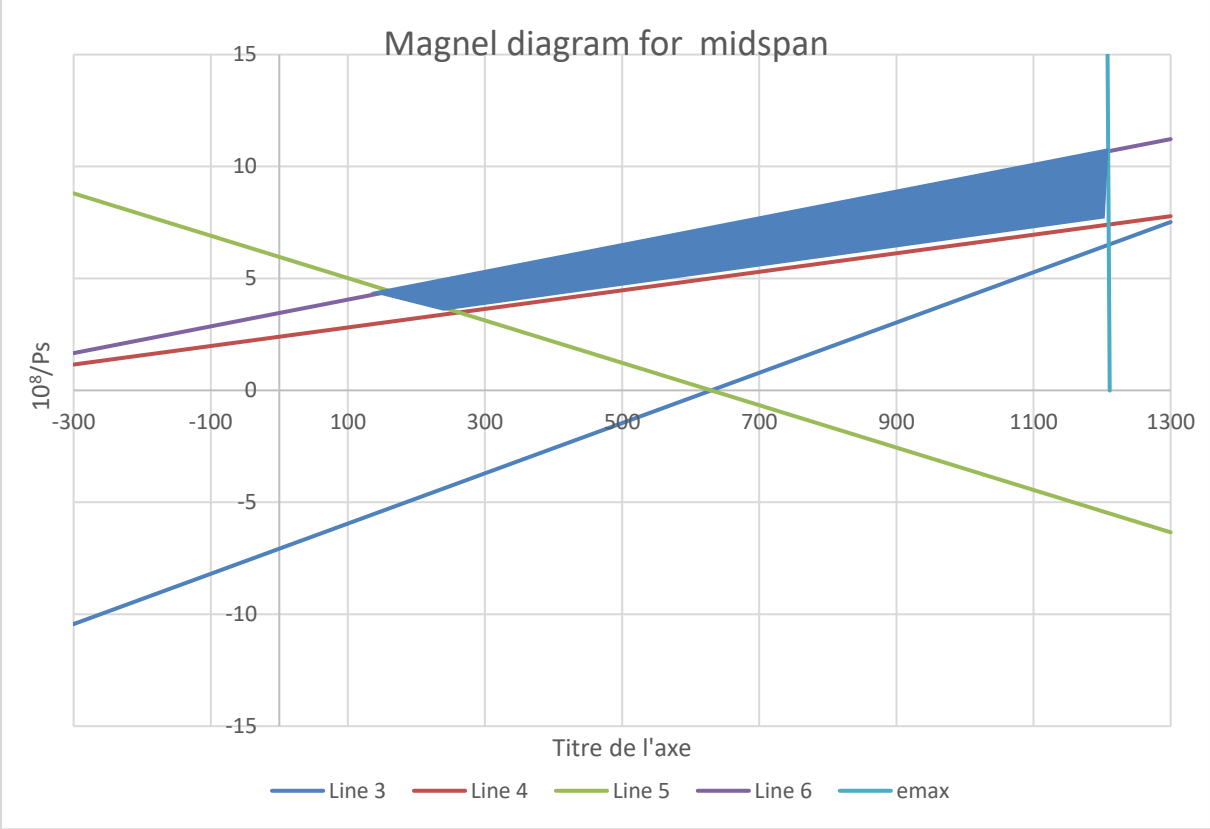

Figure 3.48. Midspan region Magnel diagram for the beam designed according to BAEL

A prestressing force P_s=9259.26 KN and an eccentricity e =1135.27 mm was obtained for the midspan section with 56 strands. At the support region, a prestressing force P_s = 4629.62 KN and an eccentricity e =1135.271 mm with 28 strands making a percentage of debonding of 50 %.This is far above the recommended value for debonding. The stress verification indicates that the stress is verified in all sections. The effective prestressing force has to be determined and to be determined and to do so,the immediate prestress losses and the long term prestress losses at support and midspan sections were computed as given in table 3.52 and 3.53 respectively.

Table 3.52 summarizes the immediate losses at support and midspan sections.

Table 3.52. Immediate losses at the support and midspan sections

Immediate losses			
	Support	Midspan	
$E_{cm,0}$	33661,49	33661,49	MPa
P_s	5497,69	10995,37	kN
e	1135,27	1135,27	mm
A_p	4200,00	8400,00	mm2
$M_{Selfweight}$	-	7713,50	kNm
σ_{cp}	-9,66	-11,78	Mpa
ΔP_{el}	-240,94	-588,02	kN
Required P_{jack}	5738,62	11583,39	kN
Prestress loss	4,16	5,08	%

Table 3.53. Long term losses at the support and midspan sections

Long term losses			
	Support	Midspan	Units
E_{cm}	36283,19	36283,19	Mpa
P_{jack}	5791,70	11583,39	KN
σ_{pi}	1378,98	1378,98	KN
f_{pk}	1860,00	1860,00	MPa
μ	0,74	0,74	
t	500000	500000	hours
ρ1000	2,50	2,50	
$\Delta\sigma_{cp,r}$	-64,65	-64,65	Mpa
M_{slab}		4406,72	
$M_{superdead}$		3247,37	
σ_{cQP}	-9,66	-5,68	MPa
$\Delta\sigma p_{c+s+r}$	55,17	55,17	MPa
Long term loss	-146,23	-139,92	KN
Ps after losses	-614,17	-1175,32	KN
percentage loss	4883,51	9820,05	%
	14,90	15,22	

The stress verifications were carried out after obtaining the prestressing force after all losses. The results of stress verification at transfer are summarized in table 3.54.for the transfer condition and table 3.55 for the service condition.

Table 3.54. Stress verification at transfer

		Prestress	eccentricity	Prestressing		Selfweight	Total
		KN	mm	comp	moment		
support	σt	5497,685	1135,271	-3,56	6,42	0	2,86
	σb	5497,685	1135,271	-3,56	-6,99	0	-10,56
Midspan	σt	10995,37	1135,271	-7,13	12,84	-7,93661	-2,22
	σb	10995,37	1135,271	-7,13	-13,98	8,641213	-12,47

Table 3.55. Stress verification at service

		Prestress	eccentricity	Prestressing		Selfweight	Traffic	Total
		KN	mm	comp	moment			
Support	σt	4883,5	1135,3	-3,17	5,70	0,00	0,00	2,54
	σb	4883,5	1135,3	-3,17	-6,21	0,00	0,00	-9,38
Midspan	σt	9820,1	1135,3	-6,37	11,47	-12,47	-7,31	-14,67
	σb	9820,1	1135,3	-6,37	-12,49	13,58	7,31	2,03

3.8.2.2. Ultimate limit state design for bending

The ultimate limit moment capacity of the beam shall be determined as discussed in section by the strain compatibility method. Due to the complex geometry of the section the position of the neutral axis was be determined by a trial-and-error procedure. Table 3.56 shows the calculation of the resisting moment of the section.

Table 3.56. Resisting moment of the girder section.

Young modulus of steel	Es	200000	Mpa
Width of collaborating slab	bf	2500	mm
Height of slab	hf	300	mm
Total tensile force	T	11955,76	kN
Neutral axis	x	301,41	mm
Effective depth	d	2632,14	mm
Lever arm	z	2511,58	mm
Resisting moment	Mu	30027,85	kNm

The deflection at transfer and at service were calculated using the curvature of the beam. Table 3.57 summarizes the calculation of the deflection at transfer and at service

Table 3.57. Calculation of deflection at transfer and at service

At transfer		
$K_{support}$	-1,6E-07	mm^{-1}
$K_{midspan}$	-1,2E-07	mm^{-1}
Y_t	-2,6E+01	mm (↑)
At service		
Support		
$K_{support}$	-1,3E-07	mm^{-1}
$K_{cc,s}$	-1,8E-07	mm^{-1}
K_{st}	-3,1E-07	mm^{-1}
midspan		
$K_{midspan}$	3,3E-07	mm^{-1}
$K_{cc,m}$	4,2E-07	mm^{-1}
K_{mt}	7,5E-07	mm^{-1}
Ys	114,966	mm (↓)

3.8.3. Detailing

Before a comparative study can be made, it is necessary to summarize the results obtained. A synthesis of the results obtained following the design of prestress bar according to Eurocode and BAEL was made as given by table 3.58

Table 3.58. Synthesis of the results obtained between Eurocode and BAEL

	Eurocode	BAEL
Number of strands	54	56
Effective prestressing midspan(kN)	9550.70	9820.05
Eccentricity (mm)	1138.31	1135.271
Deformation (mm)	115.06	114.97
Maximum traffic load Moment (kNm)	5751.68	5416.74
Moment M_{ED} (kNm)	28632.263	28212.98
Maximum moment M_{RD} (kNm)	29241.18	30027.85
Safety factor.	1.02	1.06

Having obtained the prestressing force, the number of strands and eccentricities, the detailing of the prestressed beams was drawn using Autocad software. The detailed section for the Eurocode design for the support and midspan region is given by figure 3.49 and figure 3.50 respectively while the detailed section for the BAEL design is given by figure 3.51 and 3.52 respectively. Having obtained a debonding pattern satisfying the stress limitations, the tendon profile was made for the beam designed according to Eurocode as given by figure 3.53.

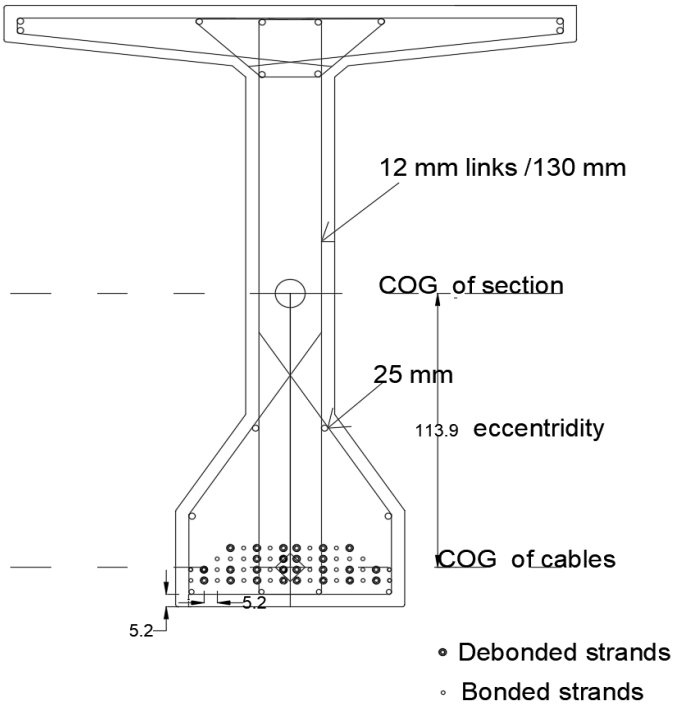

Figure 3.49. Detailed section for the precast beam at supports for the Eurocode design.

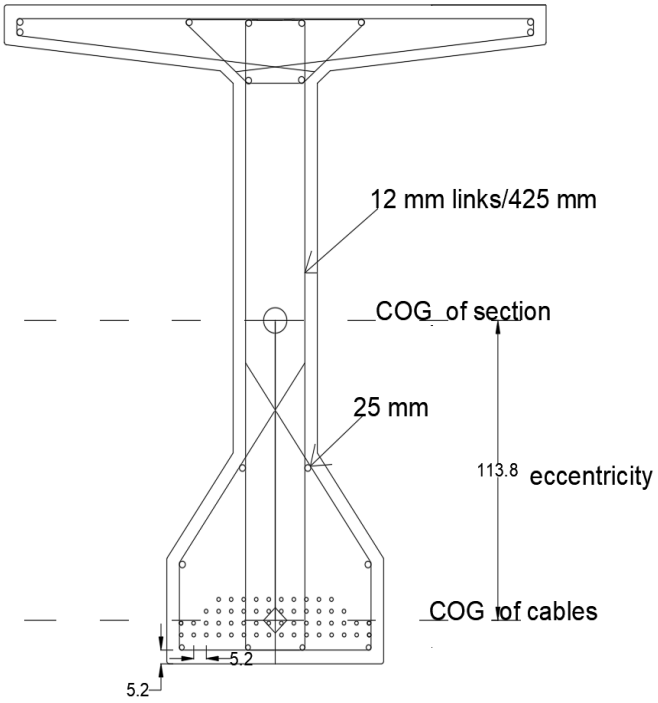

Figure 3.50. Detailed section of precast beam at midspan for the Eurocode Design

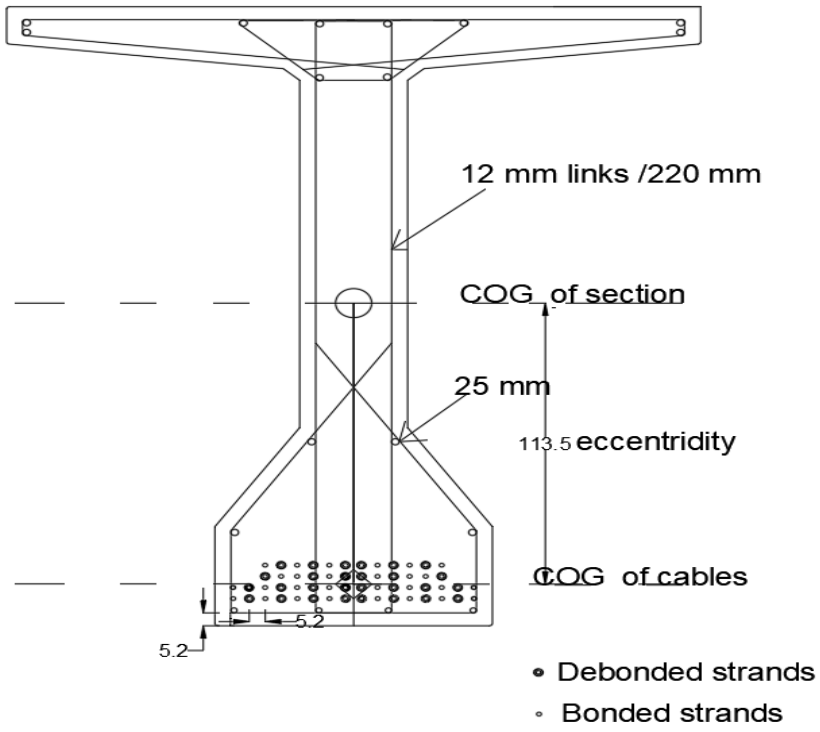

Figure 3.51. Detailed section of precast beam at supports for the BAEL Design.

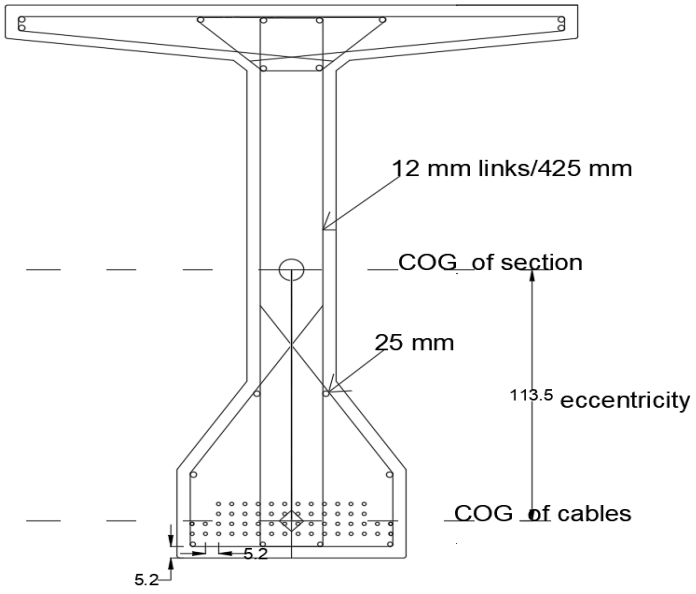

Figure 3.52. Detailed section of precast beam at midspan for the BAEL Design

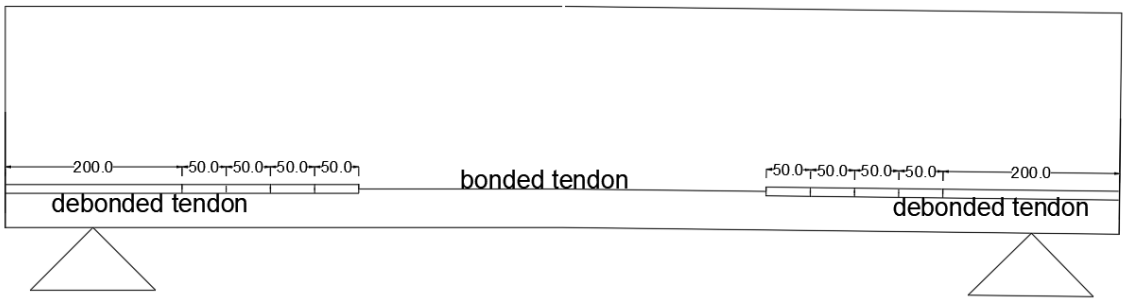

Figure 3.53. Tendon profile of the beam designed according to Eurocode

3.9.Comparative study analysis

The criteria for comparison will permit the differentiation between the two norms and obtain the norm more suited for the application. For this comparison, the criteria are number of parameters, sollicitations and design.

3.9.1. Number of parameters

For the global verifications of structural members, Eurocodes requires the application of Load Model 1 which is a tandem system made of a UDL and a double axle load .On the other hand, fascicule 61 titre 2 requires that the bridge is subjected successively to 2 systems of loads : Load System A and B. Load System A consists of a uniformly distributed load repartitioned on all the pavement surface. Load system B consists of three subsystems: traffic loads Bc, Bt and Br. Moreover, the loads of system B have to be multiplied by dynamic amplification coefficients calculated as a function of the total weight of the bridge superstructure. The characteristic values of LM1 on the other hand already take into account the load amplification coefficient and need not to be further calculated. From the observations mentioned above Eurocode takes into account fewer parameters.

3.9.2. Sollicitations

The sollicitations obtained in the edge beam after repartition with the Massonet method and Finite Element Method were more unfavorable for Load Model 1 than for all the vehicles of Load System A and B this shows that load model 1 covers most of the effects of traffic loads and the bridge designed according to Eurocode is designed to sustain more vehicular traffic.

3.9.3. Design

From table 3.58 the design of the edge beam according to BAEL required a higher prestressing force than the design according to Eurocode even though less sollicitated. Considering the fact that both designs were carried out using the permissible stress design method, a higher number of strands in BAEL is due principally to a lower elastic tensile strength admitted at transfer (3.3 Mpa) compared to Eurocode (3.79 Mpa) for the concrete class

considered. The resistances of materials for design purposes is less than that in Eurocode. The higher resistances for materials in Eurocodes are based on hypothesis regarding the workability of the materials which are not often met on the construction site.

Conclusion

The Objective of this chapter was to present the results obtained after the application of the methodology to our case study. To begin with, the presentation of the project site was made followed by the presentation of the project. Furthermore, a load analysis was done and load distribution according to Eurocode and BAEL. The numerical model was presented, with the results of numerical analysis that is vibration modes shapes and periods from dynamic analysis and solicitation diagrams from static analysis. The vibration indicate that the structures vibration was controlled with the fundamental period less than one. The sollicitations obtained in the edge beam using the Massonet method and the finite element model were then exposed and compared. This was followed by the design of the prestressed bars according to Eurocode and BAEL and the chapter ended with a comparative study of the norms following analytical and numerical analysis. The criteria for comparison permitted the differentiation between the two norms and obtain the norm performant following the criteria defined for the application. For this comparison, the criteria are number of parameters, sollicitations and design. From the evaluation, Eurocode takes into account fewer parameters than BAEL. The sollicitations obtained in the edge beam after repartition with the Massonet method and Finite Element Method using CSI bridge software were more unfavorable for Load Model 1 than for all the vehicles of Load System A and B this shows that load model 1 covers most of the effects of traffic loads and the bridge designed according to Eurocode is designed to sustain more vehicular traffic. As for the design, the design resistances of materials for design purposes is less in BAEL than that in Eurocode. The higher resistances for materials in Eurocodes are based on hypothesis regarding the workability of the materials which are not often met on the construction site.

GENERAL CONCLUSION AND PERSPECTIVES

The principal objective of this study was to design a prestressed bridge over the Mahe river according to Eurocode and BAEL the two norms of current design practice in Cameroon and apprehend the differences between the two approaches. The bridge subject to the study is a single span prestressed bridge ,10.5 m wide spanning 40 m between abutments over the MAHE river.

The methodology used to attain the above mentioned consisted of a general recognition of the site through documentation, a load analysis according to Eurocode and BAEL, numerical modeling of the bridge with static and dynamic analysis. Load repartition using the Guyon Massonet method, this was followed by the design of the prestressing using the Magnel diagram and finally a comparative study to differentiate the approaches based on the number of parameters , sollicitations and design.

The results obtained are the general presentation of site, the physical description of the project, the effects of actions on the bridge model according to Eurocode and BAEL, the numerical model of the bridge with its vibration modes, frequencies and periods, the sollicitations in the edge beam, the prestressing force and eccentricity with the detailing of the girder showing the strands and their positions. From the results obtained, the maximum moment in the edge beam due to the traffic loads according to Eurocode is greater(5751.68kNm) than the traffic loads according to BAEL (5416.74 kNm). This result are confirmed by the moments obtained using the finite element Analysis. However, a higher effective prestressing force of 9820.05 kNm provided by 56 strands at an eccentricity of 1135.271 mm is required to satisfy the stress limitations at service for BAEL compared to that of Eurocode 9550.70 kN provided by 54 strands at an eccentricity of1138.31 mm. This is due to a lower tensile stress limitation in BAEL (3.3 MPa) than Eurocode (3.7 Mpa). The outcome of the comparative study is that fewer parameters are involved to obtain the results in Eurocode compared to BAEL and the sollicitations are greater in Eurocode than BAEL thus bridges designed according to Eurocode are expected to sustain greater actions compared to BAEL. However, the design according to BAEL does not rely on strong hypotheses on material behavior and as such is stricter on resistances of materials.

As all human endeavours, this work presents certain limitations which can be improved upon. The design of the complete superstructure and substructure of the bridge including seismic analysis could not be performed for both norms.

As perspectives a more comprehensive study which includes cost analysis can be carried out after the design of the complete superstructure and substructure. This will offer the possibility of performing a cost benefit analysis of the two norms.

BIBLIOGRAPHY AND REFERENCES

AFNOR (1992), "Règle BAEL 91 révisées 99-Règles techniques de conception et de calcul des ouvrages et constructions en béton armé suivant la méthode des état limites", Issue mars 1992, vol 99, 221p.

Bares, R., & Massonnet, C. E. (1966). *Le Calcul des grillages de poutres et dalles orthotropes: selon la méthode Gruyon-Massonet-Barés*. Sante.

Bourrel, A., & Gourdou, J. (2016). II. Marchés publics. *Droit et Gestion Des Collectivités Territoriales*, *36*(1), 420–445. https://doi.org/10.3406/coloc.2016.2991

Calgaro, J.-A., & Bernard-Gély, A. (1994). *Conception des ponts*. Ed. Techniques Ingénieur.

EN 1990. (2002). *Eurocode -Basis of structural design*. British Standards Institution.

EN 1992-1-1. (2004). *Eurocode 2: Design of concrete structures*. British Standards Institution.

Gilbert, R. I., Mickleborough, N., & Ranzi, G. (2013). *Design of Prestressed concrete according to Eurocode 2* (Vol. 53, Issue 9).

Izzet, A., & Abdulhameed, A. (2017). *Prestressed Concrete: A Fundamental Approach, ACI 318-11 Code Philosophy & Stresses Limitations*.

Jaggerwal, H., & Bajpai, Y. (2014). Effects Of Skewness On Three Span Reinforced Concrete T Girder Bridges. *International Journal of Computational Engineering Research*.

Johnson, D. (2000). *Advanced Structural Mechanics: An Introduction to continuum mechanics and structural mechanics.* D. Johnson and Thomas Telford Limited. ISBN 0 7277 2860 1.

MBESSA, M. (2005). *Traite de genie civile*.

Menn, C. (1986). *Prestressed Concrete Bridges*. Springer-Verlag,Wien.

Mossot, J. (2004). *Annet-sur-Marne Bridge*. https://structurae.net/en/structures/annet-sur-marne-bridg

Okumus, P., & Oliva, M. (2014). Strand Debonding for Pretensioned Bridge Girders to Control End Cracks. *ACI Structural Journal*, *111*, 201–210.

Qaqish, M., Fadda, E., & Akawwi, E. (2008). Design of T-beam bridge by finite element method and AASHTO specification. *KMITL Science Journal*, *8*(1), 24–34.

Shreedhar, R., & Mamadapur, S. (2012). Analysis of T-beam Bridge Using Finite Element Method. *International Journal of Engineering and Innovative Technology (IJEIT)*, *2*, 340–346.

ANNEXES

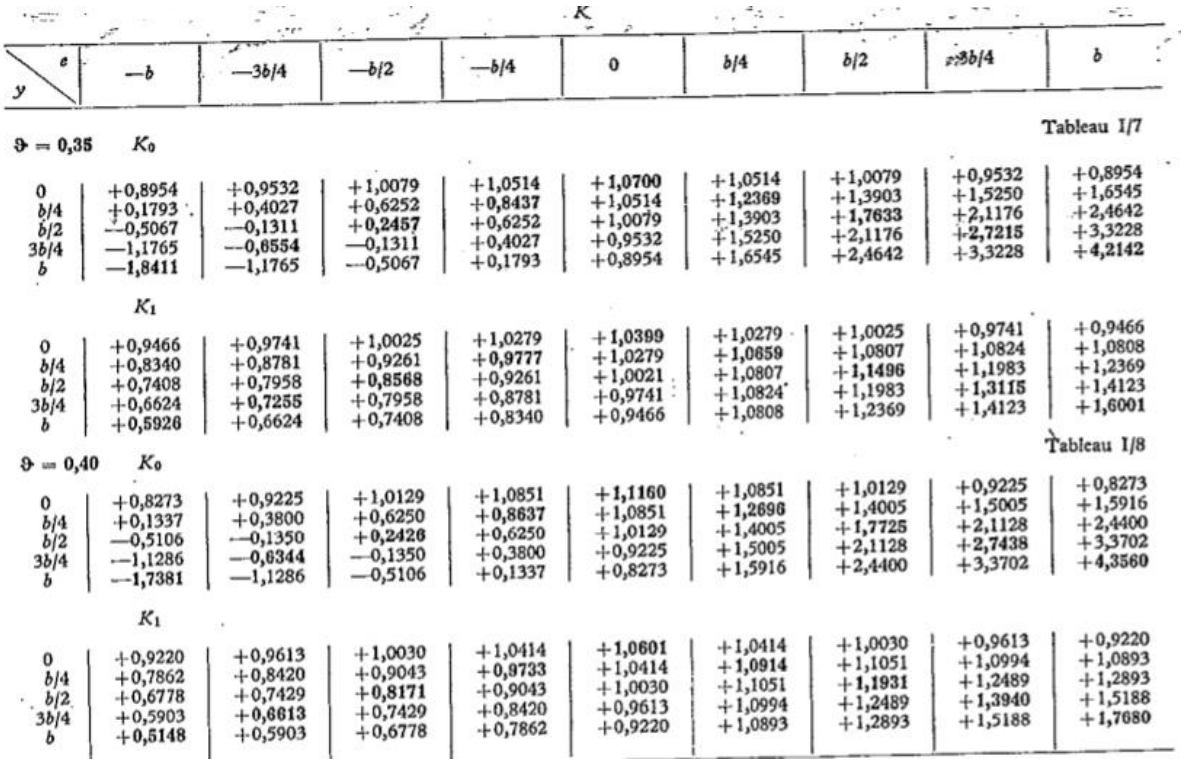

K

e / y	−b	−3b/4	−b/2	−b/4	0	b/4	b/2	3b/4	b
									Tableau I/7
ϑ = 0,35	K_0								
0	+0,8954	+0,9532	+1,0079	+1,0514	+1,0700	+1,0514	+1,0079	+0,9532	+0,8954
b/4	+0,1793	+0,4027	+0,6252	+0,8437	+1,0514	+1,2369	+1,3903	+1,5250	+1,6545
b/2	−0,5067	−0,1311	+0,2457	+0,6252	+1,0079	+1,3903	+1,7633	+2,1176	+2,4642
3b/4	−1,1765	−0,6554	−0,1311	+0,4027	+0,9532	+1,5250	+2,1176	+2,7215	+3,3228
b	−1,8411	−1,1765	−0,5067	+0,1793	+0,8954	+1,6545	+2,4642	+3,3228	+4,2142
	K_1								
0	+0,9466	+0,9741	+1,0025	+1,0279	+1,0399	+1,0279	+1,0025	+0,9741	+0,9466
b/4	+0,8340	+0,8781	+0,9261	+0,9777	+1,0279	+1,0659	+1,0807	+1,0824	+1,0808
b/2	+0,7408	+0,7958	+0,8568	+0,9261	+1,0021	+1,0807	+1,1496	+1,1983	+1,2369
3b/4	+0,6624	+0,7255	+0,7958	+0,8781	+0,9741	+1,0824	+1,1983	+1,3115	+1,4123
b	+0,5926	+0,6624	+0,7408	+0,8340	+0,9466	+1,0808	+1,2369	+1,4123	+1,6001
									Tableau I/8
ϑ = 0,40	K_0								
0	+0,8273	+0,9225	+1,0129	+1,0851	+1,1160	+1,0851	+1,0129	+0,9225	+0,8273
b/4	+0,1337	+0,3800	+0,6250	+0,8637	+1,0851	+1,2698	+1,4005	+1,5005	+1,5916
b/2	−0,5106	−0,1350	+0,2426	+0,6250	+1,0129	+1,4005	+1,7725	+2,1128	+2,4400
3b/4	−1,1286	−0,6344	−0,1350	+0,3800	+0,9225	+1,5005	+2,1128	+2,7438	+3,3702
b	−1,7381	−1,1286	−0,5106	+0,1337	+0,8273	+1,5916	+2,4400	+3,3702	+4,3560
	K_1								
0	+0,9220	+0,9613	+1,0030	+1,0414	+1,0601	+1,0414	+1,0030	+0,9613	+0,9220
b/4	+0,7862	+0,8420	+0,9043	+0,9733	+1,0414	+1,0914	+1,1051	+1,0994	+1,0893
b/2	+0,6778	+0,7429	+0,8171	+0,9043	+1,0030	+1,1051	+1,1931	+1,2489	+1,2893
3b/4	+0,5903	+0,6613	+0,7429	+0,8420	+0,9613	+1,0994	+1,2489	+1,3940	+1,5188
b	+0,5148	+0,5903	+0,6778	+0,7862	+0,9220	+1,0893	+1,2893	+1,5188	+1,7080

Annex I. Massonet table for determination of load amplification coefficient

Structural Class							
Criterion	**Exposure Class according to Table 4.1**						
	X0	XC1	XC2 / XC3	XC4	XD1	XD2 / XS1	XD3 / XS2 / XS3
Design Working Life of 100 years	increase class by 2	increase class by 2	increase class by 2	increase class by 2	increase class by 2	increase class by 2	increase class by 2
Strength Class [1] [2]	≥ C30/37 reduce class by 1	≥ C30/37 reduce class by 1	≥ C35/45 reduce class by 1	≥ C40/50 reduce class by 1	≥ C40/50 reduce class by 1	≥ C40/50 reduce class by 1	≥ C45/55 reduce class by 1
Member with slab geometry (position of reinforcement not affected by construction process)	reduce class by 1	reduce class by 1	reduce class by 1	reduce class by 1	reduce class by 1	reduce class by 1	reduce class by 1
Special Quality Control of the concrete production ensured	reduce class by 1	reduce class by 1	reduce class by 1	reduce class by 1	reduce class by 1	reduce class by 1	reduce class by 1

Annex II. Recommended structural classification

Environmental Requirement for $c_{min,dur}$ (mm)							
Structural Class	**Exposure Class according to Table 4.1**						
	X0	XC1	XC2 / XC3	XC4	XD1 / XS1	XD2 / XS2	XD3 / XS3
S1	10	10	10	15	20	25	30
S2	10	10	15	20	25	30	35
S3	10	10	20	25	30	35	40
S4	10	15	25	30	35	40	45
S5	15	20	30	35	40	45	50
S6	20	25	35	40	45	50	55

Annex III. Values of minimum cover, $\mathbf{C_{min,dur}}$requirements with regard to durability for reinforcement steel in accordance with EN 10080

Class designation	Description of the environment	Informative examples where exposure classes may occur
1 No risk of corrosion or attack		
X0	For concrete without reinforcement or embedded metal: all exposures except where there is freeze/thaw, abrasion or chemical attack For concrete with reinforcement or embedded metal: very dry	Concrete inside buildings with very low air humidity
2 Corrosion induced by carbonation		
XC1	Dry or permanently wet	Concrete inside buildings with low air humidity Concrete permanently submerged in water
XC2	Wet, rarely dry	Concrete surfaces subject to long-term water contact Many foundations
XC3	Moderate humidity	Concrete inside buildings with moderate or high air humidity External concrete sheltered from rain
XC4	Cyclic wet and dry	Concrete surfaces subject to water contact, not within exposure class XC2
3 Corrosion induced by chlorides		
XD1	Moderate humidity	Concrete surfaces exposed to airborne chlorides
XD2	Wet, rarely dry	Swimming pools Concrete components exposed to industrial waters containing chlorides
XD3	Cyclic wet and dry	Parts of bridges exposed to spray containing chlorides Pavements Car park slabs

Annex IV. Exposure classes in relation to environmental conditions according to EN 206-1.

e	-b	-3b/4	-b/2	-b/4	0	b/4	b/2	3b/4	b
	5.5	4.125	2.75	1.375	0	-1.375	-2.75	-4.125	5.5
0.4									
k_0	3.3702	2.7438	2.1128	1.5005	0.9225	0.38	-0.135	-0.634	1.128
k_1	1.5188	1.394	1.2489	1.099	0.961	0.84	0.7429	0.6613	.5903
k_α	2.255	1.931	1.5927	1.259	0.945	0.658	0.3934	0.1455	0.093
0.35									
k_0	3.23	2.72	2.12	1.52	0.95	0.40	-0.13	-0.66	-1.18
k_1	1.4123	1.3115	1.1983	1.1983	0.9741	0.8781	0.7958	0.7255	0.6624
k_α	2.1350	1.8727	1.5642	1.3275	0.9657	0.6888	0.4268	0.1758	-0.069
0.39									
k_α	2.242	1.924	1.5896	1.2665	0.948	0.6614	0.3970	0.1488	0.0912

Annex V. Calculation of load amplification coefficient for the edge beam and the central beam.